PROCESSING AND CHARACTERIZATION OF CARBON NANOTUBES REINFORCED EPOXY RESIN BASED MULTI-SCALE MULTI-FUNCTIONAL COMPOSITES

A Dissertation

by

PIYUSH R. THAKRE

Submitted to the Office of Graduate Studies of
Texas A&M University
in partial fulfillment of the requirements for the degree of

DOCTOR OF PHILOSOPHY

December 2009

Major Subject: Materials Science and Engineering

PROCESSING AND CHARACTERIZATION OF CARBON NANOTUBES REINFORCED EPOXY RESIN BASED MULTI-SCALE MULTI-FUNCTIONAL COMPOSITES

A Dissertation

by

PIYUSH R. THAKRE

Submitted to the Office of Graduate Studies of
Texas A&M University
in partial fulfillment of the requirements for the degree of

DOCTOR OF PHILOSOPHY

Approved by:

Chair of Committee,	Dimitris C. Lagoudas
Committee Members,	Zoubeida Ounaies
	Hung-Jue Sue
	Terry Creasy
Intercollegiate Faculty Chair,	Tahir Cagin

December 2009

Major Subject: Materials Science and Engineering

ABSTRACT

Processing and Characterization of Carbon Nanotubes
Reinforced Epoxy Resin Based Multi-scale Multi-functional
Composites. (December 2009)
Piyush R. Thakre, B.E., Nagpur University;
M.S., Texas A&M University
Chair of Advisory Committee: Dr. Dimitris C. Lagoudas

This research is focused on investigating the effect of carbon nanotubes on macroscale composite laminate properties, such as, interlaminar shear strength, interlaminar fracture toughness and electrical conductivity along with studying the micro and nano-scale interactions of carbon nanotubes with epoxy matrix via thermo-mechanical and electrical characterization of nanocomposites. First an introduction to the typical advanced composite laminates and multi-functional nanocomposites is provided followed by a literature review and a summary of recent status on the processing and the characterization work on nanocomposites and composite laminates. Experimental approach is presented for the development of processing techniques and appropriate characterization methods for carbon nanotubes reinforced epoxy resin based multi-functional nanocomposites and carbon fiber reinforced polymer composite laminates modified with carbon nanotubes. The proposed work section is divided into three sub-sections to describe the processing and the characterization of carbon nanotube reinforced epoxy matrix nanocomposites, woven-carbon fabric epoxy matrix composite laminates modified with selective placement of nanotubes and unidirectional carbon fiber epoxy matrix composite laminates modified with carbon nanotubes.

Efforts are focused on comparing the effects of functionalized and unfunctional-

ized carbon nanotubes on the advanced composite laminates. Covalently functionalized carbon nanotubes are used for improved dispersion and fiber-matrix bonding characteristics and compared with unfunctionalized or pristine carbon nanotubes. The processing of woven carbon fabric reinforced epoxy matrix composite laminates is performed using a vacuum assisted resin transfer molding process with selective placement of carbon nanotubes using a spraying method. The uni-directional carbon fiber epoxy matrix pre-preg composites are processed using a hot press technique along with the spraying method for placement of nanotubes. These macroscale laminates are tested using short beam shear and double cantilever beam experiments for investigating the effect of nanotubes on the interlaminar shear stress and the interlaminar fracture toughness. Fractography is performed using optical microscopy and scanning electron microscopy to investigate the structure-property relationship. The micro and nano-scale interactions of carbon nanotubes and epoxy matrix are studied through the processing of unfunctionalized and functionalized single wall carbon nanotube reinforced epoxy matrix nanocomposites. The multifunctional nature of such nanocomposites is investigated through thermo-mechanical and electrical characterizations.

To THE ALMIGHTY LORD AND MY PARENTS

ACKNOWLEDGMENTS

First and foremost, I would like to thank my advisor, Dr. Dimitris C. Lagoudas, for his constant guidance and support throughout my stay at Texas A&M. He has been an excellent mentor who has a lion's share in shaping my character. His vision to tranform his students into successful individuals never allows the student to lose his focus. He has been always challenging me to push harder and achieve greater heights. During the course of my research over the past few years, he has provided me with several opportunities to collaborate with people from outside the university which was very useful in improving my professional interaction skills. I would like to thank him for providing me with a confidence gaining platform by sending me to several national and international level conferences. Apart from training in the professional life, his ability to connect with students at the personal level indeed makes him a great mentor. His job as my Ph.D. advisor might be over, however, I would not be able to find a better mentor and would need his mentoring for many years to come. I also want to sincerely thank my committee members, Dr. Zoubeida Ounaies, Dr. Hung-Jue Sue, and Dr. Terry Creasy, for their guidance and support throughout the course of this research.

I have had the pleasure of many interactions with Dr. Ounaies during my graduate studies at A&M. Dr. Ounaies has provided me with her valuable advice in many circumstances and I admire her ability to understand and precisely respond to students' questions. She had been my graduate teaching academy advisor and with her help I was able to finish the fellow program of the teaching academy. I also had the pleasure of working with her on extracurricular activities through the Nanotechnology and Nanoscience Student Association.

I am also truly indebted to Dr. Sue for teaching me three polymer classes without

which this research would not have been possible. Many basics of my research have been taught to me by Dr. Sue. His ability to formulate precise and understanding based questions for exams is admirable and definitely provide important concepts to students. His advice about asking good critical questions in class has also helped me to think critically about my research. I am also thankful to Dr. Creasy for being very approachable and being always there for guiding students. He has provided some good suggestions during my prelim exam which helped in shaping up this dissertation in the current form.

Thanks also go to my friends and colleagues and the department faculty and staff for making my time at Texas A&M University a great experience. I would like to thank my friend and colleague, Dr. Gary Seidel, who has been a wonderful peer and I have learned a great deal of things from him. There have been many technical and non-technical discussions with Gary over the past years which helped in shaping up a special friendship with him. Special thanks also goes to my long time friend and colleague, Amnaya Awasthi, who has always been there whenever I needed any help. I have also enjoyed a lot of philosophical discussions with him which helped me grow philosophically as well as spiritually. There have been many friends and colleagues who have been a part of my life for a long time at Texas A&M University like Luciano Machado, Olivier Bertacchini, Parikshit Kumar, Darren Hartl, Bjoern Kiefer, Sampath Jambunathan, Anil Patnaik and Pranav Nagarnaik, who have made my memories really cherishable. I would also like to thank Dr. Yordanos Bisrat and Dr. George Chatgeorgiu for brainstorming discussions and providing many useful thoughts related to my research. I also want to extend my gratitude to all the people involved directly or indirectly during the course of this research.

I want to acknowledge the TiiMS (NCC-1-02038) and NRA (NNX07AB86A) projects by NASA, which provided the funding source during my research. I have

had the pleasure of working closely with Dr. Jaret Riddick (ARL), Dr. Sarah-Jane Frankland Pillsbury (NIA)and Dr. James Ratcliffe (NIA) from whom I have learned a lot of things during the course of our interactions over the last few years. Late Dr. Thomas Gates remains in my memory for his valuable advise and mentoring during my work at NASA Langley. I have also been privileged to work with Dr. Enrique Barrera at Rice University and with his post-doc Dr. Jiang Zhu (who later worked with NanoRidge Inc.). That collaborative effort has resulted in many of the material presented in this dissertation.

Finally, thanks goes to my mother and father for their constant encouragement and their belief in my abilities. Mother's love and father's inspiration have always been my strength along with my sister's unconditional love. Last but not least, many thanks goes to my wife for her love, patience and support. Especially lot of patience was required on her part during the demanding final stretch of my Ph.D. work.

TABLE OF CONTENTS

CHAPTER Page

CHAPTER Page

LIST OF TABLES

LIST OF FIGURES

FIGURE Page

FIGURE Page

FIGURE Page

FIGURE Page

CHAPTER I

INTRODUCTION

A. Problem Statement

The aerospace, automotive, infrastructure and other industries along with defense applications for army, navy and air-force have wide use for composite materials due to their light weight, high fracture toughness, high strength to weight ratio, good chemical resistance and good fatigue life. Particularly, epoxy resin based composites have been of interest in the aerospace industry due to epoxy resin being used as a matrix material for many of the high performance advanced composites. Epoxy resin based composites have been of particular interest due to the flexibility of modifying mechanical properties, thermal properties and chemical resistance by controlling curing kinetics. However, one of the limitations on the use of composite laminates has been their susceptibility to delamination, i.e. separation of individual plies resulting from out-of-plane loads. Another limitation has been the inherent brittleness and low fracture toughness of epoxy resin. The increasing demand for better mechanical, thermal and electrical properties has made it necessary to develop new composites with multifunctional properties, better processing techniques and good out-of-plane properties without adding weight penalties.

Carbon nanotubes have been reported to be one of the most promising reinforcement materials for providing multifunctionality with excellent mechanical, electrical and thermal properties. Therefore, it is proposed, based on the interest in the aerospace industry, to develop carbon fiber reinforced epoxy matrix composites with selective placement of carbon nanotubes, so as to optimize the use of nanotubes at

---

The journal model is *IEEE Transactions on Automatic Control.*

the places of weak interfaces and introduce possibility for multifunctional properties. There is a presence of multiple length scales in these advanced composites, such as, the macro-scale of the ply and the composite laminate, the micro-scale of the carbon fibers, and the nano-scale of the carbon nanotubes. A multi-scale characterization effort is required to identify contribution from nano- and micro-scale reinforcement at each length scale and to investigate the physical mechanisms behind the changes in the bulk properties.

B. Objectives

Based on the problem statement mentioned in the previous section, the following objectives are defined for the research.

1. Processing technique is required for nanotubes reinforced epoxy matrix based multi-functional nanocomposites such that a good dispersion and distribution of nanotubes is achieved. Covalent functionalization of carbon nanotubes is one way to improve CNT-epoxy interface and better load-transfer through the interphase region surrounding nanotubes in addition to providing better dispersion. Several parameters, such as, stability of suspension in solvents, mixing speeds, solvent evaporation times, etc. are needed to be studied to come up with a optimum method for processing nanocomposites. The weight fractions will be varied for the pristine and the functionalized carbon nanotubes to study the effect of quantity of nanotubes on the mechanical and the electrical properties. It is important to investigate the effect of addition of nanotubes to epoxy matrix by measuring strength, modulus and glass transition temperature of the nanocomposites. The fracture mechanisms at the nano-scale are studied using

transmission and scanning electron microscopy. The multi-functional nature of such nanocomposites is investigated by measuring electrical properties, especially the percolation behavior. This objective allows the investigation of carbon nanotube-epoxy matrix interactions and the effectiveness of nanotube functionalization on multi-functional properties.The information collected by characterizing nanocomposites is also useful for validation of effective mechanical and electrical properties predicted using multi-scale micromechanics based modeling using input from molecular dynamics simulations for interphase properties.

2. Processing techniques and characterization methodology is required for woven carbon fiber reinforced epoxy matrix composite laminates along with a technique for the selective placement of pristine and functionalized carbon nanotubes. The woven carbon fibers are chosen as the material of interest based on wide industrial application in advanced composites. The interlaminar fracture toughness is of particular interest, as the advanced composites are known to have poor out-of-plane performance due to delamination initiation and propagation. The interlaminar shear strength is also investigated to identify contribution of nano-scale inclusion on the bulk property and some qualitative input regarding effectiveness of the selective placement of nanotubes, can be provided for appropriate modification of the processing technique. The physical mechanisms introduced by the selective placement of nanotubes are investigated by using optical microscopy for micro-scale observations and scanning electron microscopy for nano-scale observations. The different length scales in the energy dissipation mechanisms introduced due to the presence of the carbon nanotubes can be understood by this objective.

3. A methodology is required for the processing and characterization of uni-directional carbon fiber pre-preg composite laminates with selective placement of pristine and functionalized nanotubes. The purpose of using unidirectional carbon fibers is to provide better understanding of mechanisms as the complications due to weave structure is absent in such composites and also to facilitate validation of multi-scale modeling of such composites for more accurate predictions. The woven fiber composites have wide industrial applications; however, for modeling purposes it presents complexity due to woven configuration of fibers and complex stress-states. Mechanical testing includes three point bending tests and in-plane shear tests to characterize the longitudinal, the transverse and the shear response of unidirectional composites. The structure-property relationship is studied by investigating microstructures using optical and scanning electron microscopy and studying the mechanisms introduced by carbon nanotubes. Double cantilever beam experiments are performed to characterize the interlaminar fracture performance of such composites, in addition to investigating the fracture mechanisms associated with the delamination process as a result of the interlaminar fracture.

CHAPTER II

LITERATURE REVIEW

A. Carbon Nanotubes

The discovery of carbon nanotubes by Iijima [2] is considered to be one of the most significant achievements of contemporary science. Carbon nanotubes are fullerene-related structures which consist of graphene cylinders closed at either end with caps containing pentagonal rings. They were discovered in 1991 by the Japanese electron microscopist Sumio Iijima who was studying the material deposited on the cathode during the arc-evaporation synthesis of fullerenes. He found that the central core of the cathodic deposit contained a variety of closed graphitic structures including nanoparticles and nanotubes, of a type which had never previously been observed. A short time later, Thomas Ebbesen and Pulickel Ajayan, from Iijima's lab, showed how nanotubes could be produced in bulk quantities by varying the arc-evaporation conditions. A major event in the development of carbon nanotubes was the synthesis in 1993 of single-layer nanotubes. The standard arc-evaporation method produces only multilayered tubes. It was found that addition of metals such as cobalt to the graphite electrodes resulted in extremely fine tube with single-layer walls.

An alternative method of preparing single-walled nanotubes was described by Richard Smalley's group in 1996. Like the original method of preparing C60, this involved the laser-vaporization of graphite, and resulted in a high yield of single-walled tubes with unusually uniform diameters. These highly uniform tubes had a greater tendency to form aligned bundles than those prepared using arc-evaporation, and led Smalley to christen the bundles nanotube 'ropes'. Initial experiments indicated that the rope samples contained a very high proportion of nanotubes with a specific

armchair structure. Subsequent work has suggested that the rope samples may be less homogeneous than originally thought. Nevertheless, the synthesis of nanotube ropes gave an important boost to nanotube research, and some of the most impressive work has been carried out on these samples. Fig. 1 shows different configurations of folded graphene layers in the schematic of carbon nanotubes.

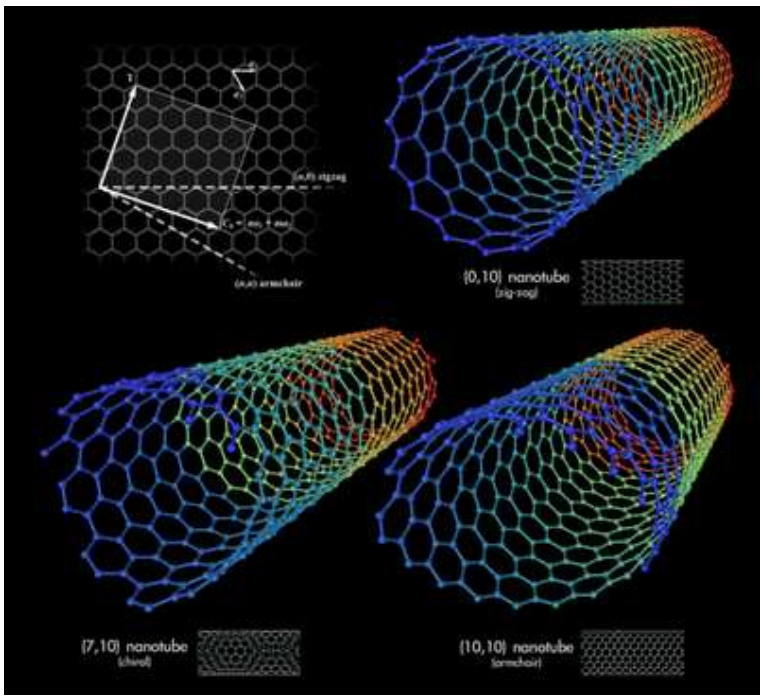

Fig. 1. Schematic of carbon nanotubes showing folded layer of graphene.[1]

1. Carbon Nanotube Synthesis Processes

Some of the known synthesis processes for carbon nanotubes as given below are compared in Table I. PLV Process: Pulsed Laser Vaporization Process / Laser Ablation, CVD Process: Chemical Vapor Deposition Process, CAD Process: Carbon Arc Discharge Process, HiPCO Process: High Pressure Carbon Monoxide Process.

The HiPCO process has evolved to the point that now it can be used for large scale production of carbon nanotubes. This process has been developed by Dr. Smalley's group at Rice University and the technology was transferred to Carbon NanoTechnologies Inc. for upscaling the process. In this process, a carbon containing gas, carbon monoxide, is passed over metal catalyst particles, mostly iron and nickel, under high pressure and temperature. The carbon nanotubes start growing from the catalyst particles into bundles of long nanotubes. The nanotubes used in the current research presented in this dissertation are made using HiPCO process. A short summary of other processes is given below in Table I.

2. Carbon Nanotube Physical Properties

Physical properties of carbon nanotubes are given below in Table II. Carbon nanotubes have excellent mechanical properties [3] such as Young's modulus of around 1000 GPa and tensile strength of around 200 GPa with small dimension (diameter 1nm) and high aspect ratio (10000). One of the major applications of carbon nanotubes is in composites which may be used in structural applications or multifunctional applications. Nanotube based composites could offer outstanding strength to weight ratio, which is an order of magnitude higher than today's structural materials. Therefore defense agencies (NASA, AFRL, ARL) have heavily invested in developing nanotube based composites for use in future spacecrafts. Experiments in fabricating and testing of composites showed improvements in mechanical properties like modulus, strength and toughness [4–7].

The use of high shear mixing, ultrasonication, surfactants, chemical modification and polymer chain wrapping have been some of the research efforts towards accomplishing better SWCNTs reinforcement. But the difficulties in dispersion of SWCNT bundles and processing challenges have resulted in only moderate improvements in

Table I. Comparison of CNT synthesis processes

Method	*Arc Discharge Method*	*Chemical Vapor Deposition*	*Laser Ablation*
Who	Ebbesen and Ajayan, NEC, Japan 1992	Endo, Shinshu University, Nagano, Japan	Smalley, Rice, 1995
How	Connect two power rods to a power supply, Place them a few millimeters apart and throw the switch. At 100Amps carbon vaporizes and forms a hot plasma	Place substrate in oven and heat to 600 deg. C and slowly add a carbon bearing gas as methane. As gas decomposes it frees up carbon atoms, which recombine in the form of NTs	Blast graphite with intense laser pulses; Use laser pulses rather than electricity to generate carbon gas from which the NTs form. Try various conditions until hit on one that produces prodigious amounts of SWNTs.
Typical Yield	30 to 90%	20 to 100%	Up to 70%
SWNT	Short tubes with diameters of 0.6 -1.4 nm	Long tubes with diameters ranging from 0.6 to 4 nm	Long bundles of tubes (5-20microns) with individual diameters from 1- 2 nm
M-WNT	Short tubes with inner diameter of 1-3 nm and outer diameter of approximately 10 nm	Long tubes with diameters ranging from 10 240 nm	Not very much interest in this technique, as it is too expensive, but MWNT synthesis is possible
Pros	Can easily produce SWNT, MWNTs; SWNTs have few structural defects; MWNT without catalyst, not too expensive, open air synthesis possible;	Easiest to scale up to the industrial production; Long length, simple process; SWNT diameter controllable, quite pure;	Primarily SWNTs with good diameter control and few defects; The reaction product is quite pure;
Con	Tubes tend to be short with random sizes and directions; often need lot of purification;	NTs are usually MWNTs and often riddled with defects;	Costly technique because it requires expensive lasers and high power requirement, but is improving;

Table II. Physical properties of single wall carbon nanotubes

Physical Properties of Carbon Nanotubes			
Below is a compilation of research results from scientists all over the world.			
All values are for Single Wall Carbon Nanotubes (SWNT's) unless otherwise stated.			
Electrical Transport			
Conductance Quantization		(12.9 k)-1	[4,5,19]
Resistivity		10-4 -cm	[2]
Maximum Current Density		1013 A/m2	[5,12]
Thermal Transport			
Thermal Conductivity		2000 W/m/K	[6,15,16]
Phonon Mean Free Path		100 nm	[15]
Relaxation Time		10-11 s	[15]
Elastic Behavior			
Young's Modulus (SWNT)		1 TPa	[3,7,8,9,12]
Young's Modulus (MWNT)		1.28 TPa	[8]
Maximum Tensile Strength		100 GPa	[18]

mechanical properties [4, 6]. Significant work has been targeted in improving the dispersion of SWCNTs in polymer matrices through functionalization [4, 5, 8], but the deformation behavior of such composites at micro and nanoscale remain poorly understood. Detailed Studies of the deformation behavior at micro/nanoscale using advanced characterization methods will help us understand SWCNTs dispersion, interfacial bonding and load transferring mechanisms.

B. Multifunctional Nanocomposites

There is significant research going on in the polymer based nanocomposites for a wide range of properties such as electrical, thermal, mechanical and magnetic properties [9–15]. What makes the polymers attractive host material is their light weight and ability to tailor fracture toughness, tensile strength, glass transition temperature, electrical and thermal conductivities. In addition, one can easily modify the physical properties of the polymer by using fillers and still keep some of the excellent inherent properties. For example, the conducting polymer composites are made by the addition of conductive fillers into an insulating polymer matrix. Introduction of fillers such as carbon black and iron powder has long been pursued by researchers to modify the electrical properties of the polymers [16, 17]. However, such fillers tend to degrade the modulus, the strength and the glass transition temperature of the nanocomposites. One of the promising filler material is considered to be carbon nanotubes since they provide good thermal and electrical properties at low loadings due to their large surface area to volume ratio compared to carbon black or other metallic reinforcements [18, 19].

Several studies have shown that various processing parameters affect the properties of the resulting nanocomposites [20–27]. Martin et al. [23] reported the effect of

stirring rates, shear forces and curing temperatures on epoxy matrix nanocomposites with 0.01 wt% of CVD grown MW-CNTs. They suggested high stirring rates and shear forces for separating nanotubes in the initial phase and then, after adding hardener, use of high curing temperatures to enhance the mobility of nanotubes resulting in a better network formation of nanotubes. Similar study was undertaken in this research to find optimum processing parameters for EPON 862 epoxy with different types of hardeners and also different types of nanotubes.

To maximize the inherent properties of nanotubes, dispersion and reinforcement of SWCNTs in polymer matrix has been one of the major issues of interest. The process of covalent and non-covalent functionalization has been suggested as one of the options for better dispersion of nanotubes [4, 5, 8, 18, 22, 28, 29]. Thakre et al. [8] reported better dispersion of SW-CNTs as a result of silane functionalization, however, no significant improvement in mechanical properties. The chemical modification of the nanotube surface through covalent functionalization results in reduction of the aspect ratio along with the formation of sp^3 carbons on nanotube surface resulting in reduction of electrical conductivity of the nanotubes [8, 18, 22]. Therefore, such issues have been addressed in this dissertation while studying the influence of nanotube functionalization on mechanical properties e.g. flexure modulus, strength, storage modulus, loss modulus, and compared with as-received nanotubes i.e. pristine nanotubes embedded in epoxy matrix nanocomposites for optimizing the multifunctional properties of the nanocomposites. The fracture surface analysis has also been presented in detail to identify possible toughening mechanisms by incorporation of nanotubes in epoxy matrix. Studying the epoxy-nanotube interaction would be useful when moving on to the more complex systems at laminate scale with additional reinforcement of woven or unidirectional carbon fibers.

The effects of the aspect ratio, the aggregate size and the dispersion process

as a result of functionalization has been reported to affect the percolation limits of nanocomposites [18–23, 30–35]. Gojny et al. [18] reported an increase in percolation threshold for smaller aspect ratio and Li et al. [22] reported similar observation and developed an analytical model based on interparticle distance concept to explain the effect of dispersion state and aspect ratio of nanotubes on the percolation threshold. Seidel [36] showed that the percolation threshold is related to the formation of conductive networks of nanotubes and aspect ratio. Improvement in dispersion of nanotubes in polymer matrix has been reported to improve electrical and mechanical properties [20, 21, 30, 31, 33]. Aggregation of nanotubes due to Van der Waals interactions and shear forces during mixing has been reported to cause a drop in electrical conductivity [18, 35, 37]. Sandler et al. [38] reported ultra-low electrical percolation threshold of about 0.005 wt% for epoxy matrix nanocomposites with CVD grown aligned multiwall carbon nanotubes (MW-CNTs). The electrical conductivity of the nanocomposites with aligned MW-CNTs was found to be an order of magnitude lower than that with entangled MW-CNTs. Owing to high aspect ratio and good dispersion, nanotubes can reach conductivity thresholds at lower loading levels and can create networks that facilitate electron transport. As seen from the literature study, the electrical conductivity has been significantly improved by addition of nanotubes and very low electrical percolation limits have been reported for nanocomposites with single walled and multi-walled nanotubes [38–50]. However, the cost comparison with cheaper reinforcement particulates does not proportionately favor the use of nanotubes.

The XD-CNT (˜$50 per gram) produced by a high yield process is much cheaper than SW-CNT ($350 to $1000 per gram), however, the difference in mechanical and electrical properties of nanocomposites consisting of these nanofillers was not known. Thus, a part of this dissertation examined the electrical and the mechanical

properties of XD-CNT and SW-CNT filled epoxy matrix nanocomposites. The study of electrical properties at nanocomposite scale would also be useful in determining the contribution of matrix conductivity improvement to the laminate scale conductivity measurements.

C. Advanced Composite Laminates

There has been an increase in the use of epoxy resin-based composite laminates in the aerospace industry in recent years due to their light weight, desirable mechanical properties and ability to be molded into complex shapes [51–55]. Epoxies find wide applications in composites due to their good chemical resistance and heat resistance along with good thermo-mechanical properties such as strength, elastic modulus and glass transition temperatures, which can be tuned by adjusting chemical composition and curing kinetics [56, 57] as per the desired performance requirements. However, conventional epoxies exhibit inherent brittleness and low fracture toughness, and consequently, epoxy-based laminates can be susceptible to delamination i.e. and separation between individual plies [58–61]. Increasingly demanding requirements for mechanical, thermal and electrical properties of composite laminates has made it necessary to develop new material systems without adding weight penalties and simultaneously introducing the possibility for multifunctionality.

Recent efforts have been reported in that direction to combine the advantages of traditional advanced composites with nano and micro sized reinforcements to enhance thermo-mechanical and electrical properties [62–70]. Some of these efforts were directed towards resolving a critical issue in textile composites associated with the formation of matrix rich regions in textile composites. The polymer matrix rich region has been reported to be one of the reasons for the poor out-of-plane properties and

a contributing factor to crack initiation and propagation, resulting in poor resistance to delamination growth.

In the past, particulate reinforcements have been used in composites in an effort to improve the interlaminar fracture toughness [62, 64–67, 71–75]. For example, hybrid composites with alumina, silica, rubber and glass spheres forming secondary phases in the epoxy matrix were studied by Kinloch et al. [71]. It was shown that rubbery particles improved the fracture toughness of a thermosetting epoxy polymer, but reduced its strength. In fact, a combination of rubber and glass particles showed a better improvement in toughness. Sohn et al. [72] reported improvement in ILFT with introduction of KEVLAR short fibers in fiber-reinforced polymer composites. There was little effect on the initiation toughness values, but extensive fiber bridging led to a significant increase in propagation toughness, indicating increased resistance to delamination growth.

Sela and Ishai [54] reported methods for improving ILFT by introducing tough interleaves instead of particulate reinforcements and using thermoplastic matrices. Such interleaved composites showed a significant improvement in impact resistance. However, the major disadvantage of a composite with tough interleaves was shown to be the weight penalty along with low stiffness and strength of tough layers which proportionately reduced stiffness and strength of the laminate. Thermoplastic matrices in interleaves showed an order of magnitude increase in ILFT; however, low thermal stability, interfacial wetting problems, poor chemical resistance to solvents and acids, and creep problems associated with the thermoplastic matrices limit their use in aircraft structures. Reinforcing polymer matrix rich regions with particles or using interleaves did not provide adequate improvements in toughness and resulted in reduced strength and glass transition temperature [57, 71, 72].

Carbon nanotubes have been reported to be used as reinforcement in poly-

mer matrices due to their outstanding electrical, thermal and mechanical properties [5, 8, 62–67, 76–83]. Extensive research has been performed in characterizing [5, 8, 56, 78, 79, 83] and modeling [76–78, 80, 82, 84] carbon nanotube-polymer matrix nanocomposites. One of the methods to disperse the carbon nanotube bundles and form enhanced interaction between the nanotubes and the surrounding polymer matrix has been by the process of covalent functionalization of nanotubes which involves attaching chemical functional groups that can form bonds with the particular matrix in addition to dispersing the nanotube bundles [4, 5, 8, 64, 78, 85] . The reinforcement of conventional composites with carbon nanotubes may play an important role in realizing the potential of such composites in structural applications as well as introduce multifunctional properties. Recently, Wichmann et al. [67] reported about 16% improvement in interlaminar shear strength while the interlaminar fracture toughness was unaffected as a result of introduction of carbon nanotubes in glass fiber-epoxy composites. The carbon nanotubes were mixed in the epoxy matrix before impregnating glass fibers to produce the laminated composite. An improvement of about 300% in mode-I ILFT was reported by Veedu et al. [66] by growing nanotubes on SiC fabric composites. Bekyarova et al. [62] reported the use of electrophoresis for selective deposition of nanotubes on woven carbon fabric. The interlaminar shear strength was improved by about 30%, along with improved out-of-plane electrical conductivity. Functionalized SWCNTs showed an improvement of about 40% in the shear strength by adding 0.5 wt% SWCNT as reported by Bekyarova et al. [63]. Such efforts suggest the feasibility of improving ILFT by introducing carbon nanotubes. However, there have been several unresolved issues, such as, the addition of nanotubes to epoxy resin results in a significant increase in the viscosity of epoxy matrix leading to processing difficulties on a larger scale. Furthermore, direct mixing into epoxy resin distributes nanotubes throughout the composite laminate, reinforcing critical as

well as non-critical areas and therefore leads to unnecessary cost increase. The chemical vapor deposition method to grow nanotubes on fiber preforms or fabric material could be potentially difficult to implement on an industrial scale.

As an alternate approach, we propose in the present work to use nanotubes in small quantities at critical regions, i.e. and at the interfaces susceptible to delamination. The objective of this paper is to understand the influence of such selective reinforcement of carbon nanotubes on the mode-I interlaminar fracture toughness of woven carbon fiber-epoxy composites processed using vacuum assisted resin transfer molding (VARTM) technique. A novel spraying technique was used for the selective placement of nanotubes without increasing the viscosity of the epoxy matrix. The spraying process is easier to scale-up to the industrial production and ensures limited use of carbon nanotubes only in the susceptible areas. Several panels were processed using VARTM method incorporating functionalized as well as unfunctionalized (pristine) carbon nanotubes.

The VARTM process has been chosen as it is widely used for applications in commercial, military and aerospace composite structures. One of the advantages of the VARTM process is that it is easier to scale up to industrial production. For a successful application, the matrix properties which govern processing characteristics like viscosity must be considered in addition to meeting the requirements for mechanical properties in service. A number of low-viscosity epoxy resins have been developed to meet the processing requirements associated with the VARTM. An epoxy with room-temperature curing agent was selected for this study on the basis of lowest viscosity for easier VARTM processing. The nanotubes were functionalized for better dispersion in the epoxy matrix along with enhanced compatibility with epoxy through better bonding characteristics. The presence of nanotubes on the intended region of the laminate, after VARTM processing, was confirmed from the microscopy images.

The mode I interlaminar fracture toughness, G_{Ic}, of the laminates considered in the current study was characterized using the double cantilever beam (DCB) test. This test was conducted in accordance with the guidelines contained in the ASTM International Standard, D5528-01 [86]. The major exception in the current study to the guidelines of D5528-01 was that the DCB specimens were made from fabric. Similar tests conducted on either textile or fabric-based laminates have been reported previously. Choi et al. [61] and de Morais et al. [87] have studied the delamination resistance of multidirectional composites and reported higher values for interlaminar fracture toughness as compared to unidirectional composites. The delamination resistance of unidirectional and plain weave fabric IM7/8552 were compared by Paris et al. [88] using the DCB test. The average value of initiation G_{Ic} of the fabric IM7/8552 was reported to be 263 J/m^2 [88]. This value is only 3% greater than the initiation G_{Ic} value reported by Hansen and Martin of tape IM7/8552 [89]. Although the coefficient of variation was higher for the fabric specimens reported by Paris [88], this similarity in initiation values of G_{Ic} suggests that reliable values of initiation G_{Ic} may be obtained from DCB tests conducted on fabric material systems.

In short, a method for selective placement of carbon nanotubes in woven carbon fabric composites and unidirectional pre-preg composites is presented in this research. The characterization results using three point bending and shear tests has been presented for unidirectional fiber composites. The mode-I interlaminar fracture toughness using DCB tests and detailed study of fracture mechanisms using scanning electron microscopy has been presented in this dissertation for woven as well as unidirectional fiber composites.

CHAPTER III

MULTI-FUNCTIONAL NANOCOMPOSITES

The commercial application of CNT nanocomposites has been limited due to the problem of transferring the inherent CNT properties to the polymer matrix. This limitation is mainly due to CNT agglomeration in nanocomposites, along with poor interface between the polymer and the nanotubes . There have been several techniques to minimize CNT agglomerations, such as, ultrasonication, high shear mixing, non-covalent and covalent functionalizations. Usually some solvent is used as a medium for the dispersion of CNTs before adding to the polymer matrix. Studies have shown that chemical functionalization of CNTs improves the dispersion and strengthens the interfacial bonding with the polymer.

In order to improve the properties of nanocomposites, a good dispersion of nanotubes in the matrix is required, and understanding the effects of the various processing parameters of nanocomposites is a key to multifunctional property improvement. In this chapter, some of the processing parameters are studied, such as, stability of CNTs in particular solvents, stirring/mixing rates and curing time and temperature. Study of these processing parameters will provide some help for better reinforcing different types of nanotubes into the epoxy matrix. These nanocomposites are then characterized using different techniques to study the effect of covalent functionalization and weight fractions of nanotubes on mechanical and electrical properties. Comparison of the electrical percolation thresholds and plausible reasons for differences in percolation are also presented. The mechanical testing of nanocomposites using three point bending and dynamic mechanical analysis is followed by detailed analysis of fracture surfaces using optical microscopy, transmission and scanning electron microscopy.

A. Effect of Processing Parameters on Nanotube Dispersion

A key to achieve good dispersion of nanotubes in nanocomposites involves finding suitable processing parameters such as, proper solvent for initial dispersion, ultrasonication time, stirring speeds, curing/pre-curing time and temperature. These parameters change depending on the type of nanotubes (single wall/multi wall), type of functionalization and also for different weight fraction of nanotubes. A sample study of some of these parameters is presented in this section for one particular type of nanotubes (XDCNTs).

1. Stability of Nanotube Dispersion in Solvents

N,N'-Dimethyl formamide (DMF), N,N-Dimethyl acetamide (DMAC), tetrahydofuran (THF), toluene, methylene chloride(MC), acetone, ethanol, and a mixture of 1:1 toluene and ethanol were used as solvents. XD grade carbon nanotubes were selected as sample filler material in the nanocomposites samples. The polymer resin matrix consisted of EPON 862 resin and EPIKOTE Curing Agent W as the hardener for the high temperature curing. EPIKOTE Curing Agent 9553, EPIKOTE Curing Agent Accelerator 537, and air release agent were used with EPON 862 for studying the room temperature curing.

XD grade carbon nanotubes (10 mg) were added into a vial containing a solvent (20 ml) and sealed with a cap. A ratio of 1 mg per 2 ml was maintained for all weight fractions. The vials were then bath sonicated for 1 hour at 40 kHz and 100 W. After sonication, the vials were left in a quiescent state with pictures taken every five minutes for the first one hour. The dispersion stability of each solvent was determined by observing the suspension of the CNTs in the vials. Solvents in which the CNTs were sedimented after an hour of being in a quiescent state were classified as solvents

showing poor dispersion stability. Solvents which showed black color even after an hour were classified as good solvents for stability of nanotube dispersion.

The same vials were sonicated using a probe sonicator instead of the bath sonicator to see if a better dispersion of CNTs could be achieved. Each vial containing the solvent/CNT solution were sonicated for a total of 2 minutes using a probe sonicator with an intensity of 40 KHz. Pictures of the vials were taken every five minutes, and categorized by the same criteria as before.

Good solvent stability is necessary to obtain good dispersion of CNTs in nanocomposites. The dispersion process involves breaking of big agglomerates of CNTs into smaller ones and ultrasonication process precisely serves this purpose. Then it depends on the solvent type whether the nanotubes are going to remain suspended in solution or are going to settle down and agglomerate. In a first study various vials containing a mixture of CNTs and a solvent were bath sonicated for 1 hour, and then observed for the quality of the suspension of CNTs. An example of a solvent with bad stability is acetone. The nanotubes are almost immediately sedimented even after one hour of ultrasonication. Fig. 2(a) shows the various vials immediately after sonication, and in the acetone vial, most of the CNTs have sedimented. This behavior was also observed in DMAC, but not to the extent of acetone, as can be seen in Fig. 2(a). After half an hour of being in a quiescent state, the CNTs in toluene, DMAC, acetone, and the 1:1 mixture of ethanol and toluene had partially sedimented or were in partial swollen state. The CNTs in ethanol floated (swollen state) instead of sedimenting as can be observed in Fig. 2(b). It was observed that after an hour toluene, acetone, ethanol, and 1:1 mixture of toluene and ethanol had almost sedimented which is shown in Fig. 2(c). After an hour of being in a quiescent state, the best solvents were observed to be DMF followed by THF and MC, respectively as shown in Fig. 2(d). In these solvents, a portion of the CNTs were in

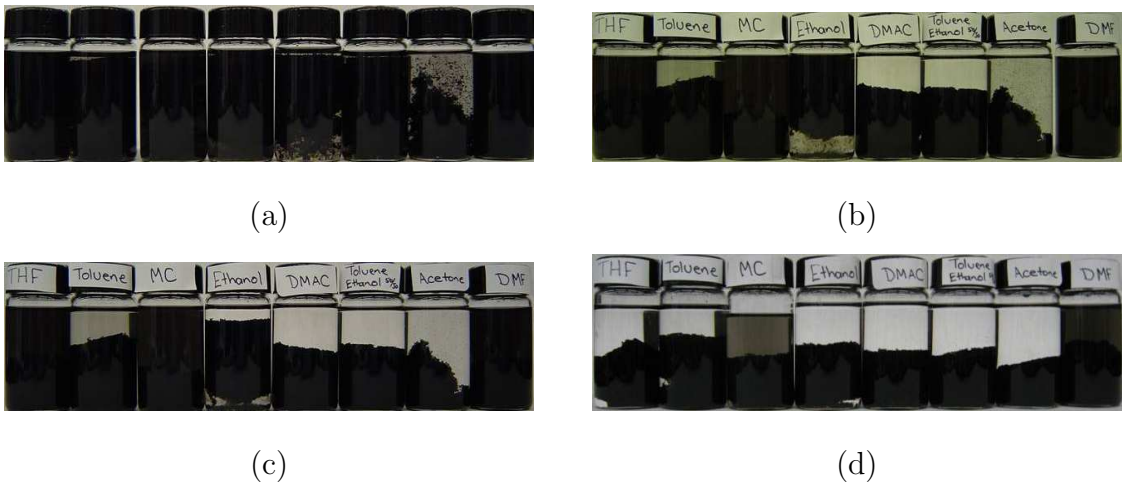

Fig. 2. Vials containing nanotubes in different solvents. 2(a) Immediately after sonication, 2(b) After one hour, 2(c) After two hours, 2(d) After three hours.

sedimented/swollen state, but a black uniform color in the solvent was maintained as can be seen in Fig. 2(b), 2(c) and 2(d). A darker color suggests that dispersed CNTs are well suspended in the solvent as compared to a lighter color. In another study the same vials were used to test a different method of breaking the CNT agglomerates. This second method consisted of utilizing a probe sonicator for the dispersion of the CNTs in a solvent. The vials were probe sonicated for a total of 2 minutes under a frequency of 40 Hz. This method seemed to provide very high shearing energy in the solvent and lot of heat was also generated in short time. Thus in order to prevent breaking down of CNTs into shorter lengths or introducing defects on the CNTs, the probe sonication time is limited to just 2 minutes. The exact time of probe sonication which will start introducing defects is not studied here. Fig. 3 only shows the results for the best three solvents. It seems that probe sonication reduced the suspension stability of THF and MC. Fig. 3 show that immediately after sonication THF and MC have formed big swollen state. After half an hour, both THF and MC had agglomerated and no black color in the liquid was present as compared to the previous

Fig. 3. Dispersion after probe sonication.

results. Even DMF was affected by probe sonication. Just after half an hour, the CNTs started to agglomerate and in one hour, they almost sedimented. While probe sonication is a faster process to break bigger bundles into smaller ones, it appears that probe sonication also induces the CNTs to agglomerate faster. For this reason the bath sonication was utilized in the processing of the nanocomposites. Ham et al. investigated dispersions of single-walled carbon nanotubes (SWCNTs) in various solvents to correlate the degree of dispersion state to the Hansen solubility parameters as below.

$$(\delta_t)^2=(\delta_d)^2+(\delta_p)^2+(\delta_h)^2$$

Several solvents with different total solubility parameters (δ_t) values were selected. Single-walled carbon nanotubes (1 mg) were added to a solvent (15 g) and sonicated for 20 hours. After sonication, the vials were left in a quiescent state for 480 hours with pictures taken every 24 hours. Their investigation showed that nanotubes were dispersed very well in solvents with certain dispersive component (δ_d). They were sedimented in solvents with high polar component (δ_p) values or hydrogen-bonding component, (δ_h) values. Hansen solubility parameters and the dispersion state of the SWCNTs are listed in Table III. In this particular Table, only those solvents used

in our study are listed to correlate our observations with their findings. The dispersion states of SWCNTs in various solvents was classified as "dispersed," "swollen," and "sedimented." Dispersed means that the liquid maintains a uniform black color without any agglomeration and precipitation during sonication. Swollen means that the SWCNTs aggregated and phase separation is observed during sonication and the aggregation is maintained in a quiescent state. Sedimented means that big particles are scattering in the solvent during sonication and all nanotubes are precipitated within 10 min after sonication. To correlate the dispersion state of the nanotubes to the Hansen solubility parameters, Ham et al. first plotted the dispersion state against the dispersion component δ_d. It was observed that dispersed group solvents distributed in the value range of 17-18 $MPa^{1/2}$ while the swollen group distributed in the value ranges of 15.8-17 or 18-19 $MPa^{1/2}$. When the three Hansen solubility parameters were plotted in a 3-dimensional plot, there seemed to be a certain space where the dispersed group solvents were located. This suggests that δ_d is the most influential in the dispersion of nanotubes, and that dispersion solubility parameter rather than the total solubility parameter can explain the interactions between the nanotubes and the solvents. According to this study, again DMF seemed to be the best solvent for suspending dispersed nanotubes.

2. Effect of Stirring Rate on Nanotube Dispersion

Agglomeration of nanotubes in composite materials can be affected by the stirring rates at which composites are processed. Martin et al. [23] conducted a study in which they varied the stirring rate following the addition of the hardener. Three samples were initially stirred for one minute at 50 rpm to insure good hardener dispersion. After the 1 minute, the stirring rates were varied to 0 rpm, 50 rpm, and 200 rpm. They found that if no stirring was applied the nanotubes remain well dispersed. When

Table III. Hansen dispersion parameters for different solvents

Organic Solvents	δ_d	δ_p	δ_h	δ_t	Dispersion
	$(MPa^{1/2})$	$(MPa^{1/2})$	$(MPa^{1/2})$	$(MPa^{1/2})$	State
N,N-Dimethylformamide	17.4	13.7	11.3	24.8	Dispersed
Tetrahydrofuran	16.8	5.7	8	19.4	Swollen
Toluene	18	1.4	2	18.2	Swollen
Methylene Chloride	18.2	6.3	6.1	20.3	Swollen
N,N-Dimethylacetamide	16.8	11.5	10.2	92.5	Sedimented
Acetone	15.5	10.4	7	20	Sedimented
Ethanol	15.8	8.8	19.4	26.5	Sedimented

the stirring rate was increased to 50 rpm the nanotubes tended to create nanotubes clusters. In another sample stirred at 200 rpm clustering of nanotubes also occurred, but the resulting agglomeration is more homogenous than in sample with 50 rpm stirring. These observations agree well with former results on carbon black particles in the epoxy matrix [14, 16, 90]. Schler et al. showed that the application of shear forces could induce agglomeration of initially well-dispersed carbon black particles, explaining that the shear forces provide the particles with sufficient kinetic energy to overcome the repulsive interactions of the electric double layers. At the same time, agglomerates can be disrupted by high shear forces. Hence, there is likely to be an equilibrium diameter for the nuclei, an interpretation that would match the different nanotube aggregate sizes that was observed for the samples prepared with 200 and 50 rpm stirring rates.

In this study, processing the nanocomposites with the different hardeners required very distinct techniques. The only common ground between the different processing techniques was the stirring rate for solvent evaporation which was set at

400 rpm. This stirring rate was selected to ensure that enough shear forces were present to prevent CNT agglomeration. This high stirring rate also ensures that the CNTs were well homogenized into the resin. In both the pre-cure and high temperature curing processes, during the degassing of the resin/hardener the stirring rate was reduced to 200 rpm due to the viscosity of the mixture. When a higher stirring rate was utilized the magnetic stirrer was not strong enough to overcome the shear forces and as a result stopped. This is not desired because we needed the hardener to be homogenously mixed with the resin. A lower stirring rate ($\leq$ 200 rpm) was not applied because we wanted to have the highest stirring rate to ensure that no CNT agglomeration occurred during degassing. In the case of using the 9553 hardener, the stirring rate during degassing of the hardener was lowered to 130 rpm because of the viscosity too. The room temperature starts gelation process in short time. This was the highest stirring rate that could be achieved to ensure that no agglomeration occurred when using 9553. The choice of stirring rate depends on the type of nanotubes used and also on the type of the curing agent used.

3. Effect of Curing Temperature on Nanotube Dispersion

The temperature at which the hardener is added can influence the dispersion of nanocomposites. It is interesting to note that the agglomeration process at higher temperatures leads to finer and more evenly distributed nanotube clusters, consistent with a lower barrier to aggregation and a higher cluster nucleation rate. These observations clearly indicate that the agglomeration process of nanotubes is temperature-dependent. To some extent, this effect can be attributed to changes in viscosity. Since the nanotube agglomeration is controlled and the diffusion coefficient is inversely proportional to viscosity, it becomes clear that the agglomeration process is accelerated for high temperatures. However, since the difference in viscosity is rel-

atively small for the two higher temperatures, it is likely that the increased kinetic energy of the particles at higher temperatures also helps to surmount the remaining potential barrier.

It was observed that the curing temperature of the nanocomposites had the greatest effect on the dispersion of CNTs. It was observed that when the mixture was poured into the mold it was viscous, but as the temperature increased during the high temperature curing the viscosity was greatly reduced. Due to the inherent van der Waals forces present between CNTs, the reduced viscosity meant that the barrier between CNTs was reduced and hence led to agglomeration in the nanocomposite. The idea behind the pre-cure process is that the CNTs will be locked into the resin which would prevent agglomeration. However, once the temperature increased to 121 ^{o}C, the viscosity was greatly reduced and again led to agglomeration of the CNTs. To verify that the temperature was a parameter affecting dispersion, a study was conducted in which a hardener at room temperature could cure. This would show that if the CNTs still agglomerated than the temperature was not the reason. Because the degassing and curing of the nanocomposites were done at room temperature the viscosity did not change immediately and hence CNT agglomeration did not occur as severely as in the high temperature curing. This is because the viscosity is not reduced and hence does not allow the CNTs to agglomerate. The reason being the van der Waals forces between the CNTs are not strong enough to overcome the resistance of the resin/hardener. Several samples were prepared and cured at room temperate followed by a post cure which consisted of 1 hour at 100 ^{o}C followed by an additional hour at 160 ^{o}C. In the resulting samples dispersion of the nanotubes was good and no agglomeration was visible.

All samples in this study contained 0.03 wt% XD carbon nanotubes. In one study a sample was cured at the manufacturers' recommended curing cycle which is to 2

hour at 121 ^{o}C followed by 2 hours at 177 ^{o}C. Due to the high pre-curing temperature the viscosity was greatly reduced and agglomeration of the nanotubes occurred. In another study twenty percent of the stoichiometric hardener ratio was added and stirred at 400 rpm and 120 ^{o}C to form cross-linking, as this allows the mixture to remain viscous. After pre-curing the mixture for three hours, the remaining hardener was added and followed by a slow cure process. The slow cure process consisted of curing the sample at 40 ^{o}C for 8 hours followed by the manufacturers' recommended curing cycle. The objective behind the low temperature cure is to allow enough cross-linking to form to prevent a reduction in viscosity at the elevated temperatures. Some agglomeration were still visible but not in the degree of the regular curing cycle. It seems from observations that the key parameter controlling the degree of agglomeration of the nanotubes is the viscosity of the epoxy/hardener mixture.

4. Nanocomposite Processing Method

Based on the study of the above parameters, an optimum processing method was developed as described below. Initially, the nanocomposites samples for the high temperature curing were created by first dissolving 10 mg of XD grade CNTs in 20 ml DMF. The DMF/CNT solution was then bath sonicated for 1 h to separate large CNT agglomerates into smaller ones, which leads to better CNT dispersion. After sonication, the DMF/CNT solution was added to a flask containing 26 g of EPON 862 resin. To evaporate the solvent, the flask was placed on a hot plate at a temperature of 80 ^{o}C and stirred with a magnetic bar at 400 rpm. A vacuum was applied to evaporate the solvent faster. Once the solvent had evaporated, the temperature on the hot plate was reduced to 60 ^{o}C and allowed to cool to the new temperature. The stirring rate was left unchanged and no vacuum was applied. After the temperature equilibrated to 60 ^{o}C, the required amount of EPIKURE Curing Agent W was added

(100:26.4 is the recommended resin to hardener ratio) and the stirring reduced to 200 rpm. A vacuum was applied to effectively degas the mixture. After all the bubbles were removed, the mixture was put into an aluminum cast mold, which was preheated to 60 ^{o}C, and cured by the following process: 2 h at 122 ^{o}C followed by 2 h at 177 ^{o}C.

The fabrication process for the pre-cured sample was very similar to the high temperature curing. The same amount of nanotubes was dissolved in DMF, and bath sonicated for 1 h. After sonication, the DMF/CNTs were added to 26 g of EPON 862 resin and stirred at 400 rpm. The temperature on the hotplate was set at 60 ^{o}C, and a vacuum was applied to evaporate the solvent. After the solvent was evaporated, the temperature was raised to 100 ^{o}C. The mixture was allowed to equilibrate at the new temperature for 15 min. Following the 15 min, 20% of the required EPIKURE Curing Agent W amount was added to the CNT/resin mixture while stirring at 400 rpm with a magnetic stirrer but no vacuum was applied. The pre-curing process was carried out for 3 h and 20 min at 185 ^{o}C. Once the pre-curing was obtained, the temperature on the hotplate was turned off and the mixture was allowed to cool for 30 min while stirring at 400 rpm. After the 30 min, the remaining 80% of the hardener was added to the mixture. The temperature was once again set to 100 ^{o}C and a vacuum was applied to degas the mixture for 30 min. After the 30 min, the temperature was turned off and the stirring rate reduced to 200 rpm. The mixture was allowed to degas for an additional 15 min. After degassing, the mixture was pour into an aluminum cast mold which had been pre-heated to a temperature of 40 ^{o}C. The curing cycle for this pre-cure sample is the following: 40 C for 8 h, followed by 2 h at 122 ^{o}C and another 2 h at 177 ^{o}C.

The nanocomposites fabricated with curing agent 9553 were processed in the following ways. XD grade CNTs wee dissolved into 20 ml of MC and bath sonicated

for 1 h. After sonication, the MC/CNT solution was added to a flask containing 26 g of epoxy, and stirred at an initial rate of 60 rpm. Once all the MC/CNT solution was added the stirring rate was increased to 400 rpm. To evaporate the solvent a vacuum was applied and the temperature on the hot plate was set at 50 ^{o}C. After the solvent had evaporated, the CNT/resin mixture was then allowed to cool to room temperature, while stirring but no vacuum applied, before the addition of the hardener. The rpm was reduced to 130 rpm. After all the bubbles were removed from the mixture, it was added to an aluminum cast mold and allowed to cure at room temperature for about 15 h. These samples were then post-cured at 100 ^{o}C for 1h followed by another hour at 160 ^{o}C.

B. Effect of Functionalization and Weight Fraction of SWCNTs on Mechanical Properties

Experiments in fabricating and testing of composites showed improvements in mechanical properties like modulus, strength and toughness [4–7]. The use of high shear mixing, ultrasonication, surfactants, chemical modification and polymer chain wrapping have been some of the research efforts towards accomplishing better SWCNTs reinforcement. But the difficulties in dispersion of SWCNT bundles and processing challenges have resulted in only moderate improvements in mechanical properties [4, 6]. Significant work has been targeted in improving the dispersion of SWCNTs in polymer matrices through functionalization [4, 5, 8], but the deformation behavior of such composites at micro and nanoscale remain poorly understood. This study will help us understand SWCNTs dispersion, interfacial bonding and load transferring mechanisms and consequently enable the optimization of processing parameters. The results from the present work can be useful in validating results from modeling efforts.

1. Experimental Procedure

a. Materials

Carbon Nanotechnology Inc. provided the HiPCO processed single wall carbon nanotubes in pristine form. The supplied material consisted of micron scale aggregates (individual SWCNT diameter 1-1.4 nm). The Young's modulus is 1.4 TPa and expected elongation to failure is 20-30% [4]. The epoxy resin was diglycidyl ether of bisphenol-A (DGEBA epoxy) EPON 862, and was obtained from Resolution Performance Products along with aromatic diamine curing agent EPICURE W.

b. Nanotube Functionalization

Hydrogen bonding and condensation reactions occur between hydroxylated nanotubes and trialkoxy silanes as shown in Fig. 4 (where Y represents organofunctional groups). Fig. 5 presents the infrared spectra of the fluoronanotubes (F-SWNTs), hydroxylated nanotubes (SWNTs-R-OH), and silane treated nanotubes using methacryloxypropyltrimethoxysilane of the functional groups attached to nanotubes. After hydroxylation of the fluoronanotubes, a broad band in the 3000-3500 cm^{-1} indicates the presence of OH groups terminating the functionalities attached to nanotubes. A new band at 1095 cm^{-1} can be assigned to the C-O stretching vibration. The hydroxyl groups provide opportunities for hydrogen bonding and possible covalent linkage with the silanes. The alkoxy groups of the silanes are very easily hydrolyzed by water to form silanol group containing species. Condensation to form oligomers occurs first. The unreacted OH groups can also form hydrogen bonds with the other OH groups on the nanotube. During post-curing, a covalent linkage can be formed on the nanotubes. The strong peaks at 1713 cm^{-1} and 1636 cm^{-1} characterize the corresponding C=O and C=C stretches in the methacryl groups, which are compatible with the vinyl

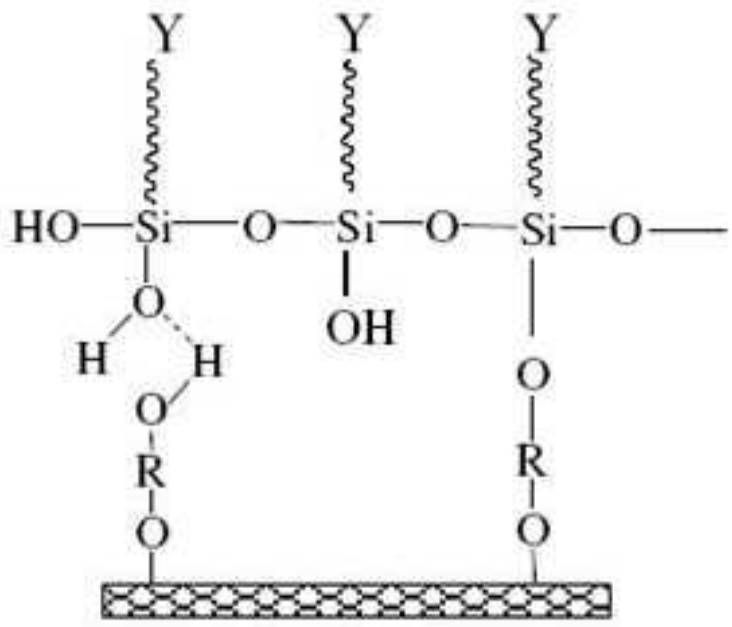

Fig. 4. Silane reaction with the carbon nanotubes.

ester. A sharp decrease of the OH band indicates that the reaction between silanol itself or potential bonding to hydroxyl groups on the nanotubes took place. The appearance of doublet peaks at 1105 cm^{-1} and 1010 cm^{-1} is clearly due to the Si-O-Si and Si-O-C asymmetric stretches respectively. The same treatment was applied to pristine nanotubes, and none of the silane features were observed from the IR spectrum. Glycidoxypropyl-trimethoxysilane was also used to treat nanotubes for epoxy. EDX element analysis gave evidence for the presence of silicon (3.5wt%) and oxygen (12 wt%) in the functionalized nanotubes. Silane-treated SWNTs exhibit significantly improved solubility and dispersion in some organic solvents including alcohol, acetone, DMF etc. SEM showed the smaller nanotube bundle sizes after the silane treatment in comparison with the pristine nanotubes, as shown in Fig. 9. This result suggests that the functional groups help to exfoliate large nanotube ropes into

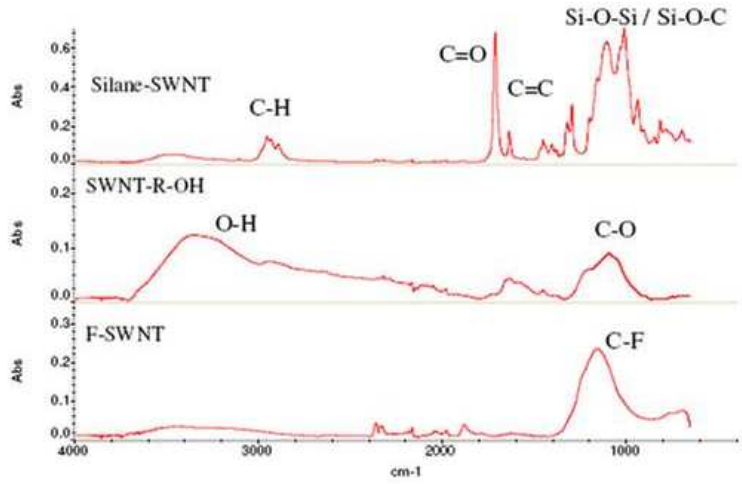

Fig. 5. FTIR spectra of silane functionalized nanotubes.

smaller bundles. Debundling of nanotube ropes allows better dispersion and more surface interaction with polymer matrix.

c. Nanocomposite Preparation

First, the nanotubes were dispersed in a solvent (chloroform) for one hour in an ultrasonicator bath (50 kHz). Epoxy resin was then added to nanotube-solvent solution and stirred on a warm plate (at about 60 ^{o}C) until most of the solvent had evaporated. Then the mixture was placed in a vacuum chamber for complete solvent removal. EPICURE W curing agent was added to the solvent free epoxy-nanotube mixture at a proportion of 100:26.4 by weight. Further mixing was performed manually followed by magnetic stirring. The mixture was allowed to degas and then cast into a custom made mold plate. A two step curing procedure was used with initial temperature set at 100 ^{o}C for 2 hours followed by 175 ^{o}C for another 2 hours in an oven. The samples were left overnight in the oven for post curing with gradual

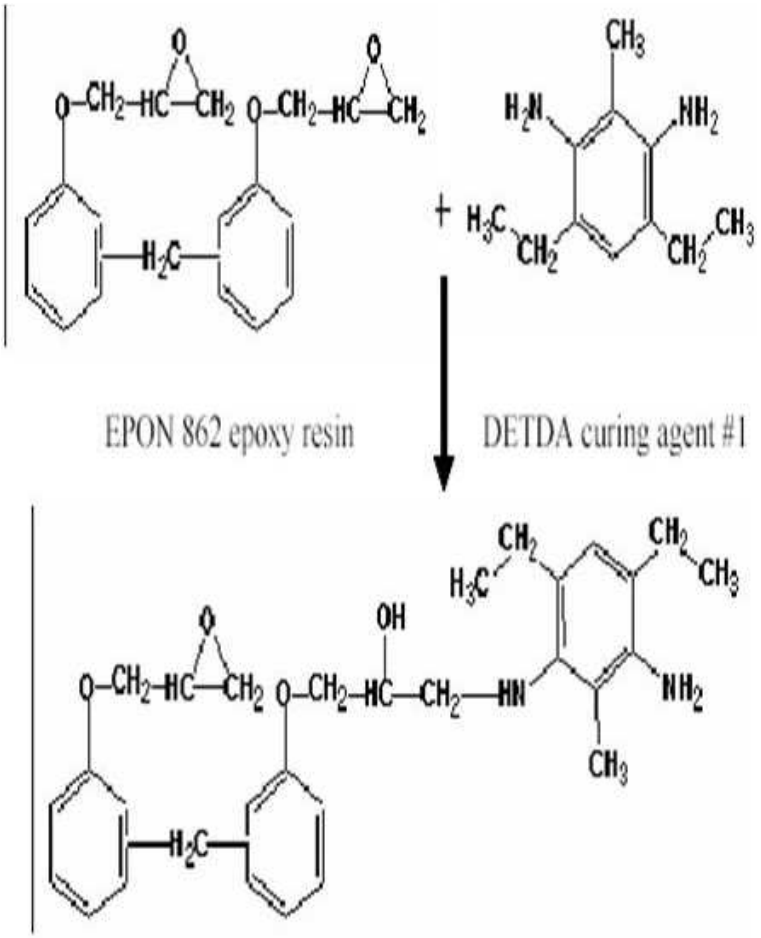

Fig. 1. Reaction of an epoxide group with a curing agent molecule.

Fig. 6. Curing reaction of epoxy EPON 862 with DETDA curing agent W.

decrease of temperature. A Band saw machine was used to cut the plate followed by grinding the sides for sizing the samples as per ASTM standards. Six different sample plates were processed following the above procedure and that consists of neat epoxy, epoxy with 0.5 and 1% pristine SWCNTs, epoxy with 0.5 and 1% of fluorinated SWCNTs and epoxy with 1% Silane functionalized SWCNTs.

d. Characterization Methods

Three point bending test was performed using custom made fixture as shown in Fig. 7(a). The Nanoindentation technique has been proven to be useful for the evaluation of deformation behavior at the nano and micro scale [7, 8, 9, 10]. Nanoindentation was performed using a Hysitron Triboscope to get the elastic modulus as shown in Fig. 8. Indents were made by a diamond Berkovich tip with nominal radius of curvature ¡ 30 nm. Dynamic mechanical analysis was carried out by TA Instruments DMA 2980 using multi-frequency 3 point bend module as shown in Fig. 7(b). The experiments were performed to obtain storage and loss modulus as well as tan δ curves at constant frequency of 1 Hz with constant temperature ramp rate from room temperature to above the glass transition temperature. The SWCNT dispersion was observed using Zeiss 1530 FE-Scanning Electron Microscope operated at an accelerating voltage of 30 kV. Fracture surfaces of the epoxy-nanotube composite specimens were observed with a Leica MEF4M metallograph equipped with a high resolution camera.

2. Results and Discussion

The Fig. 6 shows the curing reaction of epoxy EPON 862 with DETDA curing agent W [3]. The Fig. 9 and Fig. 10 shows the pristine and Silane functionalized SWCNTs providing evidence of the effective dispersion before reinforcing in epoxy matrix.

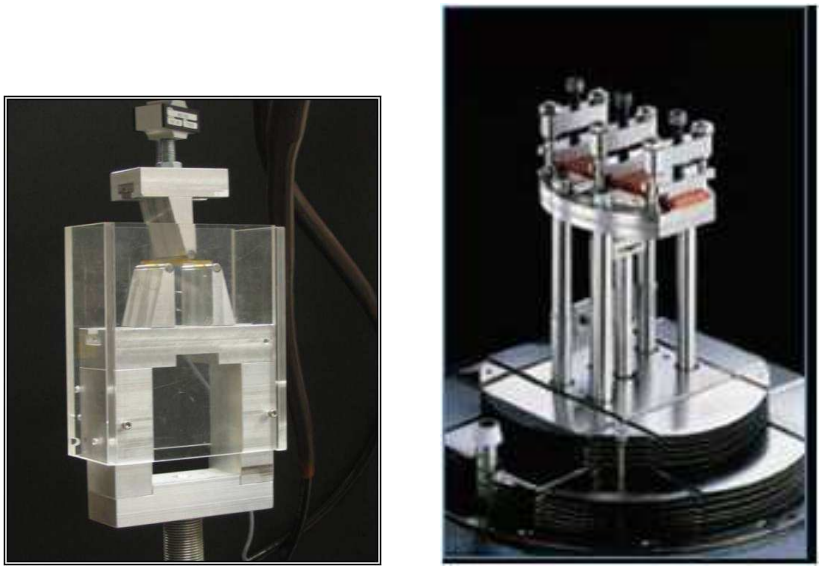

(a) (b)

Fig. 7. Three point bending and DMA set-up for nanocomposite testing. 7(a) Custom made 3PB fixture. 7(b) DMA fixture at NASA LaRC.

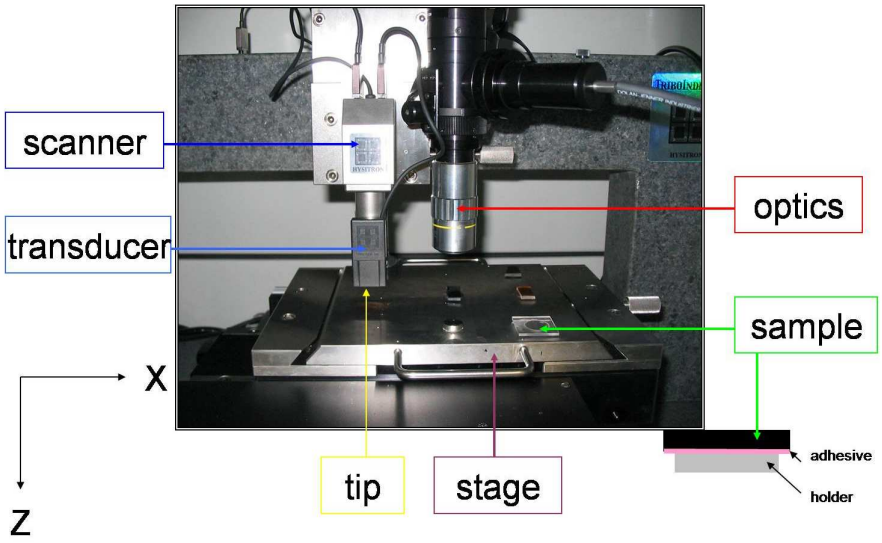

Fig. 8. Set-up for nanoidentation experiment using Hysitron Nanoindentor.

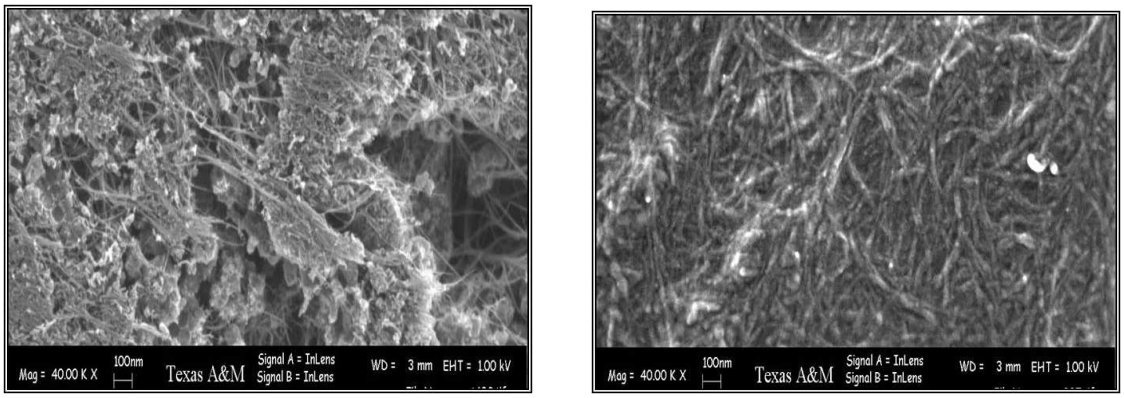

(a) (b)

Fig. 9. SEM micrographs of SWCNTs before reinforcing in epoxy matrix. 9(a) Pristine SWCNTs. 9(b) Silane functionalized SWCNTs.

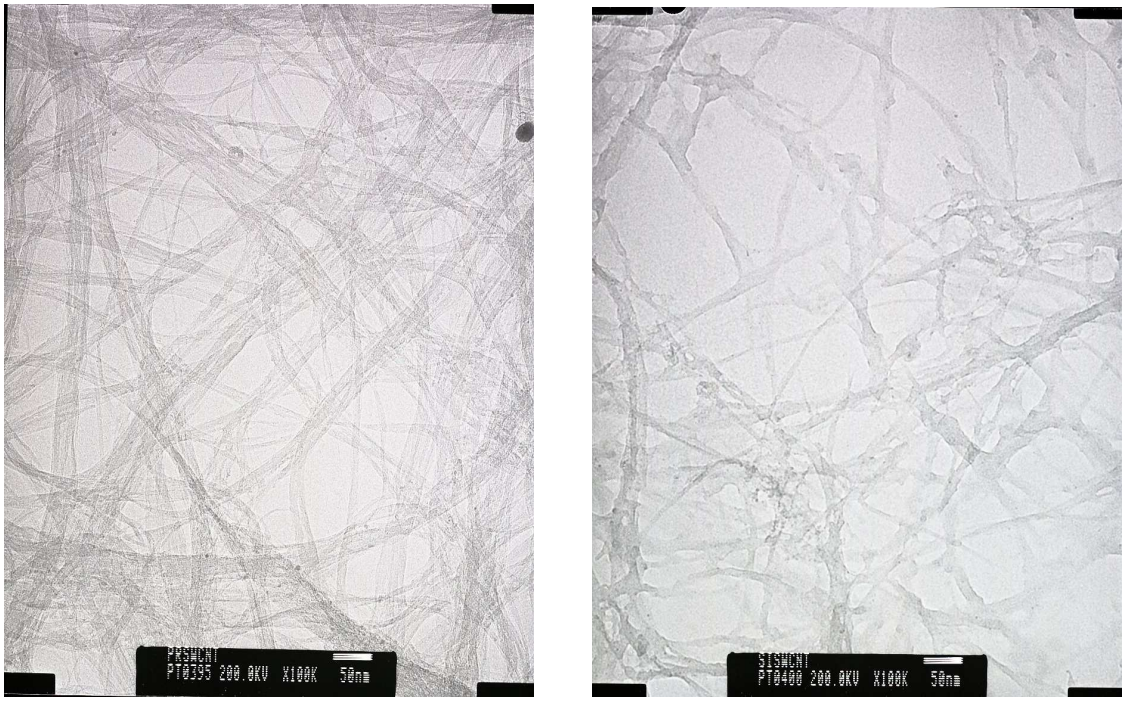

(a) (b)

Fig. 10. TEM micrographs of SWCNTs before reinforcing in epoxy matrix. 10(a) Pristine SWCNTs. 10(b) Silane functionalized SWCNTs.

a. Mechanical Characterization

The nanoindentation experiments were performed on all six specimens at a constant loading rate of 50 μN/s with loads increasing from 1000 μN to 5000 μN in steps of 1000 μN. The peak load holding of 5 sec was introduced to avoid the creep influence on the unloading curve which is used to obtain the elastic modulus of a material. The elastic modulus is obtained by fitting the unloading curve to a power law relation [91, 92]. The slope of the initial part of the unloading curve gives the stiffness, $S = dP/dh$. The elastic modulus is obtained from its relationship to measured unloading stiffness and projected contact area via the relation

$$S = 2\beta((\frac{A}{\Pi})^{1/2})E_r \tag{3.1}$$

where β is a constant depending on tip geometry (β=1.034 for Berkovich indenter) [10] and E_r is the reduced modulus which accounts for the fact the measured displacement includes contribution from both the specimen and the indenter. E_r is given as

$$\frac{1}{E_r} = [\frac{1-\nu^2}{E}]_{specimen} + [\frac{1-\nu^2}{E}]_{indenter} \tag{3.2}$$

Though it includes the contribution from the indenter, the reduced modulus truly represents the material property of specimen as the indenter modulus (diamond E_i=1141 GPa) being very high, has little effect on sample modulus (3 Gpa) [10]. The Nanoindentation results in Fig. 11 shows that the elastic modulus of epoxy increases by adding nanotubes. It can be seen that Silane functionalized samples have a lower elastic modulus as compared to pristine and fluorinated SWCNT-epoxy samples. The same trend is apparent from the results of DMA tests in Fig. 12. The lower increase for silane functionalization could be due to degradation of SWCNT surface during functionalization. Another reason could be that the presence of functional groups

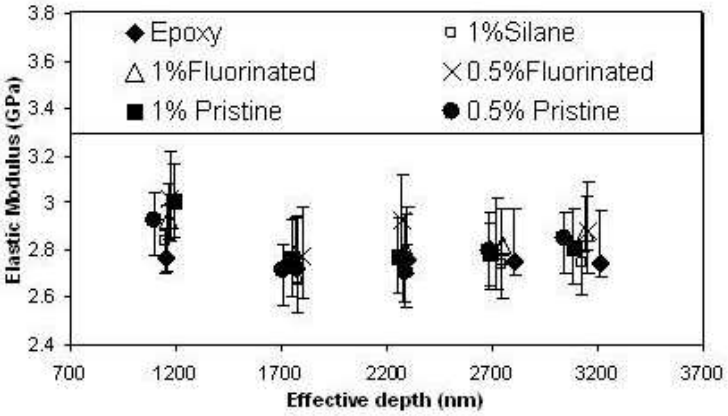

Fig. 11. Elastic modulus (GPa) measured by Nanoindentation.

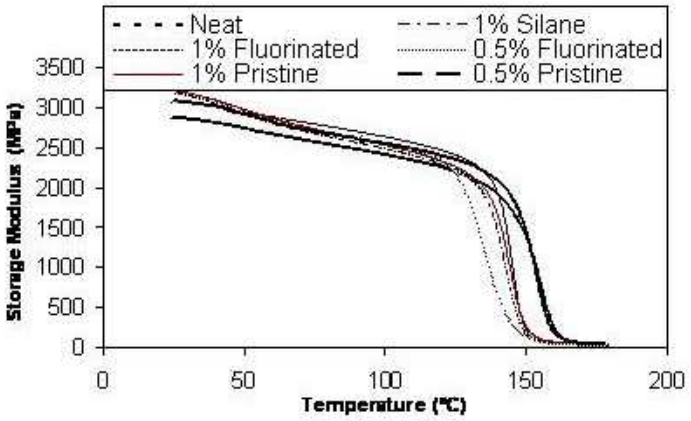

Fig. 12. Storage modulus (MPa) measured by DMA.

Table IV. Comparison of trends from DMA and Nanoindentation tests

Material	Storage Modulus DMA (GPa)	Elastic Modulus Nanoindentation (GPa)	Glass Transition DMA (C)
Neat Epoxy	2.865	2.74	162
1% Silane	2.900	2.74	150
1%Fluorinated	3.170	2.84	152
0.5% Fluorinated	3.055	2.88	143
1%Pristine	3.197	2.83	153
0.5% Pristine	3.018	2.80	160

decreases the cross link density. The Table IV gives a comparison of Nanoindentation and DMA results. We have also observed a decrease in glass transition temperatures (defined as temperature at which maximum tan δ is reached) as a result of functionalization as well as increasing weight fraction of SWCNTs. This behavior could be explained as a result of better heat distribution throughout the sample due to the presence of nanotubes allowing faster transition from glassy to rubbery state. Another possible reason is that the dispersed SWCNTs inhibits curing by its presence and thus reduce the crosslink density allowing easier molecular chain motion which results in lower glass transition temperature.

b. Fracture Mechanisms

Fig.13 shows the images of the fracture surfaces of different composites. The image analysis suggests the possibility of an increase in toughness as a result of adding SWCNTs. Though this would be just qualitative perception based on the observation of fracture growth mechanisms and quantitative data would be required from mechani-

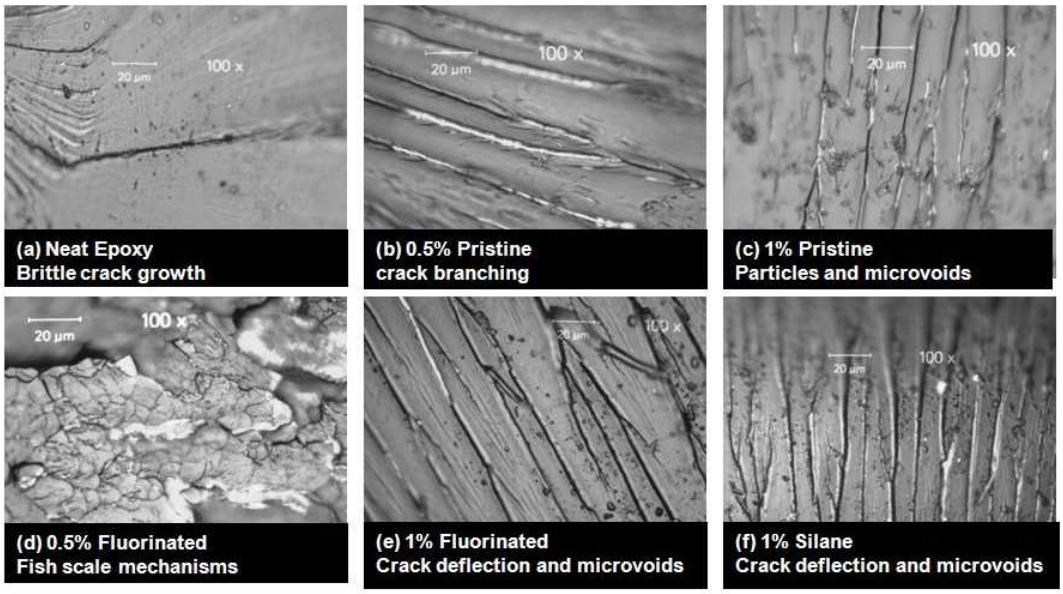

Fig. 13. Optical microscopy images of nanocomposite fracture surfaces.

cal fracture toughness tests to confirm the observation. Some of the interpretation of the mechanisms from images have been taken from the 'Polymer Toughening' book by Charles Arends and using chapter by Hung-Jue Sue [93]. Transmission electron microscopy was performed on some of the above nanocomposite specimens to investigate the plausible mechanisms of toughening process. Such TEM micrographs are shown in following figures. The presence of the functional group on the CNT is supposed to enhance the CNT-epoxy matrix interface. High resolution TEM images as shown in Fig. 14 indicates the possibility of creating such enhanced interfaces. Presence of bridging mechanism is shown in Fig. 15. Bridging is one of the mechanisms of energy dissipation caused by the nanotube-matrix debonding during bridging. Fracture of the bridging nanotubes can also contribute to the energy dissipation. One of the toughening mechanisms i.e. fragmentation of nanotubes is represented in following Fig. 16. This image shows the ability of the nanotubes to fracture inside the epoxy

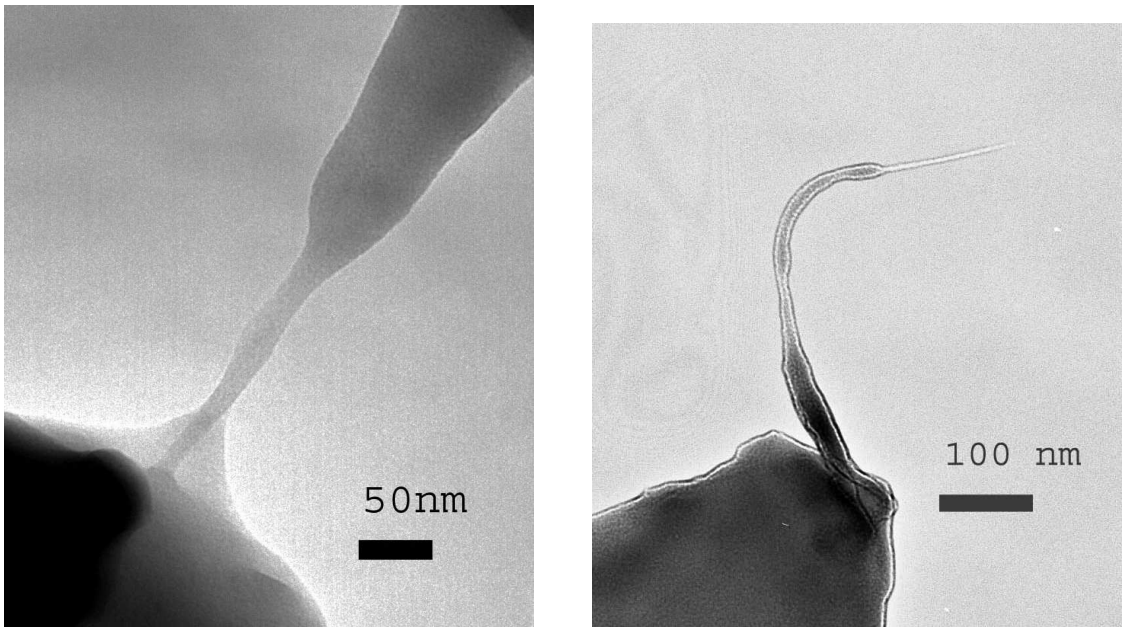

(a) (b)

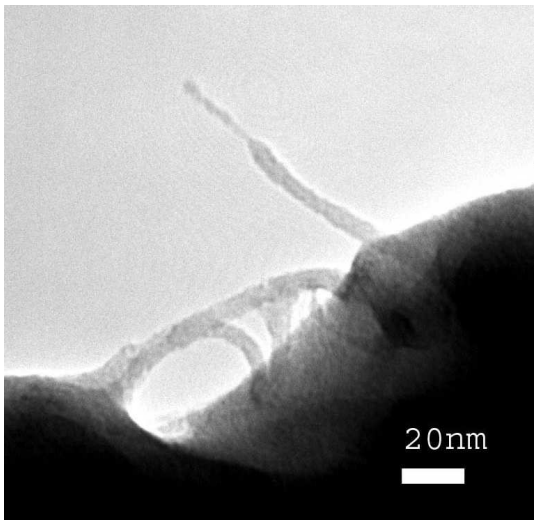

(c)

Fig. 14. TEM micrographs showing nanotubes pulled out of the matrix. 14(a) Matrix pulled out with the nanotube rope indicates good CNT-epoxy matrix bonding. 14(b) Matrix sticking to nanotube indicates good interface. 14(c) Higher magnification image showing functional group on the CNT.

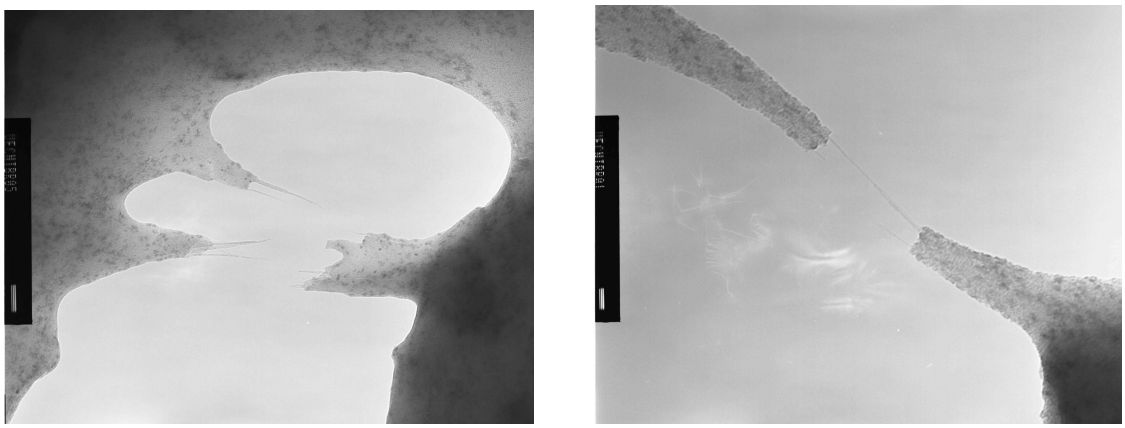

(a) (b)

Fig. 15. TEM micrographs showing bridging SWCNTs in epoxy matrix. 15(a) CNTs bridging between matrix surfaces 15(b) Higher magnification image of single bridging CNT (or rope).

matrix. The fragmentation phenomenon also means that there is a better interface between nanotube and epoxy resulting in good load transfer.

Fig. 17 shows different toughening mechanisms in our various nanocomposite systems. Significant matrix deformation is visible in areas containing nanotubes. Smooth brittle fracture is observed in areas without nanotubes also indicating poor distribution of nanotubes at some places in the nanocomposites. Microcracking and crack branching can be one of the important mechanisms of energy dissipation. The crack pinning mechanisms, although not a big contributor to the overall toughness, can be seen to be additional energy dissipation mechanism. The observation of these mechanisms indicate a strong possibility of toughening the current matrix material. However, fracture toughness experiments on nanocomposites have not be undertaken in this work, but literature on nanocomposite fracture toughness (Appendix A) has shown an improvement in fracture toughness by addition of pristine or functionalized single as well as multiwall nanocomposites. There is very limited work on the fracture

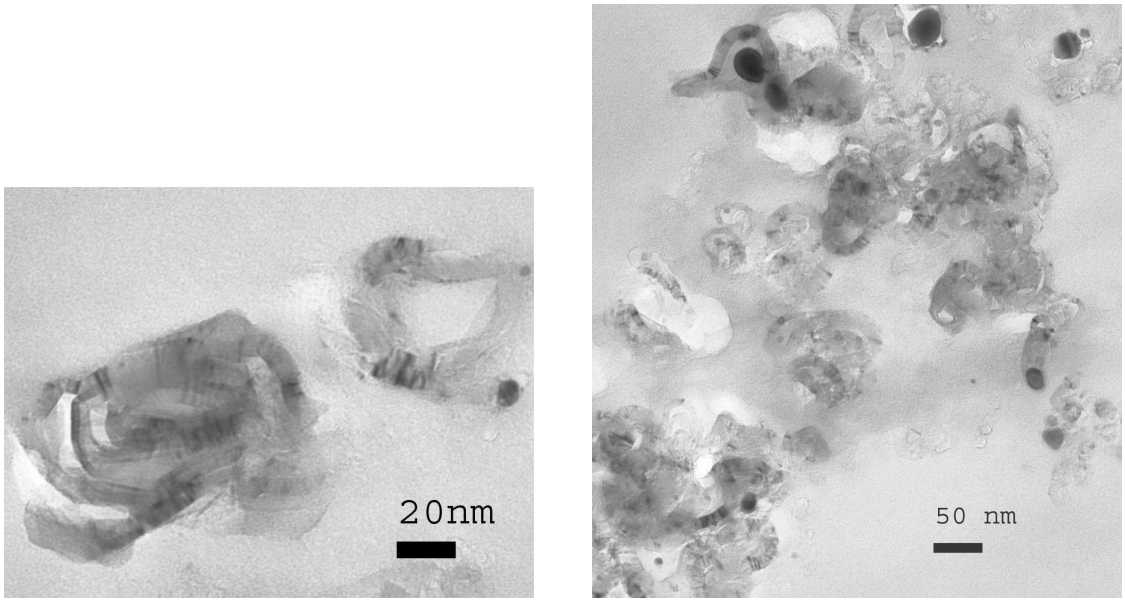

(a) (b)

Fig. 16. TEM micrographs showing fragmentation of SWCNTs in epoxy matrix. 16(a) Fragmentation represented by black rings on CNTs. 16(b) Curled CNTs around metallic impurity particle.

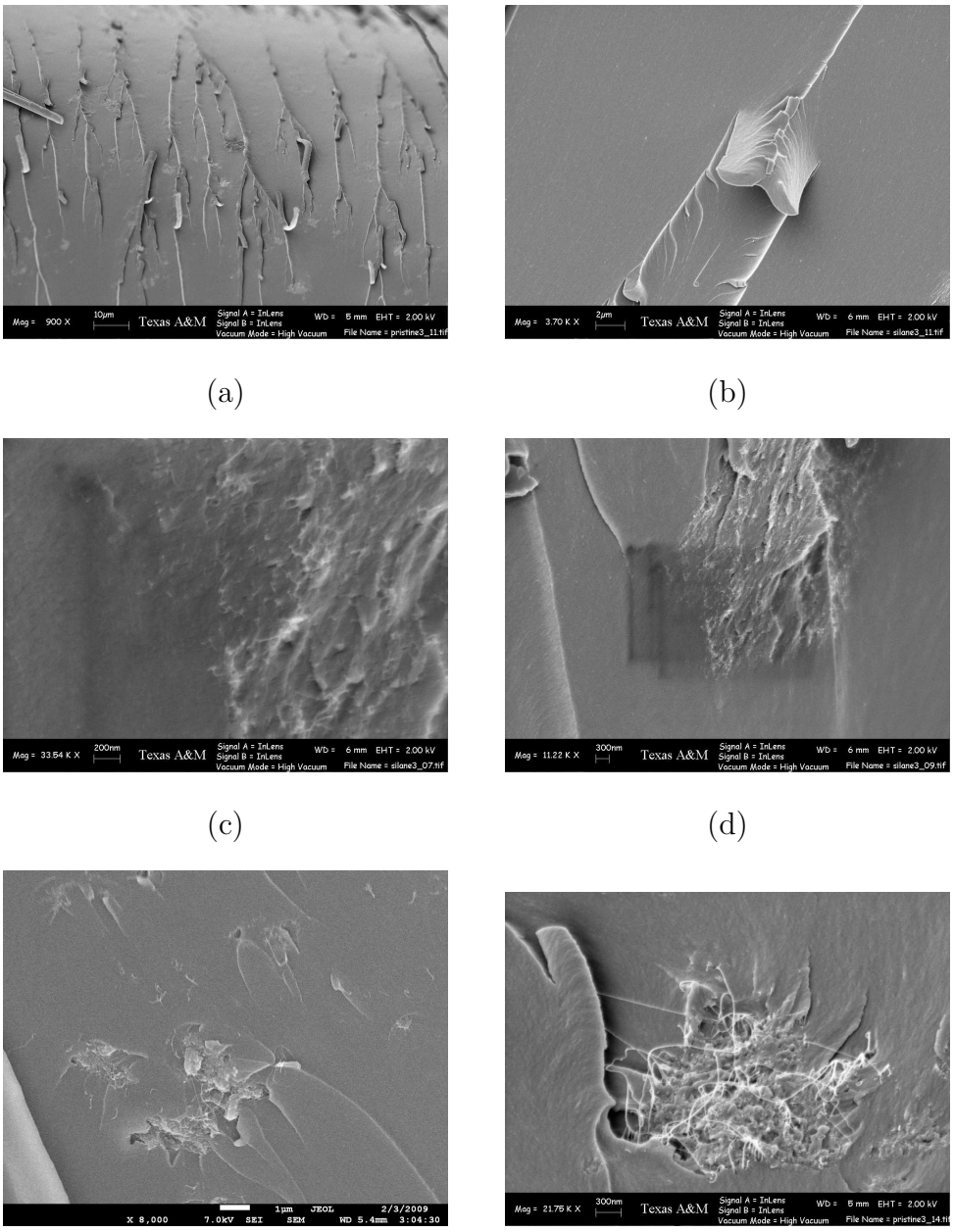

Fig. 17. Toughening mechanisms in nanocomposites. 17(a) Microcracking, crack branching and matrix peel-off mechanisms, 17(b) Matrix peel-off mechanism, 17(c) Matrix deformation mechanism introduced in the region with nanotubes (left side without nanotubes is smooth), 17(d) Nanotube rich region showing microflakes and deformation surrounded smooth regions of brittle fracture , 17(e) Crack pinning mechanisms due to entangled nanotube ropes, 17(f) Significant matrix deformation in the regions of nanotubes.

toughness of laminated composites modified using carbon nanotubes. It would be interesting to investigate the effect of nanotubes on the fracture toughness of composite laminates which are widely used in commercial applications. Such study would also help us to find if nanocomposite properties can be scaled up to contribute to the laminate scale toughness. Detailed investigation in this direction has been discussed in the next two chapters.

C. Effect of Weight Fraction of SWCNT and XDCNT on Electrical Conductivity

There is a growing demand for low cost materials in the microelectronic devices industry [94] and as a result there is significant research going on in the polymer based nanocomposites for a wide range of properties such as electrical, thermal, mechanical and magnetic properties [9–14]. The conducting polymer composites are made by the addition of conductive fillers into an insulating polymer matrix. Introduction of fillers such as carbon black and iron powder has long been pursued by researchers to modify the electrical properties of the polymers [16, 95]. However, such fillers tend to degrade the modulus, the strength and the glass transition temperature of the nanocomposites. One of the promising filler material is considered to be the carbon nanotubes since they provide good thermal and electrical properties at low loadings compared to carbon black or other metallic reinforcements[18, 19].

The effect of the aspect ratio, the aggregate size and the dispersion process as a result of functionalization has been reported to affect the percolation limits of nanocomposites [18–21, 23, 30–37, 42]. The chemical modification of the nanotube surface through covalent functionalization results in reduction of the aspect ratio along with the formation of sp^3 carbons on nanotube surface, which decreases the electrical conductivity of the nanotubes [8, 18, 22]. Therefore, as-received nanotubes have been

used in this research without any functionalization, as this work is focused on the electrical properties. As seen from the literature, the electrical conductivity has been significantly improved by addition of nanotubes and very low electrical percolation limits have been reported for nanocomposites with single walled and multi-walled nanotubes[10, 39–41, 43, 45, 46]. However, the cost comparison with cheaper reinforcement particulates does not proportionately favor the use of nanotubes.

The XD-CNT ($50 per gram) produced by a high yield process is much cheaper than SW-CNT ($350 to $1000 per gram); however, the difference in mechanical and electrical properties of nanocomposites consisting of these nanofillers is not known. Thus, the purpose of this section is to examine the electrical and the mechanical properties of XD-CNT and SW-CNT filled epoxy matrix nanocomposites. Section below describes the materials used, the nanocomposites preparation and the details of the characterization methods. Results from electrical conductivity measurements and mechanical tests along with transmission optical microscopy and scanning electron microscopy for studying dispersion are presented in following sections and the results are discussed in details giving some plausible explanations for observed percolation thresholds in different nanocomposites.

1. Experimental Procedure

a. Materials

Conductive grade XD-CNTs and HiPCO processed SW-CNTs were obtained from Carbon Nanotechnology Inc. (now Unidym), Houston, Texas [96] and Rice University. The XD-CNTs consisted of a mixture of single walled, double walled and multi-walled nanotubes along with carbon black and metallic impurities [96, 97], as shown in the transmission electron microscopy (TEM) image of typical XD-CNTs in Fig. 18. The

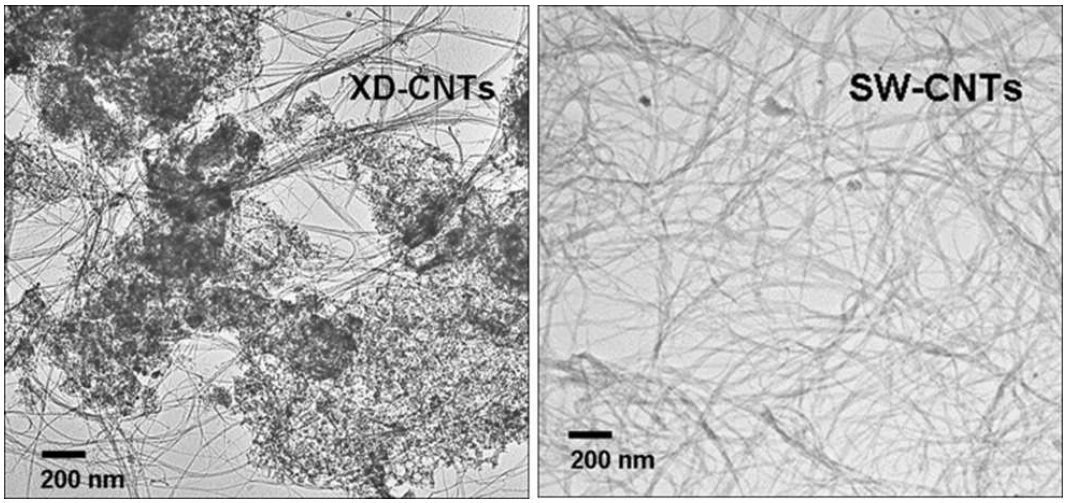

Fig. 18. TEM of XD-CNTs and SW-CNTs.

SW-CNTs consists of bundles of nanotubes (individual SW-CNT diameter 1-1.4 nm [96]). The epoxy resin used was EPON 862 along with aromatic diamine curing agent Epicure W, purchased from Resolution Performance Products.

b. Nanocomposite Preparation

The nanocomposite samples were prepared using a cast molding method. Three weight percents (0.015 wt%, 0.0225 wt% and 0.03 wt%) of SW- and XD-CNTs were used to make nanocomposites, labeled hereafter as the epoxy/SW and the epoxy/XD nanocomposites respectively. The nanotubes were dispersed in a mixture of solvents (ethanol-20 ml and toluene-15 ml) for one hour in an ultrasonicator bath (50 kHz). Epoxy resin was then added to nanotube-solvent solution and subjected to magnetic stirring on a hot plate (at about 60^{o}C), until most of the solvent had evaporated. The time required for solvent evaporation was about 30 minutes under full vacuum. Epicure W curing agent was added to the solvent free epoxy-nanotube mixture at a proportion of 100:26.4 by weight. Further mixing was performed manually, followed by magnetic stirring. The mixture was degassed for removing air bubbles until the

solution stops showing any bubbles and this process required variable time based on viscosity of solution. Degassing was followed by casting into a custom-made mold, made out of aluminum.

A two step curing procedure was used with initial temperature set at 121^{o}C for 2 hours, followed by 175^{o}C for another 2 hours. The samples were left in the oven for a few hours after the curing cycle for post curing with gradual decrease of temperature. A control epoxy specimen was processed using the same method and solvent was added to the neat resin without any CNT to investigate the effect of addition and evaporation of the solvent on the electrical conductivity, storage modulus and glass transition temperature of the control epoxy panel. Specimens were cut from the different sections of each nanocomposite panel. Rectangular specimens (30 mm x 8 mm x 2 mm) were cut for the dynamic mechanical testing, and square specimens (20 mm x 20 mm) were cut for the electrical conductivity measurements. The top and the bottom faces were polished with 600 SiC paper and a thin layer (100 nm) of silver was deposited by metal evaporation on each face to be used as electrodes. Transmission optical microscopy was performed on the square specimens used for electrical measurements, prior to the silver electrode deposition. Scanning electron microscopy was performed on fracture surfaces, which were obtained by cracking cooled specimens using nitrogen gas.

c. Characterization Methods

Electrical conductivity (AC) measurements were performed using Novo-Control Broad-band Dielectric spectrometer at room temperature with voltage amplitude of 1.0 V over a frequency range from 0.01 Hz to 10 MHz. Dynamic Mechanical Analyser (RSA-3, TA Instruments) with a three-point bend module was used to measure the storage and the loss modulus at a constant frequency of 1 Hz. The temperature was

ramped up to 200 ^{o}C from the room temperature, at a constant temperature ramp rate of 2 ^{o}C/min. A ratio of the storage and the loss modulus, given as tan δ, provided information on the glass transition temperature. For both types of characterization (electrical conductivity and mechanical), at least three samples were tested for each nanocomposite and an average is reported along with standard deviation. Transmission optical microscopy (TOM) was performed using the Nikon Stereo Photomicroscope and Scanning electron microscopy (SEM) was performed using the JSM-7500F cold emission microscope to characterize the microstructure of the nanocomposites, in order to elucidate the relationship between the resulting properties and the types and loading levels of the CNTs.

2. Results

a. Electrical Conductivity

An electrically non-conductive polymer matrix can be made conductive by the formation of conductive pathways of filler particles, when the filler content exceeds a critical volume fraction, known as the percolation threshold. The percolation threshold is characterized by a sharp rise in the electrical conductivity as a function of the volume fraction (or weight fraction) of the filler particle content for low frequencies which is identified from frequency independent response of electrical conductivity using AC measurements.

The electrical conductivity measurement as a function of frequency has been shown in Fig. 19 and Fig. 20, for XD- and SW-CNTs respectively. For low CNT loadings (less than 0.0225 wt% for XD-CNTs) the conductivity is frequency dependent, i.e., it increases with increasing frequency similar to that of the neat epoxy and the control epoxy. It should be noted that the control epoxy sample showed

similar frequency dependence to the neat epoxy, indicating that the addition of the solvents during the processing did not affect the epoxy electrical conductivity. In the vicinity and above the percolation threshold (0.0225 wt% for epoxy/XD and 0.015 wt% for epoxy/SW) the conductivity becomes frequency independent. The AC measurements allow measuring electrical conductivity as a function of frequency. The insulating (or non-percolated) specimens show frequency dependent response. As soon as conductive networks form in the non-conducting material, such a transition from non-conductive to conductive material, is represented by frequency independent response. There can be frequency dependent response at higher frequencies for not fully percolated specimens. In relation to the neat and the control epoxy, there was about seven to eight orders of magnitude increase in the conductivity at 0.01 Hz for epoxy/XD- and epoxy/SW-nanocomposites. Above the percolation threshold, the conductivity continues to increase but only marginally, i.e. and about two orders of magnitude for epoxy/XD nanocomposites (0.03 wt%) and about one order of magnitude for epoxy/SW nanocomposites (0.03 wt%). In order to compare the electrical conductivities of epoxy/XD and epoxy/SW nanocomposites as a function of weight fraction of nanotubes, Fig. 21 has been plotted using electrical conductivity data from Fig. 19 and 20 at low frequency of 0.01 Hz. The scatter in data has been plotted in Fig. 21; however, the error bars are overlapped by the size of each data point. The difference in percolation thresholds can be observed in both nanocomposites from the semi-log plots. For epoxy/SW nanocomposites, percolation occurs at a lower weight fraction (0.015 wt%) than that for epoxy/XD nanocomposites (0.0225 wt%) and corresponding frequency independence is confirmed from Fig. 19 and 20. The vertical dotted lines in Fig. 21 points to various weight fractions of XD- and SW-CNTs. Post-percolation increase for epoxy/SW nanocomposites has been observed to be from about 1E-7 S/cm for 0.0225 wt% to about 1E-6 S/cm for 0.03 wt% of SW-

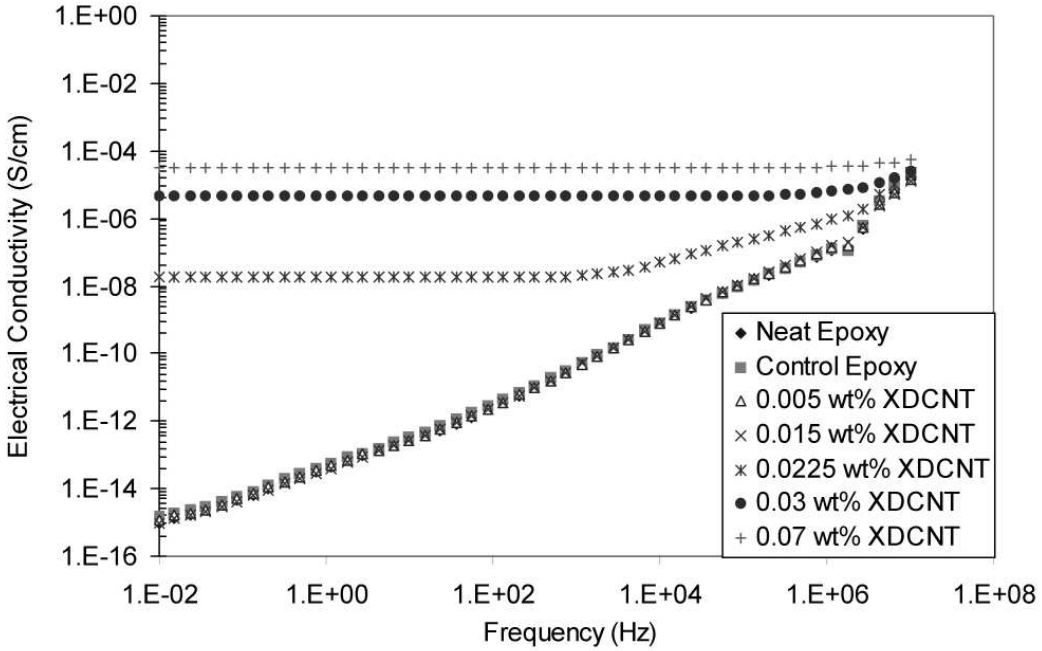

Fig. 19. Log-log plot of electrical conductivity of the epoxy/XD nanocomposites as a function of frequency for various loading weight fractions of XD-CNTs.

CNTs, while for epoxy/XD nanocomposites, from about 1E-7 S/cm for 0.0225 wt% to about 1E-5 S/cm for 0.03 wt% of XD-CNTs. Additional data points corresponding to XD-CNTs weight fraction of 0.07 wt% and 0.15 wt% and 0.07wt% for SW-CNTs have been plotted in Fig. 21 to show that the increase in conductivity becomes smaller after certain weight fraction, as indicated by the plateau in the conductivity curve after percolation. Frequency dependence of conductivity of nanocomposites is sensitive to corresponding microstructure formation of conducting networks and can be related to the percolation state of the nanofillers within the nanocomposite.

b. Microstructure-Conductivity Relationship

Transmission Optical Microscopy

The difference in percolation thresholds and the effects of higher loading of nanotubes

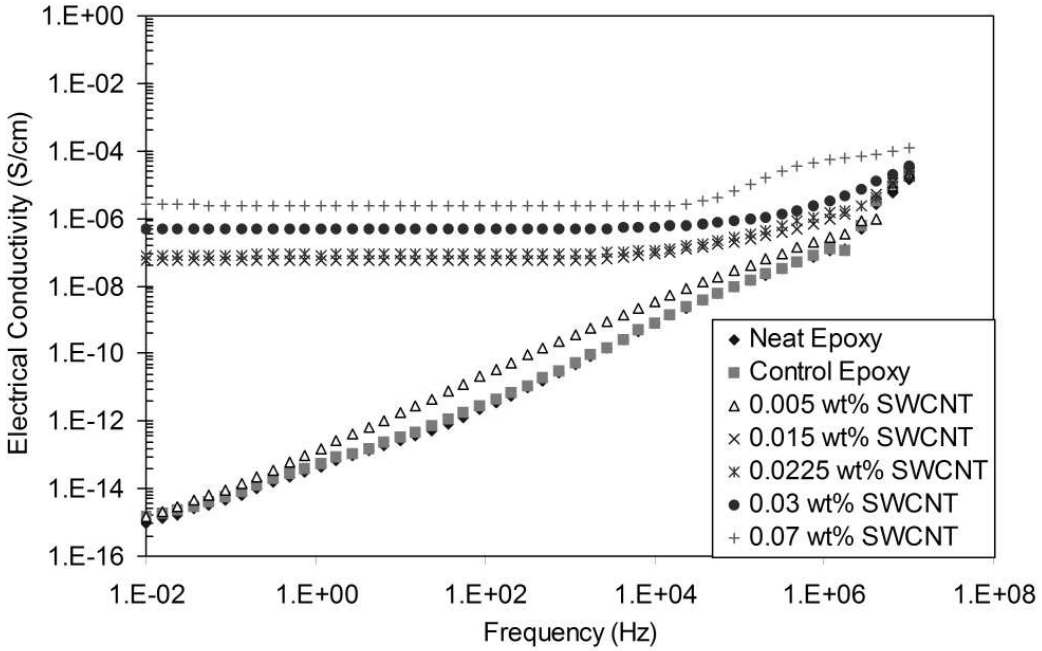

Fig. 20. Log-log plot of electrical conductivity of the epoxy/SW nanocomposites as a function of frequency for various loading weight fractions of SW-CNTs.

for these nanocomposites can be related to the formation of microstructure as a result of differences in the types of nanotubes. Fig. 22 compares the microstructures of the epoxy/SW and epoxy/XD nanocomposites at various CNT loading levels. The darker regions in the TOM micrographs represent the presence of nanotube bundles and the lighter regions represent the surrounding epoxy matrix. Fig. 22(a, c, e) shows the dispersion of SW nanotube bundles in epoxy/SW nanocomposites and Fig. 22(b, d, f) shows the dispersion of XD nanotubes in epoxy/XD nanocomposites. As it can be seen, the formation of microstructure and percolating networks is indeed different for the same weight percents of XD- and SW-CNTs. As the weight fraction of CNTs is increased for epoxy/XD nanocomposites, the nanotubes tend to form bigger clusters, unlike in epoxy/SW nanocomposites. Fig. 22 shows that the amount of agglomeration with increased loading weight fraction is higher in epoxy/XD nanocomposites

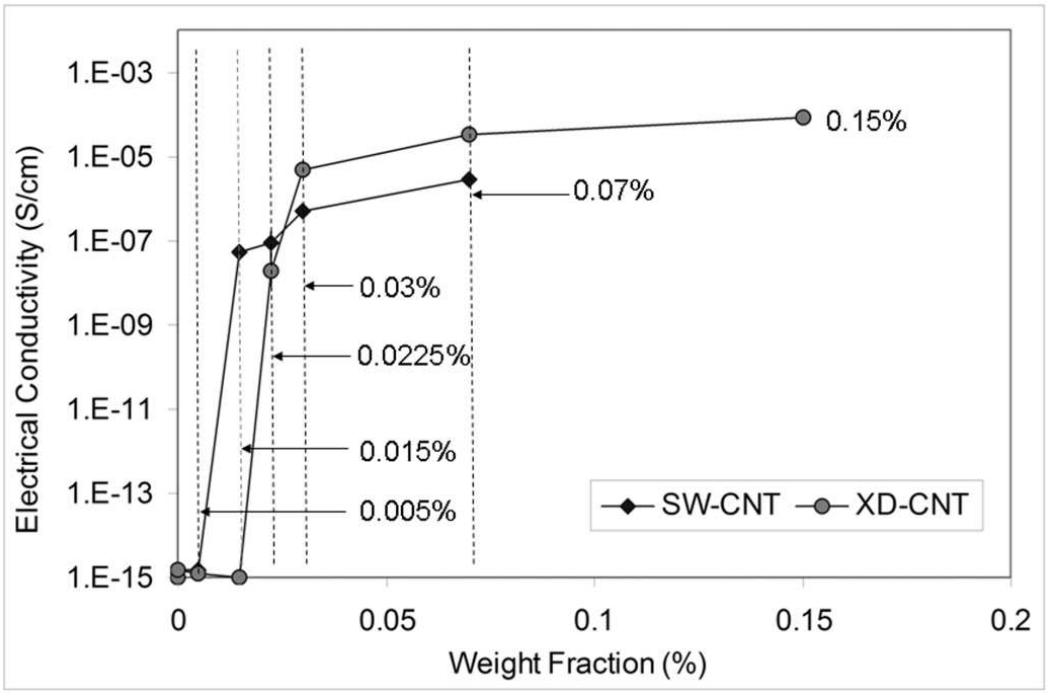

Fig. 21. Semi-log plot of electrical conductivity as a function of loading weight fractions of CNTs for epoxy/XD and epoxy/SW nanocomposites.

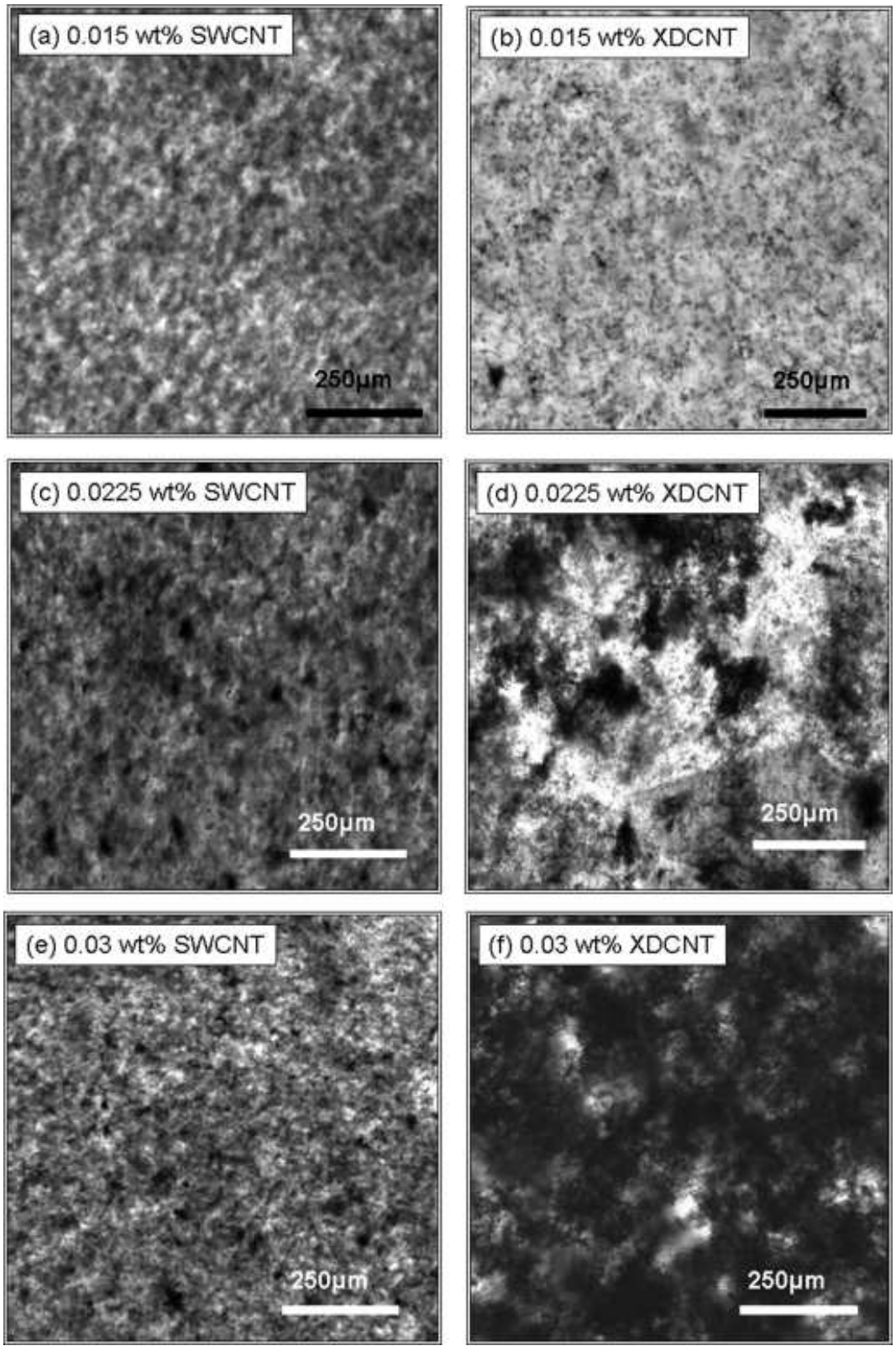

Fig. 22. Transmission optical microscopy images of epoxy/SW and epoxy/XD nanocomposites for different weight fractions of CNTs.

(b, d, f), than in epoxy/SW nanocomposites (a, c, e). The micrograph in Fig. 22 (f) is seen to be almost opaque due to big agglomerates formed by XD-CNTs.

Scanning Electron Microscopy

SEM studies on fracture surfaces were performed to study the morphological differences in the epoxy/XD and epoxy/SW nanocomposites. As seen from Fig. 23(a) and

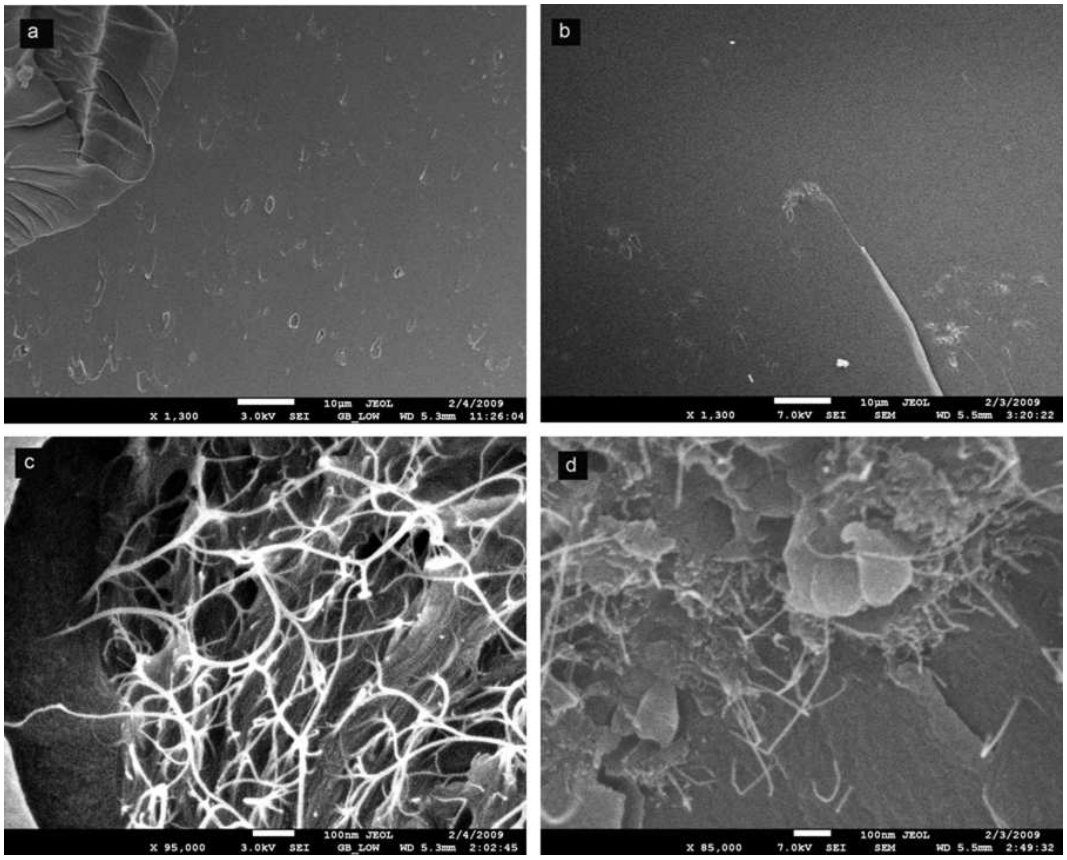

Fig. 23. Scanning electron microscopy images of epoxy/SW and epoxy/XD nanocomposites.

(b), the SW-CNTs are more homogeneously distributed as compared to XD-CNTs for 0.03 wt% specimens. Similar observations were made in Fig. 22, i.e. and XD-CNTs tends to agglomerate more with increasing weight fractions, resulting in lesser degree of homogeneity compared to SW-CNTs. Fig. 23(c) and (d) represents im-

Table V. DMA measurements for epoxy/SW and epoxy/XD nanocomposites (E' and E" reported at 30 ^{o}C).

	E' (GPa)	**E" (MPa)**	**Tg (C)**
Epoxy	2.8 0.3	91.6 12.3	129 0.1
Epoxy/SW Nanocomposites			
0.015wt%	2.5 0.1	101.6 22.1	141 1.2
0.0225wt%	2.7 0.1	110.0 23.2	148 2.0
0.03wt%	2.9 0.4	131.5 21.5	149 1.6
Epoxy/XD Nanocomposites			
0.015wt%	3.0 0.1	173.4 9.3	140 7.0
0.0225wt%	2.8 0.2	117.9 7.0	149 1.0
0.03wt%	3.3 0.2	175.1 65.4	133 1.4

ages at higher magnification to study the network formation and aspect ratio of the nanotubes. Fig. 23(c) for epoxy/SW nanocomposite shows longer length nanotube bundles (higher aspect ratio) as compared to Fig. 23(d) for epoxy/XD nanocomposites. Also a homogeneous SW-CNT network formation is visible in Fig. 23(c) as compared to agglomeration of XD-CNTs and possibly presence of some impurities in Fig. 23(d).

c. Effect on Mechanical Properties

DMA measurements were performed to find the storage modulus (E'), the loss modulus (E") and the glass transition temperature (Tg) and the results are summarized for neat epoxy, epoxy/SW and epoxy/XD nanocomposites in Table V. Carbon nanotubes have been reported to improve the mechanical properties of nanocomposites

[4, 5, 8, 13, 24, 30, 45, 63], however, the reported weight or volume fractions were much higher (50 to 100 times) than the ones used in the present study. For such extremely low weight fractions of nanotubes used in our study, minimal change is expected in the mechanical properties. The storage modulus and loss modulus values are reported in Table V for measurements at 30 ^{o}C, while the modulus values during complete temperature sweep, starting from room temperature to well above glass transition, is shown in Fig. 24. The effect of different weight fractions of SW and XD nanotubes on the storage modulus, E' (Fig. 24 a and b), and the loss modulus, E" (Fig. 24 c and d), and the tan δ curves (glass transition temperatures, Tg is measured corresponding to the peak), (Fig. 24 e and f) and comparison with neat epoxy is shown in Fig. 24. The storage modulus does not show any significant improvement or degradation as compared to neat epoxy for epoxy/SW as well as epoxy/XD nanocomposites and lies within the scatter observed from standard deviations. Higher weight fractions have not been reported in this work, as the focus of this paper is on the percolation thresholds and the post-percolation behavior of the electrical conductivity and its correlation to morphology of dispersed nanotubes. However, the loss modulus and the glass transition temperature measured from the DMA test can give some information about the dispersion state of the nanotubes throughout the specimen and the effect of localized dispersion state on the overall transition behavior from glassy to rubbery state. The changes in loss modulus are related to the changes in energy dissipation mechanisms and the change in glass transition temperature is related to the mobility of polymeric chains during the transition from glassy to rubbery state. As seen from Fig. 24(a) and Table V, the storage modulus for epoxy/SW nanocomposites is comparable to the neat epoxy modulus and lies within the standard deviation. However, the storage modulus for epoxy/XD nanocomposites seems to be slightly increased, especially for 0.03 wt% XD-CNTs.

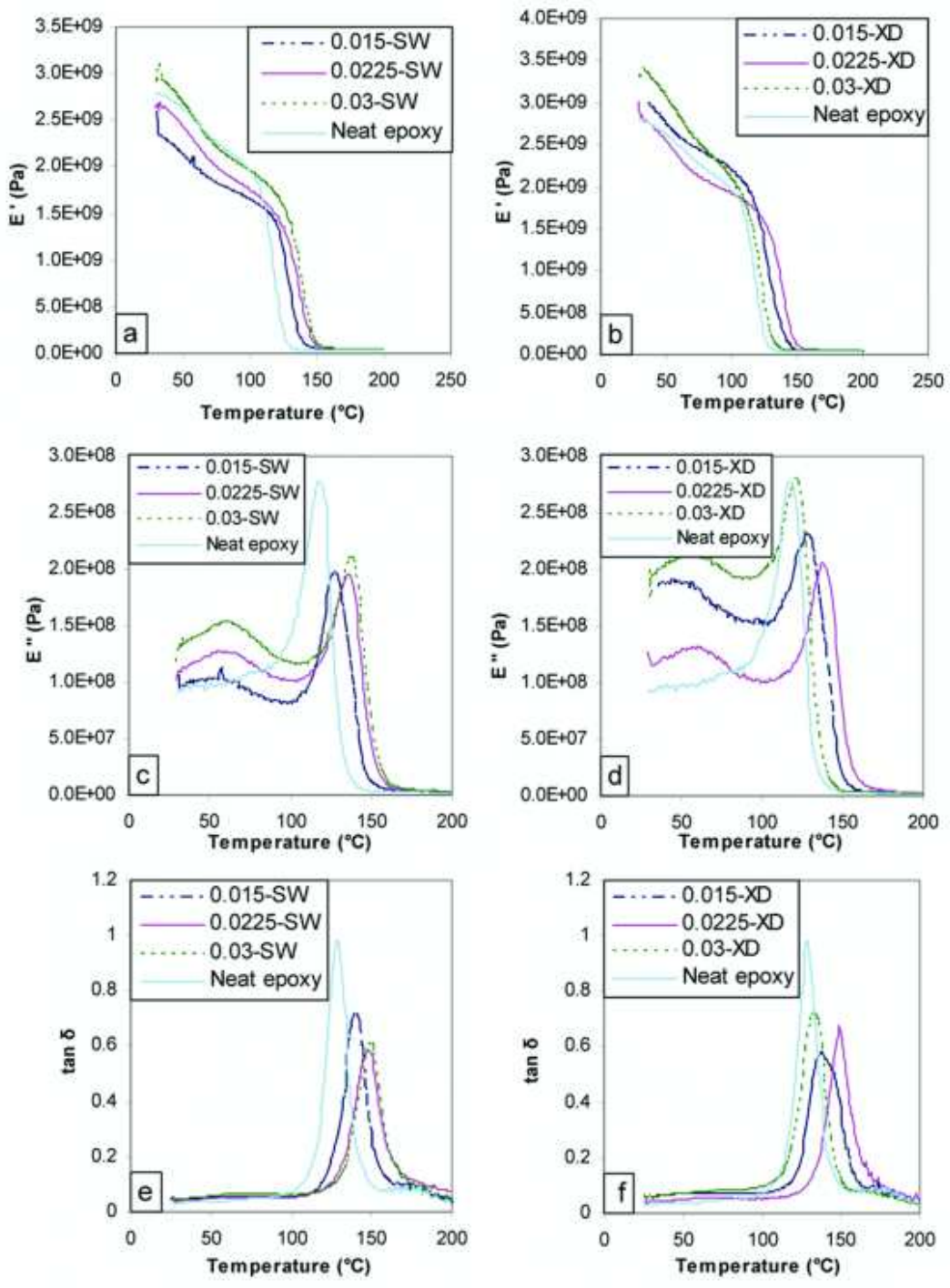

Fig. 24. DMA results for epoxy/SW and epoxy/XD nanocomposites.

The loss modulus values at room temperature showed an increase for epoxy/SW as well as for epoxy/XD nanocomposites, as shown in Fig. 24(c) and (d). The increase in loss modulus is prominent for all specimens, even after accounting for the scatter in the standard deviations. These shifts are likely to be due to the increased energy dissipation in the form of heat as a result of nanotube-nanotube friction. Energy dissipation due to crack initiation or crack growth does not seem possible, because extremely small load was applied during the DMA tests. As seen from Fig. 22 and 23, SW as well as XD nanotubes exist in the form of bundles and friction between nanotubes seems to be a plausible reason for an increase in energy dissipation at room temperature, leading to an increase in loss modulus.

Fig. 24(e) shows that the glass transition temperatures increased by about $10C$ for 0.015 wt% and about 17 to 20C for 0.0225 wt% and 0.03 wt% SW-CNTs, respectively, as compared to neat epoxy. The Tg increase for epoxy/XD nanocomposites (Fig. 24(f)) was about 10C for 0.015 wt% and about 20C for 0.0225 wt%, but insignificant change of about 3C for 0.03 wt% XD-CNTs as compared to the neat epoxy. The increase in Tg for such small weight fractions seems to be related to the localized dispersion state of nanotubes in epoxy matrix. Polymeric chains start moving during the transition process from glassy to rubbery state. The presence of nanotube bundles, as seen from Fig. 22 and 23, act as a hurdle for movement of molecular chains of polymer at temperatures near Tg, which in turn leads to an increase in the glass transition temperature.

3. Discussion

There are several parameters, like dispersion state, aspect ratio, processing method, aggregate size, presence of impurities and ratio of metallic-semiconducting nanotubes etc. and that affect the percolation threshold and the post-percolation electrical con-

ductivity. The effect of aspect ratio, inter-particle distance between nanotubes and nanotube agglomeration is discussed in the following sections. In addition, the experimental percolation thresholds have been compared with the theoretical percolation thresholds for the nanocomposites obtained from a power law model.

a. Effect of Aspect Ratio and Distance Between Nanotubes on Electrical Percolation

Nanotubes tend to agglomerate due to van der Waals interactions, particularly in absence of any surface modification through chemical functionalization. As a result of bundling, the conductive inclusions have a larger effective diameter which yields a reduced aspect ratio. Thus increased weight/ volume fraction of nanotubes is required to achieve the percolation. As seen from SEM images in Fig. 23(c) and (d), the aspect ratios of nanotube bundles for XD-CNTs are seen to be smaller as compared to the aspect ratios of SW-CNT bundles. Due to the presence of larger diameter MW-CNTs in the bundle formation of XD-CNTs, it is expected that the conductive inclusions of XD-CNTs will have a larger effective diameter as compared to conductive inclusions of SW-CNT bundles. The outcome is the reduction of the effective aspect ratio for XD-CNT bundles, as observed from Fig. 23. The lower percolation threshold for epoxy/SW nanocomposites compared to that with epoxy/XD nanocomposites indicates an agreement with Gojny et al. [18], Seidel et al. [36] and Li et al. [22] for comparison between SW and MW-CNTs embedded epoxy matrix nanocomposites.

A simplified approach has been taken for analyzing the electrical conductivity results using two possible differences between SW- and XD-CNTs. Firstly, the change in surface area to volume ratio with respect to change in nanotube aspect ratios and secondly, the change in the distance between nanotube surfaces surrounded by an epoxy interphase as a function of nanotube diameter and nanotube volume fraction. XD-CNTs consist of a mixture of MW-CNT, SW-CNT and other carbon/metallic

impurities. SW-CNTs are smaller diameter CNTs as compared to MW-CNTs and also SW-CNTs are observed to be usually longer than MW-CNTs. The surface area to volume ratio is a function of radius of the conductive inclusions. For smaller diameter conductive inclusions, the surface area or volume ratio is higher compared to larger diameter conductive inclusions. Thus the interface area available for charge conduction is higher for smaller diameter conductive inclusions. In the case of smaller diameter (high aspect ratio) SW-CNTs, higher surface area to volume ratio results in greater ability for charge conduction, resulting in lower percolation thresholds. In the case of XD-CNTs, the surface area to volume ratio is smaller due to the presence of MW-CNTs and also due to bigger conductive inclusions formed by agglomeration. Thus the observation of higher percolation threshold can be inferred qualitatively. The diameter of nanotubes can also have an effect on the electrical conductivity, as the distance between nanotube surfaces changes in case of an ideal homogeneous dispersion, for the same length and weight fraction of nanotubes. Here, a simplified geometrical approach can be used for a qualitative discussion of the results. The volume fraction can be assumed to be close to the weight fractions used in this study, because of the almost similar densities for the epoxy matrix (1.2 g/cc) and the nanotubes (1.3 g/cc). If two different nanotube diameters are considered, e.g. and 1 nm and 10 nm (1 nm representing SW-CNT and 10 nm representing XD-CNT), in an ideal case of well aligned and homogeneously dispersed nanotubes, one can plot the distance between nanotube surfaces as a function of change in volume fraction of nanotubes, as shown in Fig. 25. The distance between nanotube surfaces is calculated by approximating a concentric cylinder consisting of a nanotube surrounded by the matrix. The ratio of the radius of the nanotube and the matrix cylinder is proportional to the volume fraction of the nanotube to the matrix material. As seen from Fig. 25, for the same volume percent of nanotubes, the distance, d, between 1

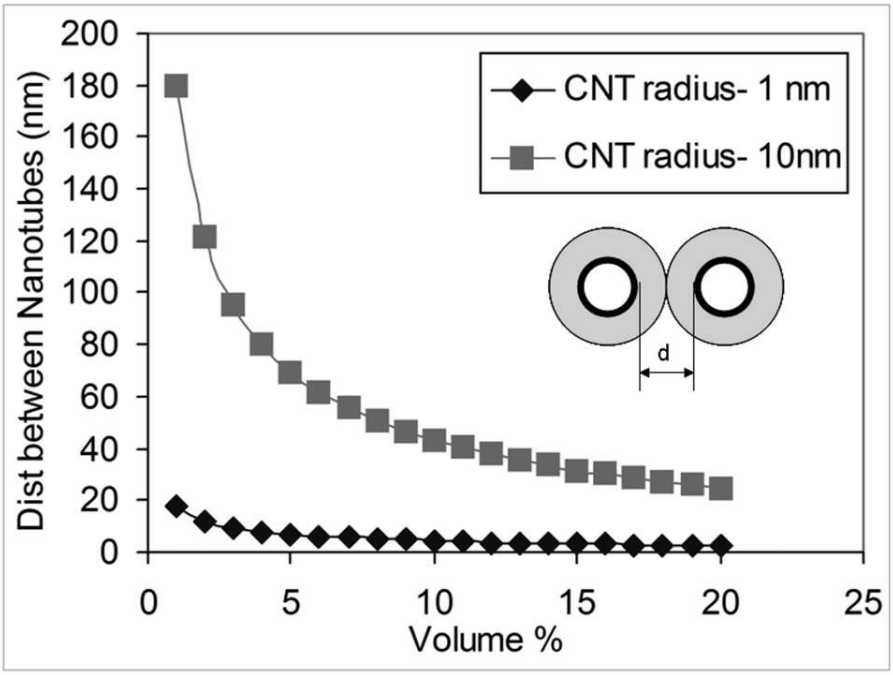

Fig. 25. Change in the distance between nanotubes surfaces, d, as a function of change in nanotube volume percent for two different nanotube diameters in an ideal case study.

nm diameter nanotubes is smaller compared to 10 nm diameter nanotubes. Thus, for the same volume percent of nanotubes in a nanocomposite, the distance between nanotubes' surfaces increases with increasing nanotube diameter. So these observations indicates a possibility for easier electron hopping in case of epoxy/SW nanocomposites due to smaller diameter nanotube bundles and thus lower separation between nanotubes, resulting in the lower percolation threshold compared to the epoxy/XD nanocomposites.

Fig. 25 represents ideal condition for aligned, homogeneously distributed and well dispersed carbon nanotubes. From Fig. 25, the separation distance between SW-CNTs is about 18 nm for 1 vol% of SW-CNTs, and for 10 vol% CNTs, the separation distance is about 4 nm. The real nanocomposites have randomly oriented bundles

of nanotubes. Also, the local volume fraction can be significantly higher than the global volume fraction of nanotubes due to bundling of nanotubes, in which case the distance between SW-CNTs can be shorter than 18 nm (from Fig. 25). However, the exact distance required for electron hopping is not known, but, it is known that electron hopping is one of the mechanisms for increasing electrical conductivity in the nanocomposite specimens, and present argument shows the effect of nanotube diameter on the distances required for electron hopping. In case of XD-CNTs, the separation distances are much greater, as seen from Fig. 25, which indicates bleak possibility for electron hopping mechanism. However, XD-CNTs also contain some proportion of SW-CNTs and thus introducing a possibility for electron hopping mechanism. This will help in reducing the percolation threshold for XD-CNTs reinforced nanocomposites. This provides a possible explanation for small difference in the percolation thresholds between SW-CNTs and XD-CNTs reinforced nanocomposites, as observed from the experimental results in the present study.

Seidel et al. [36] reported the formation of conductive networks as the principle cause for the large increase in effective conductivity for MW-CNTs, while both the formation of conductive networks and electron hopping lead to a large increase in conductivity at very low SW-CNT concentrations. The percolation threshold was reported to be lower for SW-CNT as compared to MW-CNT. The present experimental results for percolation threshold validates the modeling results from Seidel et al. [36]. However, due to the presence of SW-CNTs in the mixture of XD-CNTs, the difference in the percolation thresholds between SW-CNT and XD-CNT is not large as compared to modeling results. As seen from TOM micrographs in Fig. 22 and SEM micrographs in Fig. 23, the conductive network formation with increasing weight fraction of CNTs is more prominent (dense network) in the case of XD-CNTs, as compared to SW-CNTs, due to XD-CNT agglomeration. The dense network of nanotubes

brings more nanotubes in direct physical contact, which could be a positive attribute for post percolation electrical conductivity. This can be interpreted qualitatively, as the main reason for the larger increase in post percolation electrical conductivity for XD-CNTs, by about two orders of magnitude for 0.03 wt% XD-CNTs, as compared to one order of magnitude increase for 0.03 wt% SW-CNTs.

b. Effect of Agglomeration of Nanotubes on Electrical Percolation

In case of the MW-CNTs, multiple graphene layers are separated by 0.34 nm with van der Waals interaction between the layers, in addition to the interaction with other surrounding entities. The number of carbon atoms per unit length is more for a MW-CNT as compared to a SW-CNT.

Considering an isolated MW-CNT and a SW-CNT, each carbon atom on a MW-CNT has more number of carbon atoms to interact with surrounding species, i.e. MW-CNTs or SW-CNTs or other carbon impurities, as compared to an atom on a SWCNT. This leads to higher van der Waals interaction forces between MW-CNT and surrounding species, i.e. MW-CNTs or SW-CNTs or other carbon impurities. Hence MW-CNTs have a tendency to form bigger agglomerates and as in case of XD-CNTs (which is a cocktail of MWCNTs, SWCNTs, and other impurities), the same phenomenon is observed, as can be seen from the Figure 5.

The effect of interaction forces (van der Waals forces) between nanotubes on the percolation threshold has been studied by Grujicic et al. [98] through analytical and numerical modeling. They reported that the interaction between nanotubes due to van der Waals forces increased the percolation threshold as compared to nanotubes without interaction forces. Also it was seen from their numerical model that the nanotubes tended to agglomerate in an attempt to align themselves when interaction forces were introduced between the nanotubes (Fig. 4 in [98]). The analytical

percolation model predicted similar behavior of increased percolation threshold by introduction of interaction forces between nanotubes. The predictions of the model are in good agreement with our experimental observation of higher percolation threshold for epoxy/XD nanocomposites and agglomeration of XD nanotubes.

In addition to higher van der Waals forces between MW-CNTs, the tunneling resistance, as shown by Li et al. [22] for higher diameter nanotubes is lower and the cutoff thickness for tunneling distance is shown to be 1.8 nm. Therefore, MW-CNTs with 0.34 nm distance between inner layers would have comparatively greater electron tunneling as compared to SW-CNTs, thus leading to higher post percolation conductivity for the nanocomposites. Before percolation, formation of conducting network will govern the percolation threshold value. The XD-CNTs form bigger agglomerates resulting in inhomogeneous distribution through out the specimen and poor physical contact during network formation as compared to corresponding weight fraction of SW-CNTs (as seen from SEM and TOM images). Hence SW-CNTs are expected to percolate earlier; however, post percolation conductivity of XD-CNTs is expected to be higher as seen from our results.

c. Comparison with Theoretical Percolation Threshold Using Power Law Model:

The theoretical percolation threshold in composite materials has been given by the following power law model [98, 99]:

$$\sigma = A(V - Vc)^t \text{ ..... } (1)$$

Where σ is the electrical conductivity, V is the filler volume fraction, Vc is the critical volume fraction (volume fraction at percolation) and A and t are percolation parameters. The filler volume fraction, V, is selected for the conductive nanocomposites

and the critical volume fraction, Vc, is varied such as to obtain best power law fit. The volume fractions in Eq. (1) are replaced with weight fractions used in the experimental study. Since the matrix and the nanotube densities are about the same, the volume fractions and the weight fractions would be almost same. The value for t has been reported from 1.30 to 3.10 as per Ounaies et al. [99] and from 0.87 to 1.79 as per Grujicic et al. [98]. The value of A should ideally converge to the electrical conductivity of the nanotubes [98]. However, the value of A is usually found to be much lower than the theoretical electrical conductivity of nanotubes ($\sim$ 1000 S/cm [36]). One of the reasons for lower value for A is due to the presence of contact resistance within the conductive path, i.e. and between two adjacent nanotubes, which decreases the effective conductivity of the nanotubes. At low weight percents of nanotubes, a physical contact between nanotubes, which is required to form paths between conductive inclusions in direct contact, is absent. Thus, the value of A is found to be much lower than expected. Power law fitting of the log σ vs log (V-Vc) yielded best fit for 0.0225 wt% of XD-CNTs with fitting parameters, A and t, being 7.0E-04 and 1.02 respectively. Ounaies et al. [99] reported values for A of 6.7E-04 and t of 1.38 for their nanocomposites (percolation at 0.5 wt%).

Grujicic et al. [98] presented percolation results for interacting versus non-interacting nanotubes through analytical and numerical modeling. The interaction was considered by the presence of van der Waals forces between the nanotubes. The value of t was reported to be 0.87 and 1.17 for non-interacting and interacting nanotubes respectively. The corresponding value of A was 1.6E-06 for non-interacting nanotubes and 2E-05 for interacting nanotubes. It seems that the value of fitting parameters, t and A, increases with increasing interaction of nanotubes. The variations in reported A and t values in literature are expected to be due to different processing methods, dispersion state of nanotubes, bundle sizes and interaction be-

tween nanotubes and with impurities. It is estimated by the power law model that the percolation for epoxy/XD nanocomposites occurs around 0.0225 wt%. So the theoretical predictions from the power law model are in good agreement with our experimental results.

The theoretical results for SW-CNTs also showed good agreement with the experimental results. Power law fitting yielded A of 2.6E-03 and t of 2.04 for Vc of 0.016 wt% SW-CNTs. This seemed to be the best fit possible after consideration of a lot of various critical weight fractions. The increased value of A indicates better physical contacts in the formation of conductive network, yielding higher effective conductivity of SW-CNTs as compared to XD-CNTs. An increase in the value of t may represent better interaction between SW-CNTs at low volume fractions as compared to XD-CNTs. The theoretical prediction of percolation threshold for SW-CNTs is in good agreement with experimental observation of percolation threshold, i.e. and close to 0.015 wt%, for epoxy/SW nanocomposites.

4. Summary

Several processing parameters were studied in this chapter for getting good quality nanocomposites. Processing methods were developed for preparing nanocomposites containing varying weight fractions of SW-CNTs, functionalized SW-CNTs and XD-CNTs, whose mechanical and electrical properties have been investigated in this work. The results are presented with respect to the variation of the microstructure as observed from transmission optical microscopy and scanning and transmission electron microscopy. The mechanical property improvement was not found to be as significant as the electrical properties. The dispersion of SWCNTs improved as a result of functionalization. The modulus values improved by 2% for Silane functionalization, 10% for pristine nanotubes and 12% for fluorinated nanotubes. The modulus also

increased with increasing nanotube content, for example, the increment for pristine nanotubes was 6% by adding 0.5% nanotubes and 12% increment by adding 1% nanotubes. However, the glass transition temperature decreased by adding SWCNTs. The fractographic analysis qualitatively indicates an improvement in toughness of the composite materials by adding SWCNTs. Further characterization to quantify the fracture toughness and study the load transfer through the interface needs to be done on these material systems.

Electrical percolation threshold for epoxy/SW nanocomposites (0.015 wt%) is found to be lower than the percolation threshold for epoxy/XD nanocomposites (0.0225 wt%). The increase in electrical conductivity after percolation is found to be higher for XD-CNTs by an order of magnitude as compared to SW-CNTs at 0.03 wt% of nanotubes. The major enhancement of the electrical conductivity is achieved without compromising the storage modulus with the addition of either SW- or XD-CNTs. One of the important outcome of this work is that a significant improvement in the electrical conductivity has been achieved for both epoxy/SW and epoxy/XD nanocomposites as compared with neat epoxy by about seven to eight orders of magnitude at percolation and about eight to ten orders of magnitude post percolation. The improvement for epoxy/XD nanocomposites comes at a much lower cost than epoxy/SW nanocomposites, even after considering additional weight fraction of XD-CNTs due to the differences in the percolation threshold. It would be interesting to investigate if this improvement in matrix electrical conductivity could be transferred at the composite laminate scale.

The investigation of structure-property relationships in nanocomposites also lead to another important finding of several toughening mechanisms with different types of nanotubes. The presence of these toughening mechanisms indicate a possibility of transferring these mechanisms to the composite laminate scale. Investigations

regarding this concept of transferring nanocomposite toughness and multifunctional properties to the laminate scale has been pursued in the next couple of chapters.

CHAPTER IV

MULTI-SCALE WOVEN COMPOSITE LAMINATES

Polymer matrix composite laminates have the benefit of light weight, good mechanical properties and ability to be molded into complex shapes. Susceptibility to delamination is one of the major weaknesses of many advanced laminated composite structures. The information about composite materials' resistance to delamination is useful for product development, material selection as well as damage tolerance analysis of composite structures. The delamination properties like interlaminar shear strength and interlaminar fracture toughness are important properties to be investigated. It is necessary to develop new material systems that meet the demanding requirements of aerospace industry without adding weight penalties. There have been several efforts in improving the delamination behavior by modifying the fiber-matrix interface in the past [100–104]. There are several recent efforts directed towards similar problem [64, 105–108]. The objective of the present study is to explore the delamination behavior of conventional carbon fiber composites modified by addition of small quantity of nanoparticles without compromising the processing characteristics.

Carbon nanotubes being one of the most promising class of new nanoparticles, they have the benefits of excellent mechanical properties [3, 109] such as Young's modulus of around 1 TPa and tensile strength of around 200 GPa with small diameter ($1nm$) and high aspect ratio (10000-for pristine nanotubes). A number of research groups are assessing the possible applications of carbon nanotubes in conventional composites for structural applications or multi-functional applications [18, 64, 105, 106, 108]. Modeling and experiments have shown improvements in the mechanical properties of the SWCNT reinforced composites [78, 82, 84]. To maximize the inherent properties of nanotubes, dispersion and reinforcement of SWCNTs in polymer matrix

is one of the major issues of interest as seen from previous chapters. The need of SWCNTs at a particular location is governed by the stress concentrations due to applied load or boundary conditions depending on sample geometry and weak material interfaces. Thus the concept of selective placement of nanotubes is introduced to strengthen the material at locations of stress concentrations and weak interfaces.

In the present work, novel composites are fabricated with selective placement of nanotubes in the laminate mid-plane to improve delamination resistance of woven composites. The interlaminar properties for these composites are investigated using short beam shear tests under three point bending [110–117] and double cantilever beam tests. The fracture mechanisms at the delamination plane are investigated using detailed scanning electron microscopy.

A. Experimental Procedure

1. Materials

The purified single wall carbon nanotubes (SWCNTs) were obtained from Rice University, and were made by the high pressure carbon monoxide synthesis process (HiPCO). The supplied material consisted of micron-scale aggregates with individual SWCNT diameters reported to be 1.0 to 1.4 nm. Functionalized nanotubes were prepared through a three-step chemical treatment. The carbon nanotubes were first fluorinated in a Monel flow reactor at 150^{o}C for 12 hours following the procedure developed at Rice University [85]. Hydroxylated nanotubes were then prepared through reaction of the fluoronanotubes with lithium hydroxide treated ethyleneglycol [5]. Finally, the organosilane N-(2-aminoethyl)-3-aminopropyltrimethoxysilane obtained from Aldrich Inc. and was used to produce silane functionalized nanotubes. This procedure has been demonstrated in previous work to successfully functionalize nan-

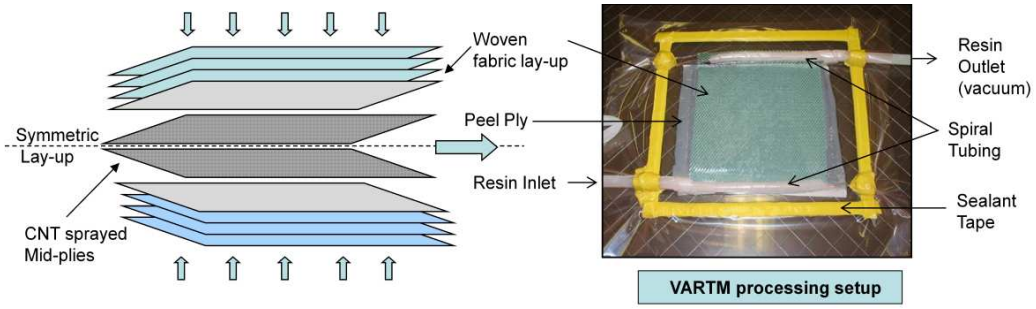

Fig. 26. Schematic representation of ply lay-up and actual VARTM process.

otubes with organosilanes [85]. For spraying the nanotubes onto the carbon fabric plies, a solution was prepared using 0.1 wt % purified pristine nanotubes in ethanol, and another solution was prepared using 0.1 wt % silane functionalized nanotubes in ethanol. The 0.1 wt % represents weight fraction with respect to weight of an individual ply of woven carbon fibers. The total weight fraction of carbon nanotubes amounts to be 0.01 wt% of the total weight of all plies.

The epoxy resin used was diglycidyl ether of bisphenol-F (DGEBF epoxy) EPON 862 (now called EPIKOTE 862), and was obtained from Resolution Performance Products along with aliphatic amine curing agent EPICURE 9553. This matrix system was selected because of desirable features such as low viscosity, good mechanical and chemical properties. The low viscosity makes this epoxy suitable for VARTM process and therefore eliminates the use of viscosity reducers and reactive diluents from the epoxy formulation. Thus, the physical and chemical resistance properties of the matrix were not compromised in pursuit of amenable processing viscosities. The woven carbon fabric used in the composite was an eight-harness satin weave (8 H.S.) of T300 carbon fibers produced by Textile Technologies Incorporation. NASA Langley Research Center (LaRC) provided the woven fabric in the form of a roll of

12 inches (30.5 cm) wide and about 40 feet (1220 cm) long. The 8 H.S. configuration of the fabric consists of woven tows such that a single longitudinal tow passes over seven transverse tows and under one transverse tow.

The VARTM process was used to fabricate laminate plates using the mold set-up as shown in Fig. 26, and detailed information about the VARTM processing and the nanotube spraying method has been provided in reference [64]. The complete VARTM set-up including all components apart from the mold is shown in Fig. 27. Each panel contained ten layers of carbon fabric plies and carbon nanotubes were sprayed at the mid-plane of the laminate (i.e. between ply number 5 and 6). The ply stacking was kept symmetric about the mid-plane as shown in Fig. 26. A PTFE film insert of size about 3 inches wide (7.62 cm) and 8 inches long (20.32 cm) was placed at the mid-plane of the fiber stack as the delamination starter material. Three different panels were processed as described in Table VI, each of dimensions approximately 8 inches (20.32 cm) wide, 6 inches (15.24 cm) in length and about 0.16 inch (0.40 cm) in depth after removing the rough edges from four sides. The measurements were performed with an accuracy of $\pm$ 0.1 mm (0.004 inch) in width and $\pm$ 0.01 mm (0.0004 inch) in thickness. The nomenclature for the DCB test specimens consisted of the panel number preceded by the specimen number, e.g. 5P2 indicates 5th specimen of the 2nd panel. The numbering of specimens from 1 to 6 indicates cutting direction from left to right in the panel i.e. specimen 1 and 6 forming the edge specimens.

2. Processing Method

The pristine nanotubes were provided in the form of aggregates. Several different techniques have been suggested for dispersing the nanotubes. Nanotubes were chemically functionalized using Silane (3-glycidoxypropyl trimethoxysilane) and it has been described in detail by elsewhere [26]. The pristine as well as silane nanotubes were

Table VI. Composite panels prepared by the VARTM technique and their nomenclature

Panel Number	Mid-plane Modification	Specimens (6 each)
P1	No nanotubes, solvent evaporated	1P1 to 6P1
P2	0.01 wt.% pristine nanotubes	1P2 to 6P2
P3	0.01 wt.% silane functionalized nanotubes	1P3 to 6P3

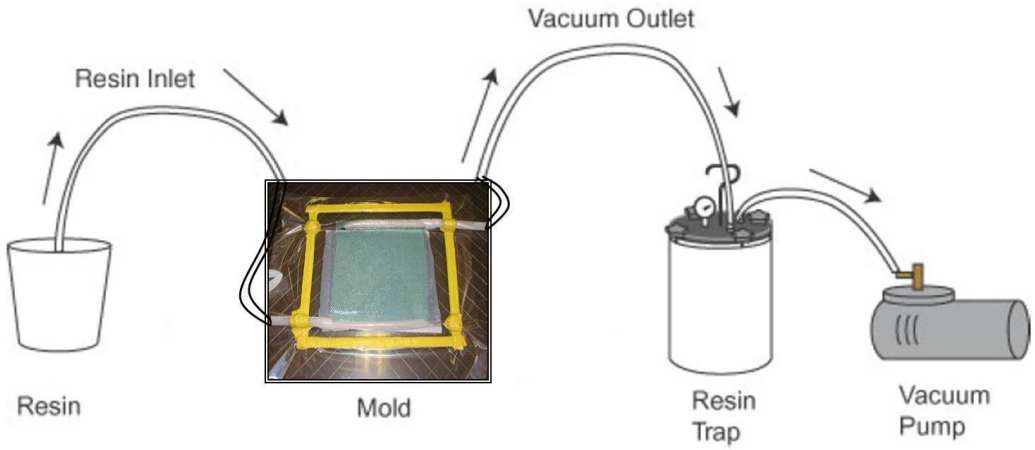

Fig. 27. Components involved in VARTM process.

mixed separately with ethanol solvent. The solutions were subjected to ultrasonication for about an hour using a 40 kHz bath sonicator to enhance dispersion. Each solution was then sprayed on the carbon fabric ply on one side only. Likewise, two plies were prepared for each solution and dried overnight. Two plies were sprayed with just ethanol to be incorporated into the baseline (no nanotubes) composite. The weight percent of SWCNTs was 0.1% of the weight of a single ply of woven carbon fabric. The solvent is evaporated during the drying process and the nanotubes form a thin layer over the carbon fiber mat. Ten layers of carbon fabric layers were stacked in

a symmetric and balanced lay-up to create a single laminate that includes two layers in the mid-plane sprayed with either the nanotubes-ethanol solution or just ethanol. The SWCNTs were introduced between ply number 5 and 6 of the 10 ply stacking with sides containing nanotubes facing each other. In the VARTM process, vacuum was created inside the sealed vacuum bag containing the stacked plies. The resin was injected through the spiral wrap tube and resin flowed through the stack of woven carbon fabric lay-up as a result of pressure gradient. The fabric infiltration time is a function of the resin viscosity, the fabric permeability and the applied pressure gradient. The resin flowed out through the vacuum outlet and into the resin trap. The stacking sequence and basic set-up of the mold prepared for VARTM process is shown in Fig. 26.

The laminate was allowed to cure under vacuum pressure for about 15 hours at room temperature. It was then subjected to heating for an hour at 120^{o}C after removing from the VARTM setup and placing in an oven. Laminates of 6"x 6" size were obtained at the end of the above procedure with thickness of approximately 3.5 mm. The fiber weight fraction of composite without nanotubes, with pristine nanotubes and with silane functionalized nanotubes was 64.77%, 64.34% and 64.35% respectively. The main focus of this research is to study the interaction of SWCNT with epoxy resin and carbon fabric at the interface and improve critical mechanical properties such as interlaminar fracture toughness and interlaminar shear response.

3. Characterization Methods

a. Specimen Preparation

The specimens were cut according to ASTM-5528 standards with length of 6 inches (15.24 cm) and width of 1 inch (2.54 cm) with an accuracy of $\pm$0.1 mm. The upper

and lower specimen surfaces were roughened using grinding paper where the piano hinges were to be bonded. The surfaces of the piano hinges were sand blasted to prepare rough surfaces for better bonding, and then the surface was cleaned with acetone to remove any contamination. The specimens were dried for four days at 60^oC in a Thermolyne Oven (Series 9000) to remove moisture absorbed during the cutting process. Two-part epoxy adhesive was used to bond the piano hinges, and the specimens were placed in an oven for two hours at 60^oC to cure the epoxy adhesive. The specimen edges were sprayed with white paint, and a scale with 1 mm resolution was placed on one of the edges of each specimen for monitoring crack propagation, as shown in Fig. 28(a). The specimens were stored in a dessicator before testing to protect them from humid conditions and also after testing to preserve the fracture surfaces for microscopic investigation.

b. Short Beam Shear Test

There is no exact method available for determination of interlaminar shear strength; however, approximate values can be obtained by various tests. The short beam shear (SBS) test is one of such most commonly used methods. The SBS test is a simple test and is attractive as a materials screening test and as a measure of quality control. The sample preparation is easier and the test is much easier and faster to perform. For this study, the SBS test as defined by ASTM D 2344 - 00 was used. As per the ASTM standards, the short beam strength obtained by this method can be used for quality control and process specification purposes. It can also be used for comparative testing of composite materials, provided that failures occur consistently in the same mode. The specimen dimensions were selected as per standards with length equal to 6 times the thickness and width equal to twice the thickness. A total of 8 samples were tested for each type of composite panel, even though, ASTM standards [118] require

only 5 samples. The tests were performed on a MTS axial load frame. A 2000 lb load cell was used and the rate of loading was 1.0 mm/min. The load was applied until fracture occurred and the fracture load was used in the calculation of the apparent shear strength of the material. The test was stopped when load dropped by about 30% or head travel exceeded the specimen nominal thickness. The short beam shear strength is calculated using eq.4.1 ,

$$F_{sbs} = \frac{3P_m}{4bh} \tag{4.1}$$

where F_{sbs} is the estimate of the shear strength; P_m is the maximum cross-head load during the test; b is the specimen width; and h is the specimen thickness or depth. The above formula is derived assuming Euler-Bernoulli beam theory, which is only approximately correct for a short beam and for the three point bending loading conditions. According to the beam analysis results, the shear stress varies parabolically through the thickness with maximum value reaching at the center plane. However, due to bending there is also a normal component of stress, which is maximum at the top and bottom of the specimen cross-section, and which might play a role in final failure, especially if there is compressive failure due to fiber microbuckling or kinking.

In most cases, because of the complexity of internal stresses and the variety of failure modes that can occur in this specimen, it is not generally possible to relate the short beam strength to a material property. However, the failures are dominated by resin and interlaminar properties, and the test results have been found to be repeatable for a given specimen geometry, material system and stacking sequence [118]. The woven configurations of fibers make the stress state more complex to analyze. Thus the method used here allows for a quantitative comparison of the short beam strengths of composites with and without nanotubes.

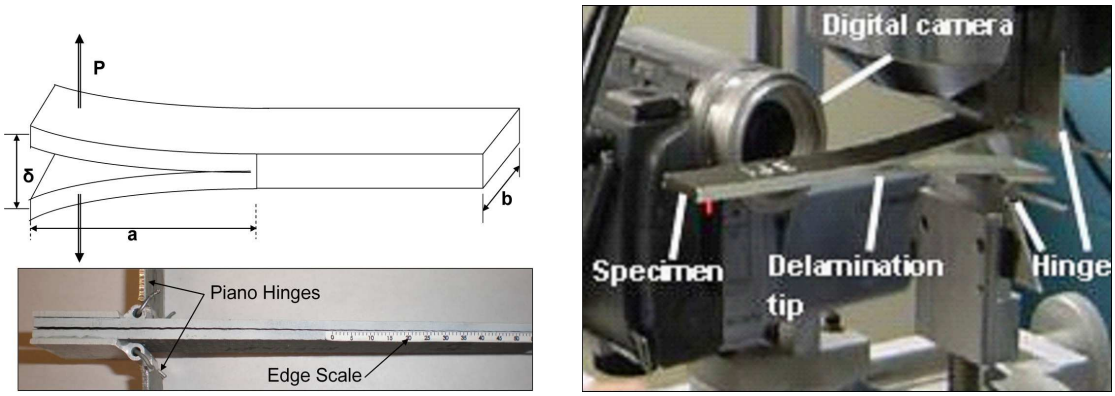

(a) (b)

Fig. 28. Double cantilever beam test. 28(a) Specimen specifications 28(b) Test Set-up.

c. Double Cantilever Beam Test

The ASTM D-5528 standard was followed for performing the DCB tests at room temperature using a servo-hydraulic test frame (MTS 858 table top system) as shown in Fig. 28(b). A 50 lbf (222.50 N) load cell with ± 0.05 N resolution (interface model 1500 ASK-50) was used for force measurement. Parameters P, δ , and a represent force, applied displacement, and delamination length, respectively. Crack propagation was monitored on a video screen connected to a video camera set at magnification of about 20X and focused on the crack tip at all times as the crack progressed. The test was conducted under displacement control at a displacement rate of 1.27 mm/min. Crack extension was recorded every millimeter of crack growth for stable crack growths, and crack propagations corresponding to start and end values of unstable crack growths were noted. The crack was allowed to propagate through a distance of at least 40 mm, after which the specimen was unloaded at a rate of 2.54 mm/min. The same procedure was repeated for the six specimens from each panel.

d. Data Reduction Method

Three data reduction methods (i.e. and the modified beam theory (MBT), the compliance calibration (CC) and the modified compliance calibration (MCC) [86]), were utilized to calculate the G_I values i.e. strain energy release rates. A comparison of the results is shown in Fig. 29(b) for a sample specimen using the three different techniques of data reduction, as per the ASTM standards. Fig. 29(b) shows almost overlapping R-curves from all three methods. Further comparison of the results for different specimens has been presented using only the modified beam theory.

Modified Beam Theory

In the modified beam theory method, each arm of the DCB specimen is considered to be a cantilever beam of length equal to the delamination length 'a'. The G_I value calculated by Euler-Bernoulli beam theory is overestimated in the absence of perfectly clamped delamination front as shown by Hashemi et al. [119]. Thus to correct for this non-perfect clamping effect, Hashemi et al. suggested a slightly longer delamination length, a+Δ, where Δ is determined from the plot of the cube root of compliance, $C^{1/3}$, versus delamination length, 'a' as shown in Fig. 29(a). The compliance, C, is the ratio of load point displacement to the applied load, i.e. C = δ/P. The strain energy release rate is calculated by using eq. 4.2 as follows

$$G_I = \frac{3P\delta}{2b(a+\Delta)} \tag{4.2}$$

where, P is the applied load for crack growth, δ is the corresponding load point displacement, 'a' is the corresponding delamination length (or initial crack length), b is the specimen width, and G_I is the strain energy release rate (G_{Ic} is the critical value known as mode-I interlaminar fracture toughness and it is considered to be a material property of the particular composite). The analysis method required the

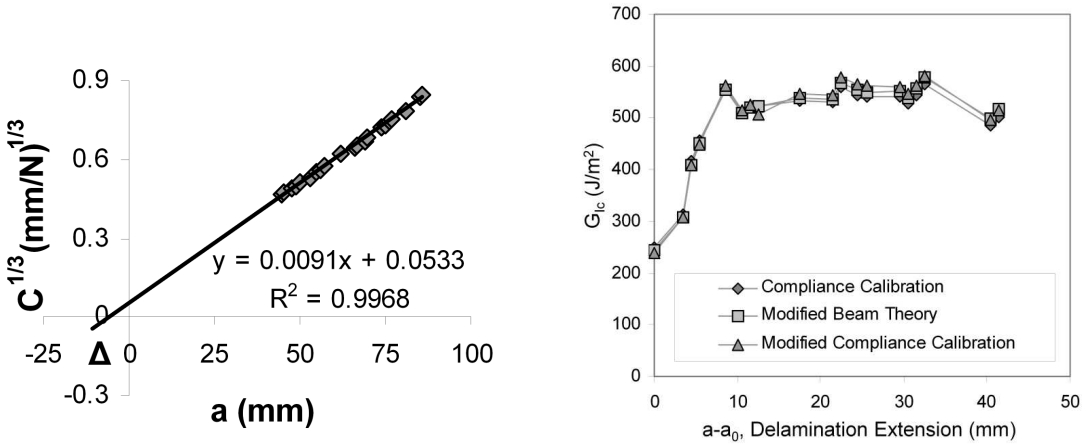

(a) (b)

Fig. 29. Data reduction method. 29(a) Method to find the correction factor, Δ, x-intercept value obtained by extending the straight line through the data points. 29(b) Comparison of R- Curves from three data reduction techniques (compliance calibration, modified beam theory and modified compliance calibration) for one representative specimen 1P2.

measurement of only three parameters i.e. P, delta and 'a' during the test, and δ was obtained using the method suggested by Hashemi et al. [119], as shown in Fig. 29(a).

e. Scanning Electron Microscopy

A Hitachi S-3700N scanning electron microscope was used for studying the delaminated fracture surfaces of the DCB specimens, and imaging was performed using Oxford Instruments INCAx-Sight Model 7962. The specimens were split open after completion of the DCB test and the mid-planes were coated with a 2 nm thick platinum layer to reduce the charging effect of the specimen surface under the electron beam. The specimens were imaged at different locations along the crack length as shown in Fig. 30, to maintain consistency in comparison for specimens from different

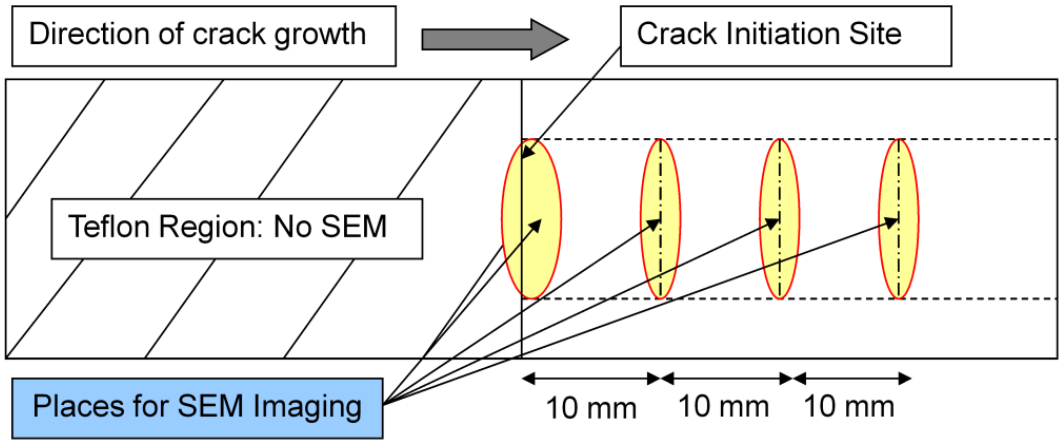

Fig. 30. SEM locations along crack length for consistency of comparison between specimens from different panels. [Not drawn to scale. Actual specimen length 16 cm and width 2.5 cm]

panels.

B. Results and Discussion

1. Interlaminar Shear Strength

As demonstrated in the scanning and transmission electron microscopy images for Fig. 31, the functionalization using silane results in good dispersion of the SWCNTs, even though they are shorter in length. Park and Jin [120] and Zhu et al [121] showed that silane coupling agent plays an important role in improving the mechanical interfacial properties like short beam shear strength and fracture toughness for the glass fiber composites. It is of interest to compare the influence of dispersion due to silane functionalization on interlaminar shear strength of carbon fiber composites using short beam shear tests. The functionalized nanotubes and the pristine nanotubes were dispersed into smaller aggregates using ultrasonication before spraying on to the woven fabric lamina. Thus a coating of nanotubes is formed on one surface of the lamina that is expected to influence the interlaminar property of that lamina when

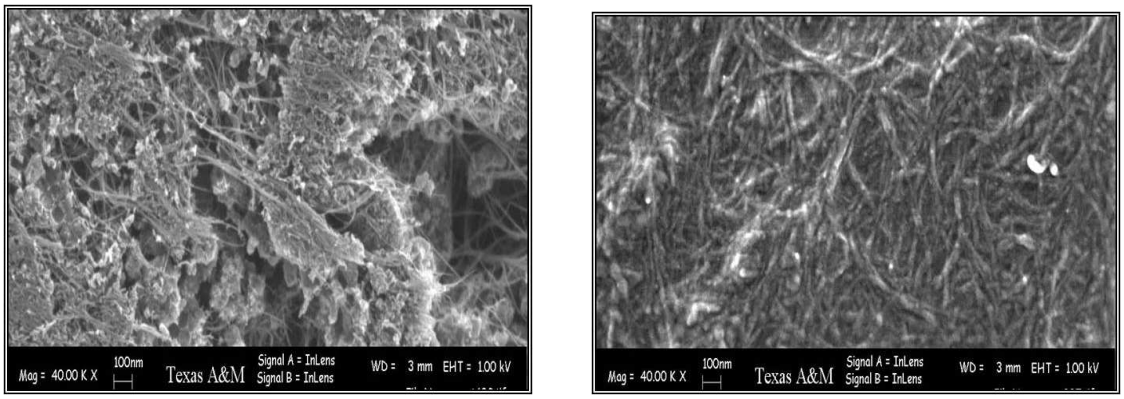

(a) (b)

Fig. 31. SEM micrographs showing dispersion of pristine and silane functionalized nanotubes. 31(a) Pristine nanotubes, 31(b) Silane functionalized nanotubes.

strategically placed at predetermined position in the lay-up. In the present work, the selective location was the mid-plane of the 10 ply laminate. Some of the composite samples were fabricated with a Teflon film in the middle plane of the laminate to form an initiation site for the delamination between midplane plies. These laminates were subjected to an opening load so as to cause delamination in the mid-plane and the resultant fracture surface was imaged using field emission SEM. The micrograph in Fig. 32(a) shows fracture surface of a composite without nanotubes and it can be seen that no matrix is remaining on the fibers indicating poor interface leading to clean fiber-matrix debonding.

It is obvious from Fig. 32(b) that the pristine nanotubes are present on the fiber surface in the form of a network of nanotube bundles. The image in Fig. 32(c) shows the fracture surface of sample with silane functionalized nanotubes. In this image, the nanotubes are not visible but fibers are covered with substantial amount of matrix showing complex fracture pattern. This indicates the possibility of enhanced fiber-matrix interface due to the presence of functionalized nanotubes. As a consequence

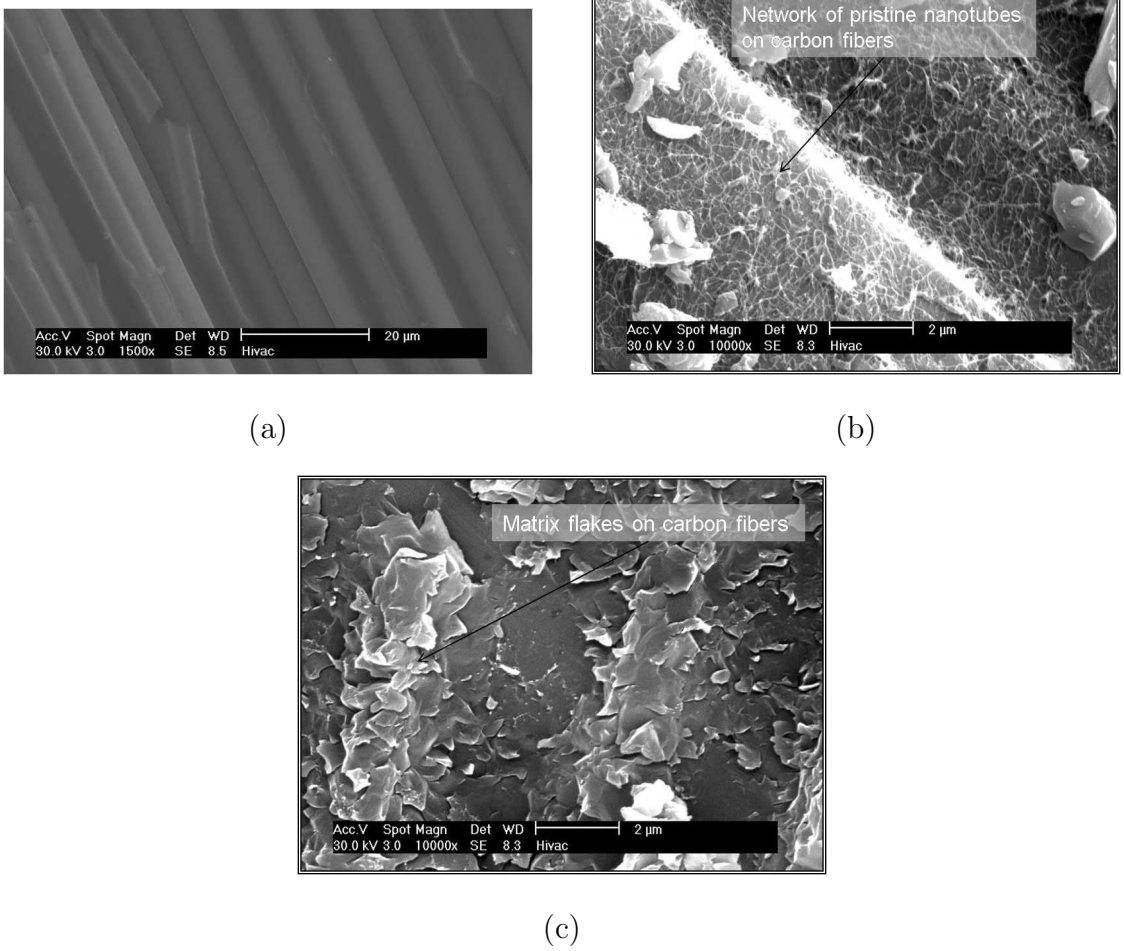

Fig. 32. SEM images of fracture surfaces of SBS test specimens. 32(a) Opened mid–plane of specimen without nanotubes. 32(b) Opened mid-plane of specimen with pristine nanotubes showing entangled network of nanotubes.32(c) Opened mid-plane of specimen with silane functionalized nanotubes showing matrix flakes.

the crack propagated through the matrix instead of the interface. Results from the SBS test are shown in Fig. 33. The specimens E1 to E6 in Fig. 33(a) represents the composite without nanotubes (base material), specimens P1 to P6 in Fig. 33(b) represents the composite with pristine SWCNTs and specimens S1 to S6 in Fig. 33(c) represents the composite with silane functionalized SWCNTs respectively. The x-axis represents the displacement of the cross-head and y-axis represents the load measured in Newtons. The rate of crosshead movement was 1 mm/min as per the ASTM standards. The initial portion of the loading curve in all figures represents an artifact caused by the take-up of slack and alignment or seating of the specimen. A linear curve follows after the artifact representing a linear increase in load till damage initiates represented by yield like curve. Then the loading curve suddenly drops significantly after the load has passed through a maximum, representing delamination as a result of discrete shear [111]. The small plateau following delamination indicates reloading of sample, however, the test was stopped and the sample was unloaded at this point as per the ASTM standards because the load drops below 30% of the maximum load.

The failure modes of all composite samples are seen to be almost identical indicating similar failure mechanisms. It is seen from the load-displacement curves that there is big difference in maximum load required for delamination for some specimens. However, it did not result in large differences in ILSS as shown by error bars in Fig. 34. This was due to difference in specimen sizes (b,h) that resulted in difference in load required for delamination. Daniels et al (1971) [111] studied about different failure mechanisms in the SBS test and classified the distinct failure modes from the load-deflection diagram.

Discrete shear failures were characterized by a single crack that may be flat, irregular or perhaps only at the side of the specimen corresponding to brittle behavior and showing sudden load drop similar to that seen in all of our specimens. It was

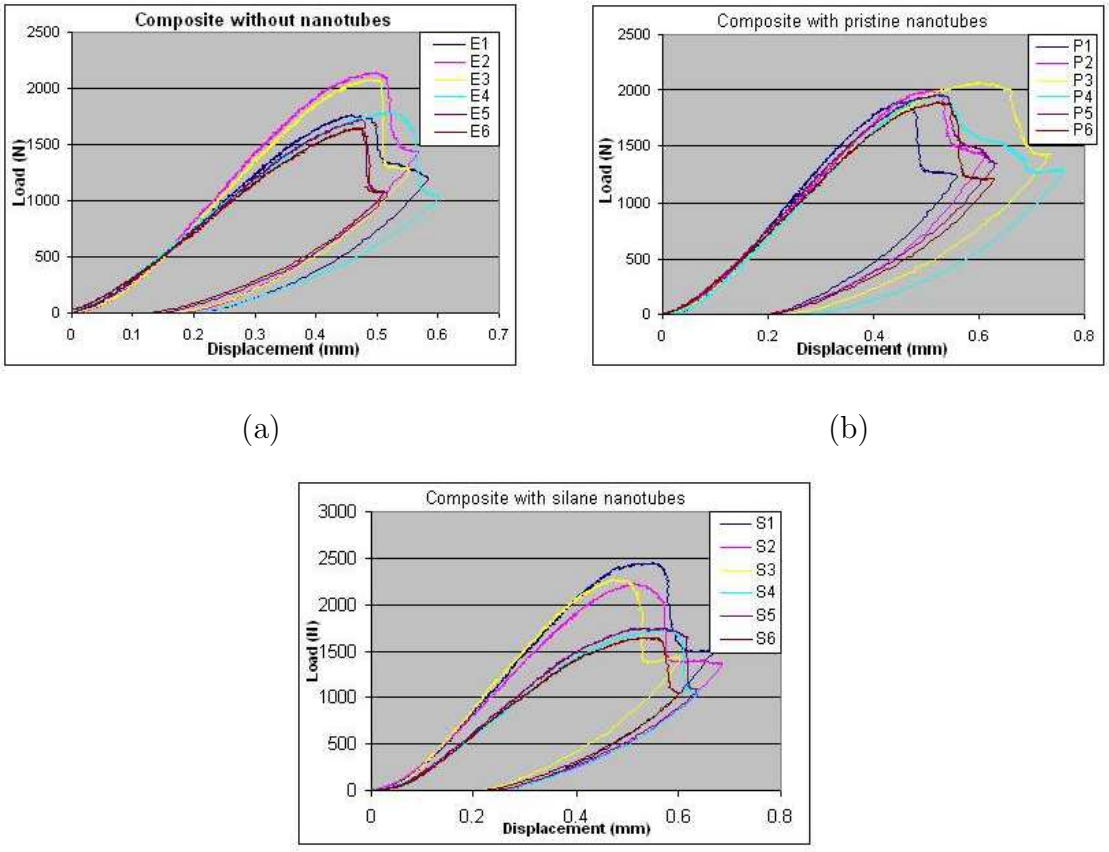

Fig. 33. Load-displacement curves showing different failure modes in SBS test specimens. 33(a) Failure modes in composite without nanotubes. 33(b) Failure modes in composite with pristine nanotubes. 33(c) Failure modes in composite with silane functionalized nanotubes.

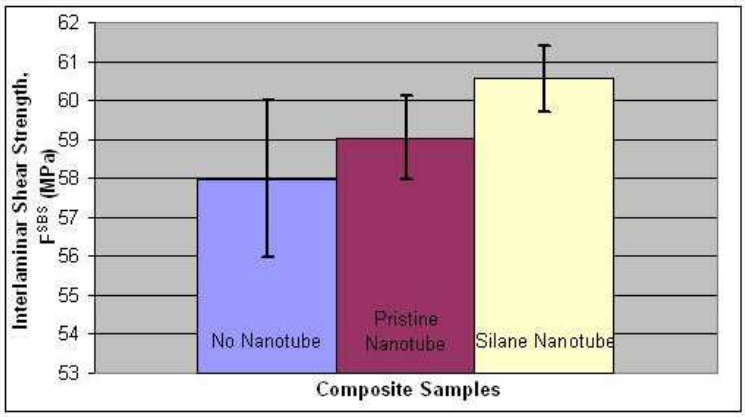

Fig. 34. Interlaminar shear strength for different composites as found from short beam shear tests.

also mentioned in the study that the compressive stress on the top surface under the loading nose could cause failure of the beam, presumably with an abrupt force drop. Therefore, the load-deflection diagrams in Fig. 33 indicate the possibility of failure due to discrete shear or compression or a combination of both. This observation from load-deflection curves is confirmed from the optical microscopy images in Fig. 35(a),36(a) and 37(a) as discussed later in this section. The white arrows in those figures represent compressive failure below the loading nose and the black arrows represent delamination due to discrete shear failure. Thus, the load-deflection curves imply that the results for the different composites can be compared due to similarity of failure modes. Fig. 34 below gives the comparison in short beam strengths for the different tested composites. The SBS strength is evaluated from eq.4.1. As illustrated from the results in Fig. 34, the interface modified with silane functionalized nanotubes provides the maximum improvement in interlaminar shear strength. The improvement was found to be about 4.4% over the baseline (no nanotubes) composite and about 2.6% over pristine nanotubes modified lamina. The coefficient of variation was 1.4% for the silane SWCNT samples. Comparatively, the improvement due to

pristine nanotubes was just about 1.8% higher as compared to the baseline composite. The coefficient of variation was 1.8% for the pristine SWCNT samples. Comparatively, the coefficient of variation for baseline samples was 3.6% respectively. The variation is shown in the form of error bars in Fig. 34. The coefficient of variations were comparable to those reported in literature [102, 103]. The numbers presented above does not indicate any strong trend towards significant improvement in ILSS.

Recently, similar results i.e. about 5% improvement in shear strength was reported by Qiu et al. [122] for multi-wall carbon nanotube integrated glass fiber/epoxy composites. Dean et al. [123] reported about 10 to 15% decrease in ILSS for silicate modified CFRP composites. Zhu et al reported 15% decrease in silane SWCNTs loaded glass fiber-vinyl ester composites without extra initiator or post cure treatment. An improvement of about 16% was reported by Wichmann et al. [67] for nanotubes modified glass fiber/epoxy composites. Nanofibrous membranes were incorporated in glass/epoxy composites by Liu et al.[124] and mechanical performance of laminates was found to be unaffected by using proper thickness of membranes. Thus our experimental results on the ILSS of the multiscale laminates seem to be consistent with the previous studies [67, 107, 121–123]. However, SBS test does not seem to provide enough information to reach a conclusion and optical microscopy of edges and scanning electron microscopy of delamination surfaces has be performed for thoroughness of screening process for these novel composites.

2. Mechanisms of Shear: Optical and Scanning Electron Microscopy

Optical microscopy was performed on the edges of the laminate after testing. Fig. 35 shows representative micrographs for a composite specimen without any nanotubes. The compressive failure under the loading nose is visible from Fig. 35(a) shown by white arrow. The interlaminar failure (delamination) along with transverse crack in

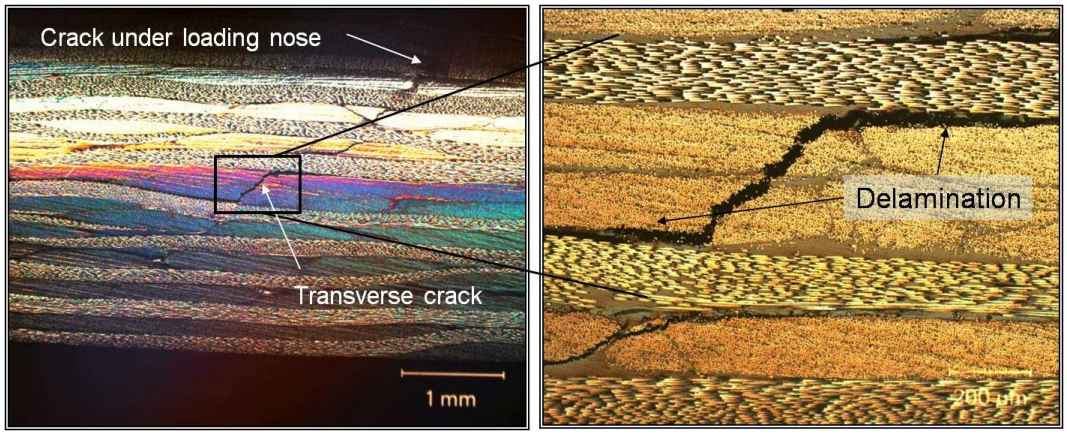

(a)

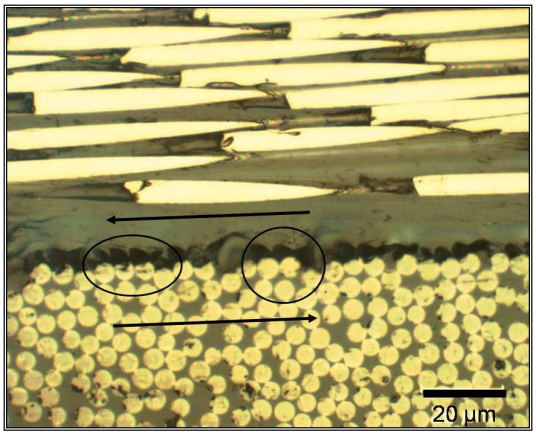

(b)

Fig. 35. Optical microscopy of SBS specimen without any nanotubes. 35(a) Edge of the specimen showing all laminae and failure modes. Magnified mid-plane shows transverse crack and delamination. 35(b) Close-up of delamination plane shows prominent shearing mechanism.

the mid-plane can be seen from Fig. 35(a) (black arrow). The magnified image of interlaminar failure as shown in Fig. 35(b), illustrates that the transverse fibers are sheared out of their cup like location in the matrix towards right side as shown inside marked ovals. This indicates that indeed the interlaminar failure was due to shear stresses. The micrographs in Fig. 36 provide images of a laminate edge with pristine nanotubes dispersed in mid-plane. The compressive failure under the loading nose is visible from Fig. 36(a) as shown by white arrow. The interlaminar failure (delamination) along with transverse crack in the mid-plane can be seen from Fig. 36(a)(black arrow). The magnified image of interlaminar failure is shown in Fig. 36(b). It illustrates that the transverse crack ends at the interface and delamination starts from that point (shown by black arrow). The longitudinal fibers show clean surface showing complete delamination. Fig. 36(c) shows the scanning electron microscopy image taken from one edge of the delaminated surface of this composite. It clearly shows the presence of nanotubes on the fracture surface indicated by arrows. The tight nanotubes shows bridging mechanism by nanotube ropes. Fig. 37 shows the optical micrograph of an edge of a composite with silane functionalized nanotubes in the mid-plane. The failure mode is consistent with the other tested samples as above i.e. the compressive failure below the loading nose (white arrow) but fewer transverse cracks and delamination (black arrow). One interesting comparison between Fig. 35(a),36(a) and 37(a) shows that the amount of damage (number of cracks) visible in Fig. 37(a) is comparatively less. The close-up of the crack in the mid-plane indicates that the crack is passing through the transverse plane away from the interface. Thus, the results indicate the presence of significant amount of matrix on the longitudinal fiber surface. This behavior was also observed in the SEM images after opening the mid-plane of the laminate as shown in Fig. 32(c). The complex matrix fracture surface is seen on the samples with silane functionalized nanotubes and the

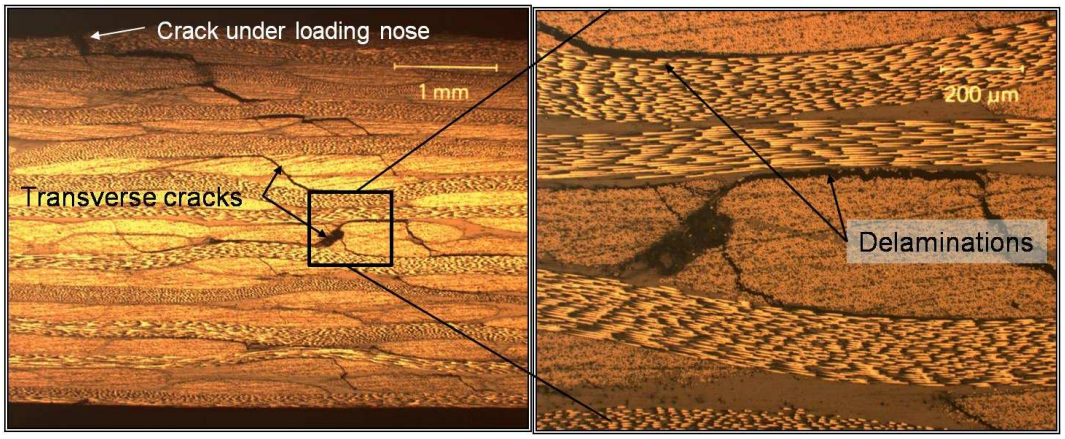

(a)

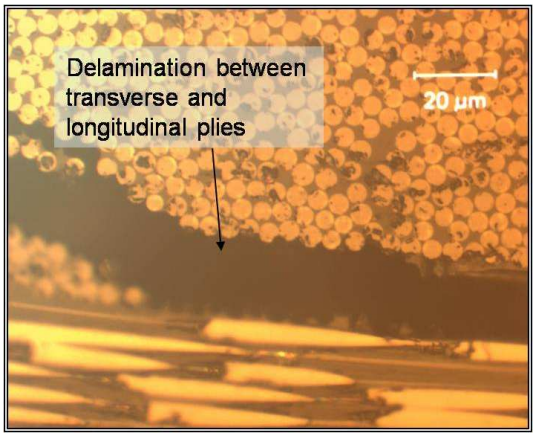

(b)

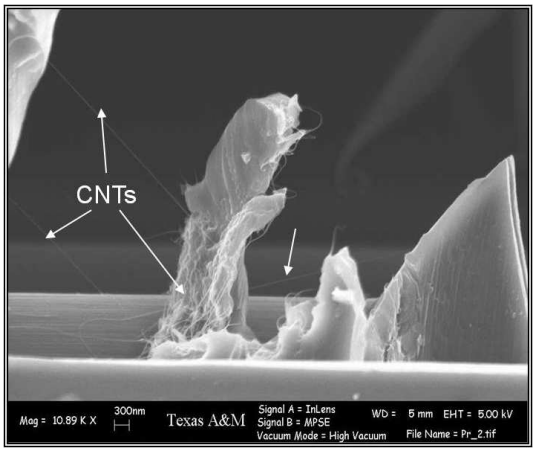

(c)

Fig. 36. Optical and scanning electron microscopy of SBS specimen with pristine nanotubes. 36(a) Edge of the specimen showing all laminae and failure modes. Magnified mid-plane shows transverse cracks and delaminations. 36(b) Close-up image shows transverse crack leading to interlaminar failure.36(c) SEM image of delamination plane shows bridging mechanism by nanotube ropes.

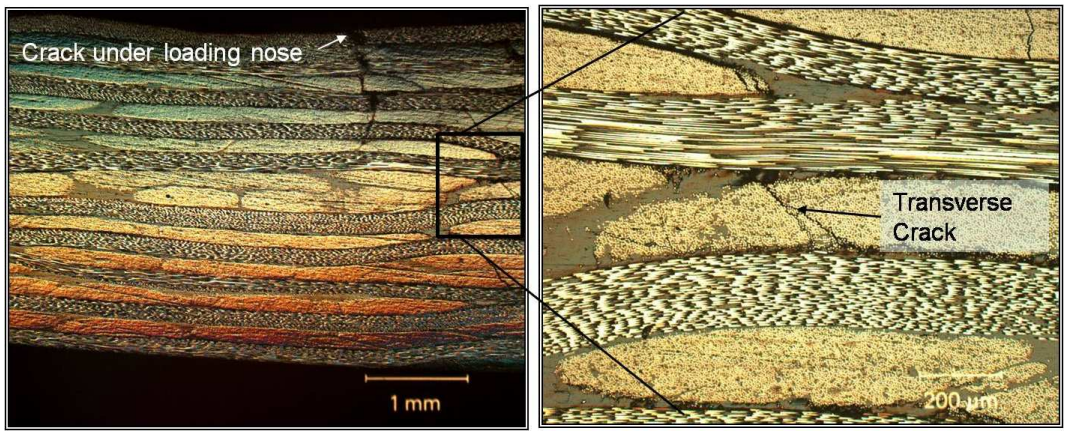

(a)

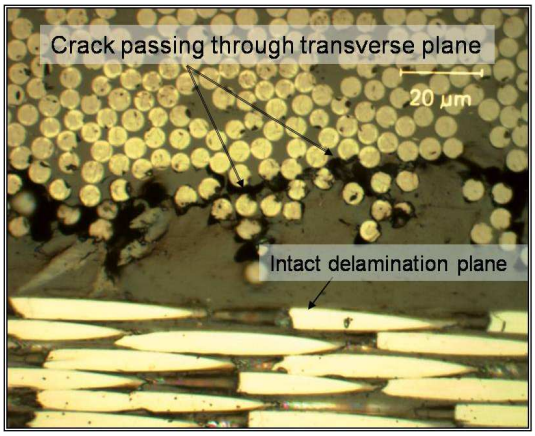

(b)

Fig. 37. Optical microscopy of SBS specimen with silane functionalized nanotubes. 37(a) Edge of the specimen showing all laminae and failure modes. Magnified mid-plane shows a transverse crack. 37(b) Close-up image shows crack passing through transverse plane avoiding delamination.

nanotubes are not visible as in composite with pristine nanotubes.

The SEM images in Fig. 32(c), showing matrix bonded with carbon fabric and the corresponding optical microscopy images in Fig. 37(b) showing the intact interface and crack passing through transverse fiber plane indicate that the silane functionalized nanotubes resulted in a better fiber-matrix interface. This can also be inferred from the small increase in interlaminar shear strength for this sample. Similar understanding can be seen from propositions made by several authors [67, 102, 103, 107, 121, 122]. Thus the use of functionalized nanotubes has clearly caused a change in the delamination process as observed from optical micrographs and SEM images. It was also observed that the number of cracks formed in specimen with functionalized nanotubes were comparatively less than observed on the edges of composites without functionalized nanotubes. It indicates retardation of matrix crack onset and damage accumulation in composites with functionalized nanotubes. Similar results have been observed recently by Yokozeki et al. [107] for cup-stacked carbon nanotubes-CFRP composites.

Although, shear is the dominant load in this test method, the internal stresses are complex and a variety of failure modes can be seen. The effects of weave pattern and constraints of adjacent layers are among few causes that are responsible for complex stress states. Elasticity solutions by Berg et al. [110], Whitney [115, 116], and Sullivan and Van Oene [114] have demonstrated inadequacies in classical beam theory in defining the stress state in the short beam configuration. These solutions show that the parabolic shear stress distribution as predicted by eq. 4.1 only occurs, and then not exactly, on planes midway between the loading nose and support points. Away from these planes, the stress distributions become skewed, with peak stresses occurring near the loading nose and reaction/support noses. The stress state local to loading nose is of particular importance in which the stress concentration combined

with transverse and in-plane compressive stresses has been shown to initiate failure. Thus SBS strength determined from this test cannot be just attributed to a pure shear property. SBS test method by itself does not seem to be a good screening test showing little difference in different composite specimens. However, optical microscopy and SEM results showed enhanced fiber-matrix interface due to functionalized nanotubes and indicated possibility of significant effect on interlaminar fracture toughness. Thus SBS tests in conjunction with optical microscopy of edges and SEM for fractured delamination surfaces can serve as a good materials screening method before moving on to more complex testing methods.

3. Interlaminar Fracture Toughness

a. Force-Displacement Response

The comparison of the delamination initiation and the delamination propagation as observed from the force-displacement curves is shown in Fig. 38(a) for representative specimens taken from the same area of the laminate from three different panels. The large unstable delamination growth behavior identified by a sudden drop in force (more than 50% of the peak force) from point A to B, as shown in Fig. 38(a), was observed only in the panel with functionalized nanotubes. The force drop results from a delamination extension of about 30 mm (point A to B) as seen from Fig.38(b). Usually, the unstable delamination growth behavior shows about 3 to 5 mm delamination extension [88, 125] resulting in about 8 to 15% drop from the peak force. The reasons for the large unstable delamination growth behavior in the specimens with functionalized nanotubes have been discussed in Section 4.2. Fig. 39 shows the force-displacement curves for six specimens from individual panels along with the average force-displacement curve (shown by a dark curve) for that particular panel.

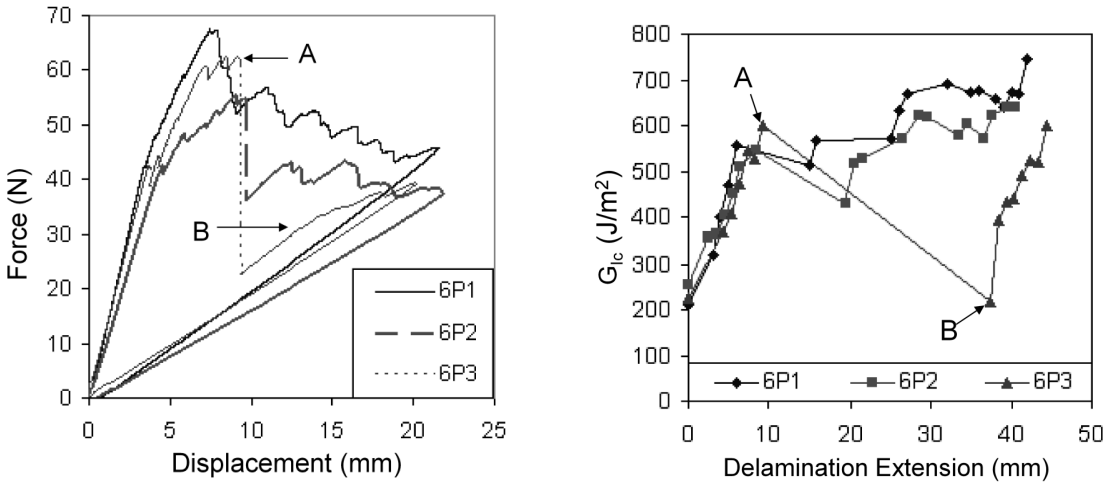

(a) (b)

Fig. 38. Representative graphs for one specimen each from 3 panels: 6P1-No nanotubes, 6P2-Pristine nanotubes, 6P3-Functionalized nanotubes. 38(a) Force-displacement curves, 38(b) R-curves (resistance curves).

The initial response for all specimens was linear until the delamination initiation. The linear response was followed by a combination of stable and unstable delamination growths. The stable response was represented by a gradual decrease in force with delamination growth. The unstable response has been characterized by sudden drop in force with delamination growth. Fig. 39(a) shows gradual decrease in force with increasing load-point displacement for all specimens from panel P1 (base laminate with no nanotubes). The difference (33%) in slope of the linear region for specimen 6P1 is due to the difference in initial delamination length which was about 6 mm shorter as compared to the average of the rest of the specimens. The slope of the linear regions overlapped for all specimens from panel P2 (pristine nanotubes). Specimen 5P2 seems to be an outlier as it is the only specimen showing large force drop (50%) out of total six specimens. From Fig. 39(c), the difference in the slope of the linear region between specimens 1P3-2P3 and specimens 3P3 to 6P3 is largely due to

the difference in initial delamination lengths. A difference of around 2.5 mm in initial delamination lengths resulted in about 17% difference in slopes. If the displacement is normalized with respect to initial delamination length ($\delta/(a_0)^3$) for the linear region then the effect of 'a' disappears from the linear slope. Large force drops (50% to 70%) were consistently observed in all specimens with functionalized nanotubes, as shown in Fig. 39(c). As can be seen from Fig. 39(c) and Fig. 39(d), large unstable delamination growth represented by force drops of about 30 to 40 N was the characteristic behavior of the panel with functionalized nanotubes as observed from the large force drops. The average drop in force is about 50% of the peak force as shown in Fig. 39(d) for the specimen with functionalized nanotubes. The average initial delamination length for the panel with functionalized nanotubes was 46 mm and for the panel without nanotubes was 46.5 mm. A small difference of 0.5 mm in initial delamination lengths resulted in about 12% difference in slopes of the linear region of average force-displacement curve and about 5% difference in slopes if the displacement is normalized with delamination length. The slope is also a function of the cube of the arm thickness, along with other differences such as specimen width, arm modulus, fiber volume fraction which can cause the difference in the initial slopes. An increase of about 6% is found in the average delamination initiation force for the panel with pristine SWCNTs over the panel without SWCNTs (with 2% coefficient of variation). The increase in case of the panel with functionalized SWCNTs is about 14% over the panel without any nanotubes, having about 5% coefficient of variation. The coefficients of variations are very small compared to values in the literature [66, 75, 81, 88, 126, 127][16, 25, 31, 47-49] (about 10 to 15%) indicating consistency in the processing technique and repeatability of the testing method.

The area under the force-displacement curve represents energy absorbed during the overall delamination growth. Fig. 39(d) represents comparison of the average of

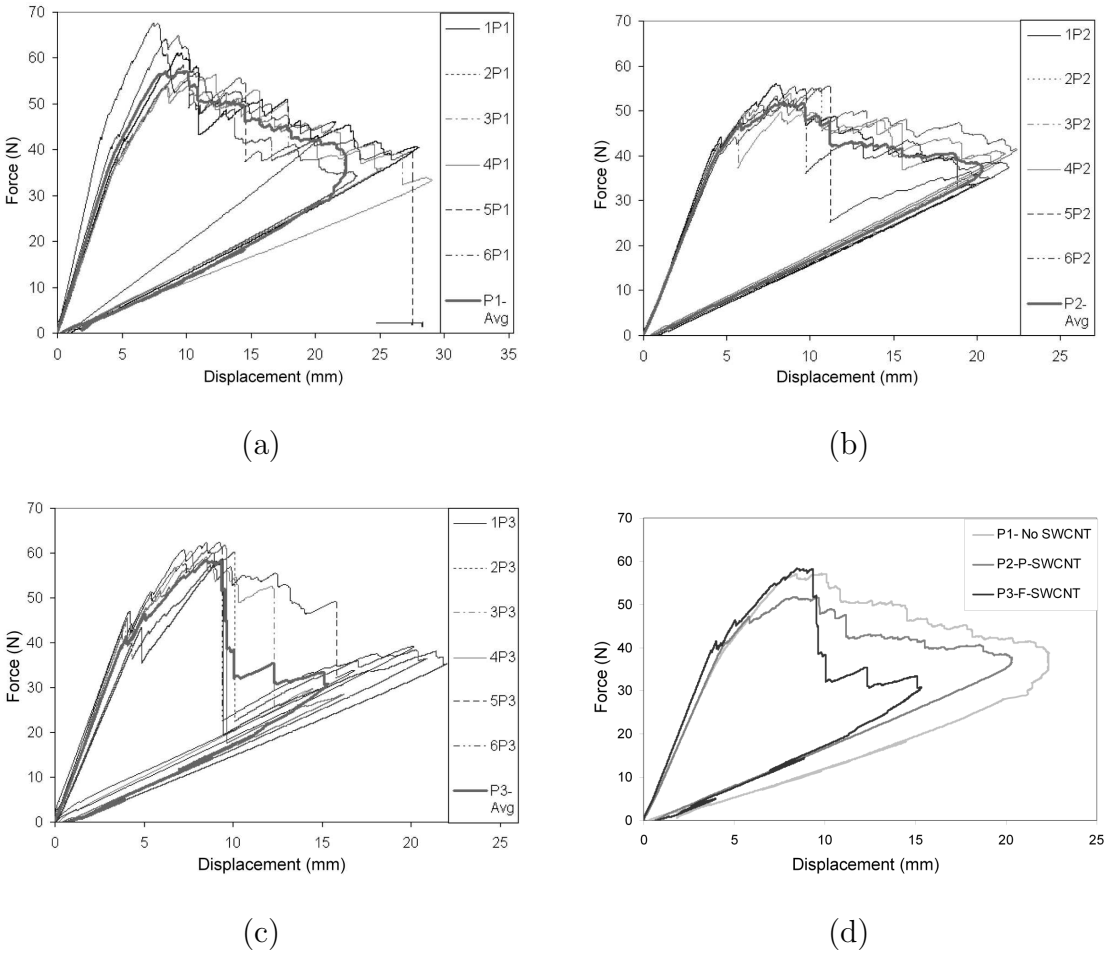

Fig. 39. Force-Displacement curves for all panels. 39(a) P1: No-SWCNT, 39(b) P2:Pristine SWCNT, 39(c) P3: Functionalized SWCNT, 39(d) Average curves.

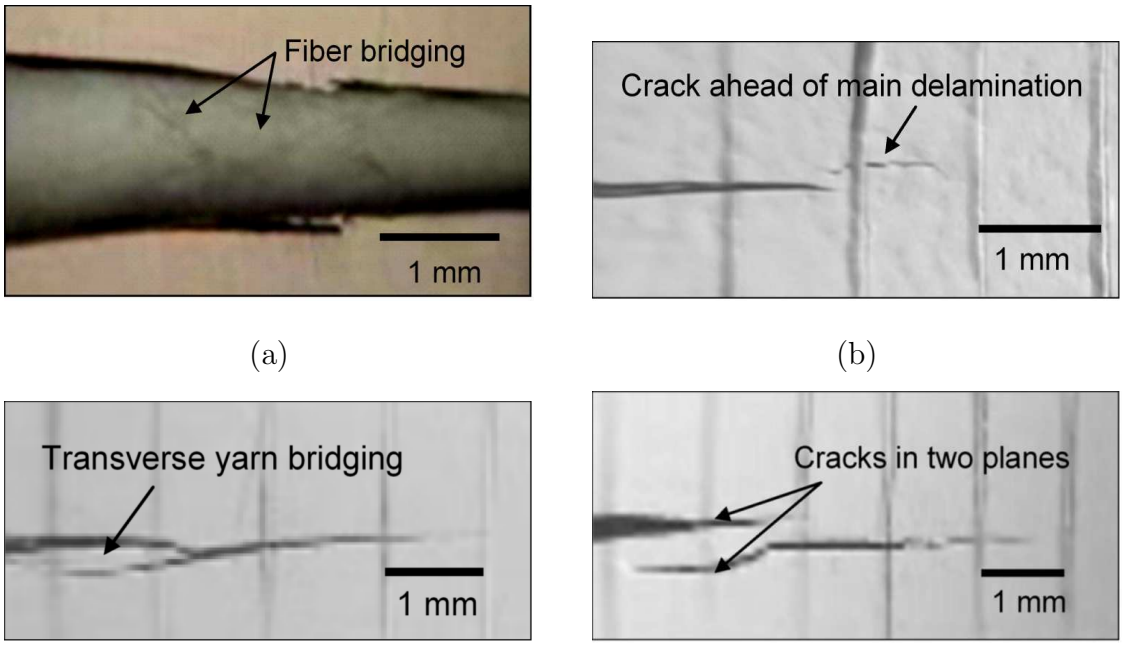

Fig. 40. Crack propagation mechanisms. 40(a) Crack initiation in front of crack tip, 40(b) Cracks in two planes, 40(c) Transverse yarn bridging, 40(d) Fiber bridging.

the force-displacement behavior for all panels. The area under the curve for panel with functionalized nanotubes is the lowest followed by panel with pristine nanotubes and panel without nanotubes showed comparatively largest area under the curve. This observation is consistent with the R-curve behavior discussed later in this section, which shows lowest propagation G_{Ic} for panel with F-SWCNTs followed by panel with P-SWCNTs and highest propagation G_{Ic} for panel without nanotubes. The delamination initiation is followed by a small sudden drop in force for all specimens. The delamination growth was visually observed at this point from the edge of the specimen thus releasing the stored energy to create new fracture surfaces. For all specimens, the initial small force drop or variation from linearity (i.e. change in slope) was followed by an increase in force till a peak. The increase in force corresponds to the presence

of fiber bridging, yarn bridging, ply bridging or a combination of these mechanisms as observed in Fig. 40. Similar characteristics were observed in woven composites by Paris et al. [88], Alif et al. [125] and Martin [128] and is termed 'ratchetting' by Martin [128]. The ratchetting of the force-displacement curve represented stick-slip propagation of the crack. The slip portion on the force-displacement response represents the delamination growth until the delamination comes to an arrest. This stick portion of the force-displacement response corresponded to fiber/yarn bridging mechanisms observed from the edge of the specimen. Sometimes an additional delamination appeared in the front of the existing delamination, tip as shown in Fig. 40(a), and grew backward around the transverse yarn. On other occasions, delamination appears to be on an adjacent plane as shown in Fig. 40(b). Similar observations were made by O'Brien et al. [88] and Alif et al. [125]. The stick portion was followed by a slip portion on the force-displacement curve represented by sudden drop in force (unstable crack growth). The slip portion of the force-displacement curve corresponded to the breakage/pullout of the bridging fibers or tows in the delamination plane (Fig. 40(d)) or debonding of the transverse yarns as shown in Fig. 40(c). Such features from Fig. 40 represent some of the mechanisms of energy dissipation. The images from Fig. 40 are taken from representative specimens from all panels and such features were common in specimens from all panels irrespective of its constitution i.e. irrespective of the presence or absence of nanotubes. The delamination extensions corresponding to slip portion were about 2 to 7 mm for the panel without nanotubes (Fig. 41) and the panel with pristine nanotubes (Fig. 42), which is quite similar to that observed in woven composites [88]. However, large slip behavior with corresponding delamination extension from 20 to 30 mm was observed in specimens from the panel with functionalized nanotubes (Fig. 43).

It is important to point out that all three panels (P1, P2, and P3) from a single

batch were processed together at the same time under exactly same processing conditions in the same VARTM set-up. Similar processing conditions were also maintained for the second batch of all three panels. The large stick-slip behavior (20-30 mm crack growth) was observed in most of the specimens from the panel with functionalized nanotubes, and from that panel only. Hence, it is indicated that this behavior has some relationship with functionalization of the nanotubes, and not with the processing conditions, since they were maintained consistently for all panels. It is discussed further in the section with respect to the observed delamination fracture surfaces by using SEM fractography.

b. Strain Energy Release Rate Measurements

The delamination extensions were noted from a marked scale on the edge, with 1 mm markings during various increments of stable delamination growth. In cases where growth was unstable, the delamination length corresponding to the beginning and end of the unstable period were recorded.

R- Curves for all tested specimens are shown in Fig. 41 to Fig. 43. These curves show the change in the strain energy release rate of the specimen as the initial delamination starts growing from the end of a PTFE insert and propagates through the specimen. A non-linearity criterion is used to calculate the initiation values for the critical strain energy release rates which are considered as the interlaminar fracture toughness values for different laminates. According to the non-linearity criterion [88], force and displacement values corresponding to first deviation from linearity on the force-displacement curve is considered as the critical values for initiation of delamination growth. The average values of initiation G_{Ic} for six specimens from each panel are presented in Table VII. The results show a 6% increase in average initiation G_{Ic} for the panel with pristine nanotubes over the panel without any nanotubes. This

Table VII. Average G_{Ic} at delamination initiation for woven CFRP composites

Panel Number	G_{Ic} Initiation (J/m^2)	CoV (%)
P1: No SWCNT	230.5	8
P2: Pristine SWCNT	245 5	5
P3: Functionalized SWCNT	231.8	9

difference lies just beyond the coefficient of variation of initiation values of G_{Ic} for the specimens with pristine nanotubes. This suggests some statistical significance to the observed increase in initiation G_{Ic} of the specimens containing pristine nanotubes. The corresponding increase in average initiation G_{Ic} for the panel with functionalized nanotubes is negligible over the panel without any nanotubes with about 8% coefficient of variation which is still lower than the reported coefficient of variation (around 14%) in literature by Martin [128], Choi et al. [61] and Paris et al. [88].

R-curves for all specimens from the panel without nanotubes are shown in Fig. 41. It shows that the G_{Ic} increases for about 7 to 10 mm of delamination growth, after which it plateaus and the delamination continues with small stable and unstable growths without significant increase or decrease in G_{Ic} values. Similar behavior was also observed for the panel with pristine nanotubes as shown in Fig. 42. The initial increase in the G_{Ic} before the plateau has been due to the fiber bridging mechanisms. The small drop after the peak G_{Ic} was observed due to breaking of bridging fibers.

Fig. 43 shows that the G_{Ic} increases almost linearly until a sudden drop in G_{Ic} with very large delamination extension. The delamination extension of about 20 to 30 mm was observed for five specimens out of total six specimens. For two specimens, the G_{Ic} starts to increase again after large delamination extension. In other specimens, the specimen length was not sufficient to be able to again notice the sta-

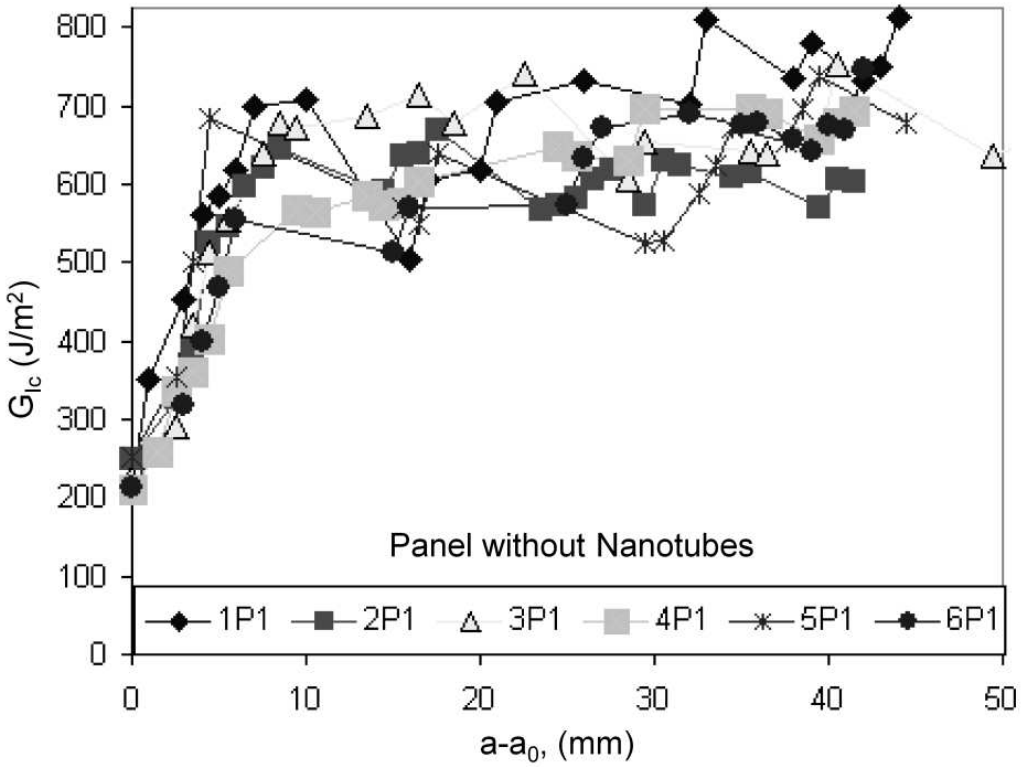

Fig. 41. R-Curves for 6 specimens from panel without any nanotubes (P1).

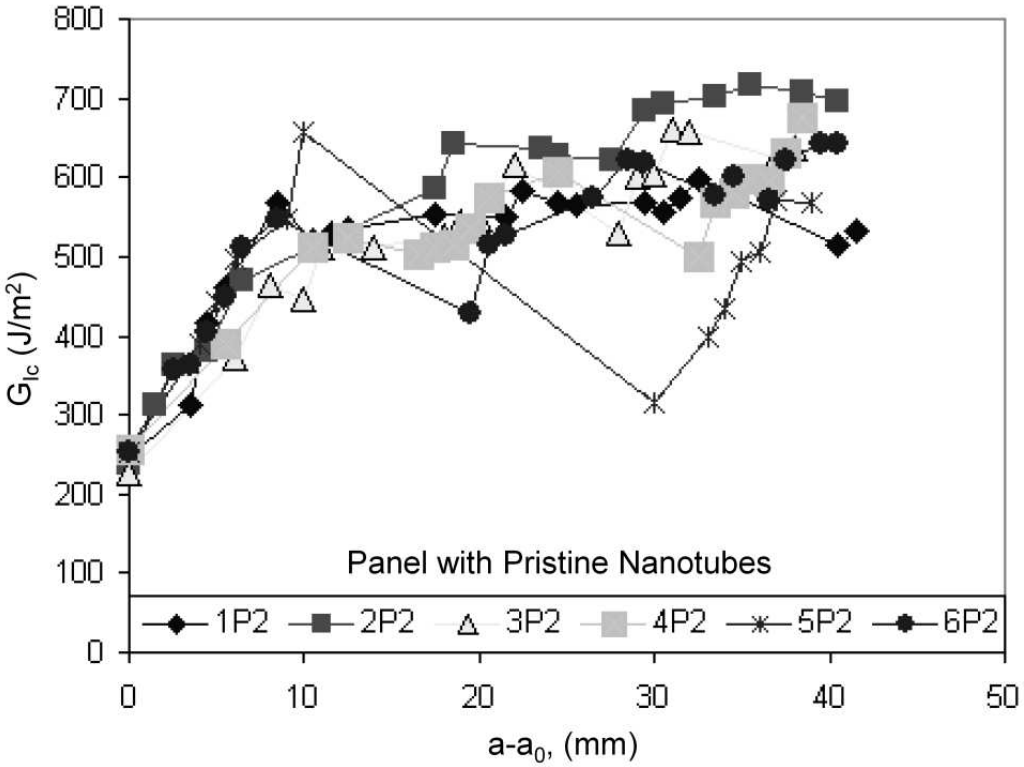

Fig. 42. R-Curves for 6 specimens from Panel 2 with pristine SWCNTs (P2).

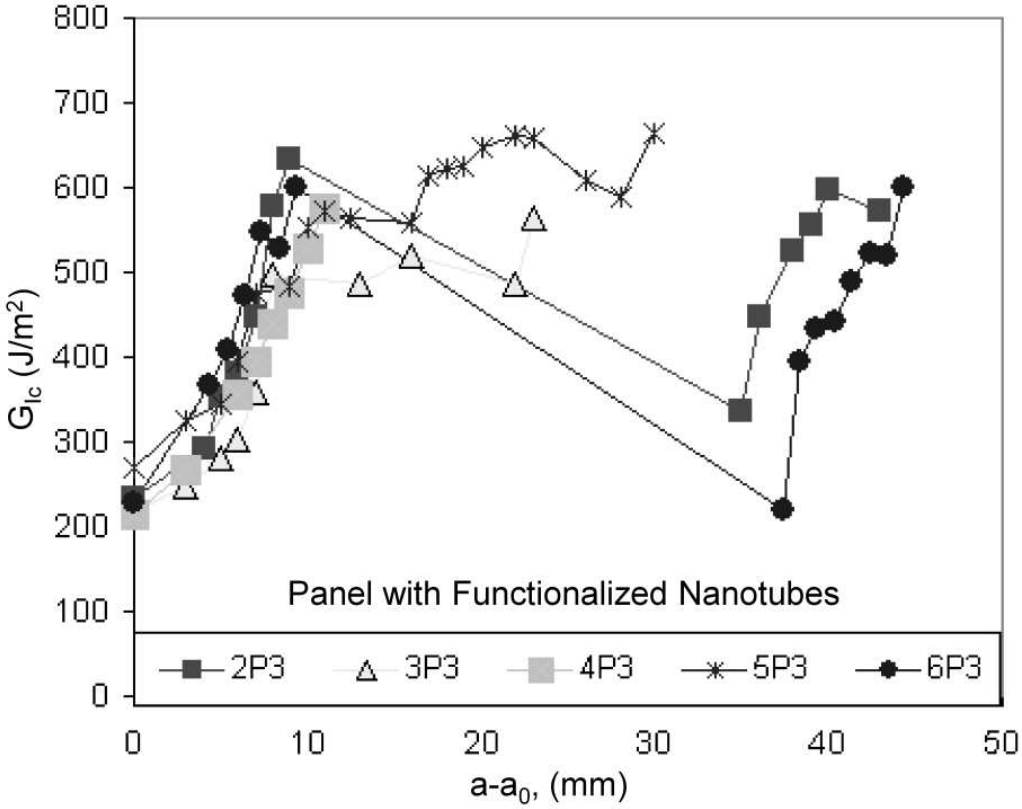

Fig. 43. R-Curves for 6 specimens from Panel 3 with functionalized SWCNTs (P3).

ble delamination extension. Such peculiar behavior of large delamination extension could be due to many reasons such as inhomogeneous distribution of nanotubes on the plane of lamina, smaller aspect ratio of nanotubes, suppression of fiber bridging mechanisms due to smaller length of nanotubes, etc. Tong et al. [129] presented numerical results revealing that the nanotube's length, density, and maximum pull-out displacement as well as the interfacial friction shear stress are important parameters affecting the delamination toughness. Especially the interlaminar fracture toughness might reduce with shorter length nanotubes. The fiber bridging mechanisms would also be suppressed due to shorter nanotube lengths. Smaller nanotubes also creates a possibility for the nanotubes to escape from the mid-plane to the adjacent planes of plies during the VARTM process resulting in poor distribution in the mid-plane resulting in observed large unstable crack growths. The average R-curve behavior for all specimens from three distinct panels is shown in Fig. 44. Values of G_{Ic} for every 2 mm of delamination extension were averaged for each panel and the average G_{Ic} data points were plotted. Polynomial curve fitting was utilized to fit these data points to get the average R-curve response for each panel.

The purpose of plotting average G_{Ic} values was to compare the general trend of crack growth in different panels. It has been seen from Fig. 44 that initiation G_{Ic} values for all the panels were very similar. However, propagation G_{Ic} values have been found to be lower for the panel with pristine nanotubes compared to the base laminate panel without nanotubes, and the plateau represented stable propagation unlike the curve for the panel with functionalized nanotubes.

The large unstable crack propagation behavior has been observed by the absence of a plateau in the propagation region for the panel with functionalized nanotubes, as shown in the Fig. 44. The propagation G_{Ic} value was not possible to calculate for this panel due to the large unstable crack propagation, and hence, insufficient

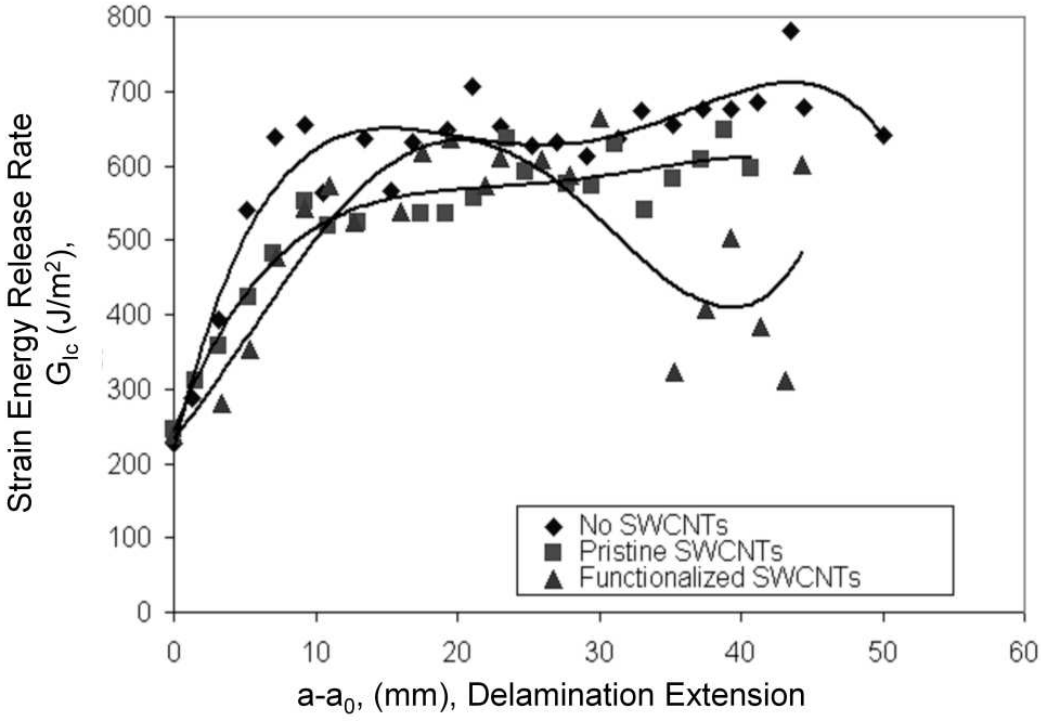

Fig. 44. Average R-curves for woven composites. Average G_{Ic} values calculated per 2 mm of crack extension and curve fitting through average G_{Ic} indicating trend of crack growth for each panel.

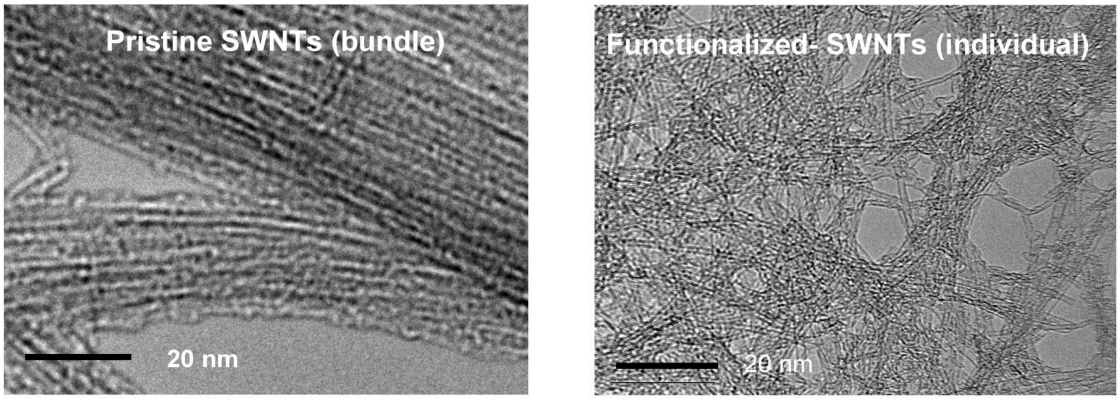

(a) (b)

Fig. 45. TEM images showing (a) Pristine SWCNTs and (b) Functionalized SWCNTs.

number of data-points. However, the peak G_{Ic} value for the panel with F-SWCNTs has been observed to be close to the propagation value for the base laminate panel and higher than the panel with P-SWCNTs. This indicates a possibility of achieving improvement in propagation G_{Ic} for the panel with F-SWCNTs compared to that with P-SWCNTs, provided the delamination propagation can be stabilized.

4. Mechanisms of Delamination: SEM Fractography

Microscopic investigation of the delaminated surfaces was performed using scanning electron microscopy (SEM) and transmission electron microscopy (TEM) for understanding the mechanisms of crack initiation and propagation [87]. Fig. 45 shows the TEM micrographs of pristine and silane functionalized nanotubes. Pristine nanotubes consisted of an agglomeration of nanotubes resulting from Van der Waals interaction resulting in larger bundle diameters. The functionalization process resulted in better dispersion with smaller nanotube bundle diameter and shorter lengths, in addition to better bonding with epoxy matrix [5, 8]. SEM images were taken at various low and high magnifications such as 20X, 100X, 5000X and 10000X at the locations shown

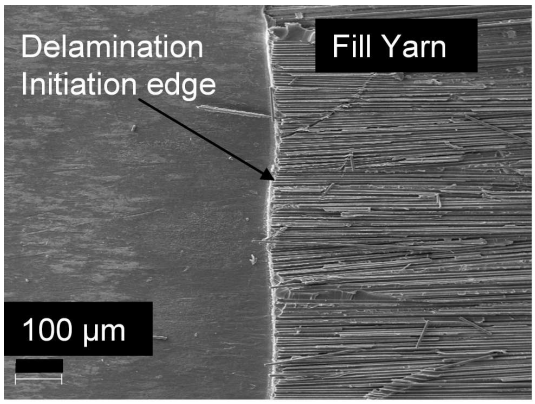

(a) 0 mm (Delamination initiation)

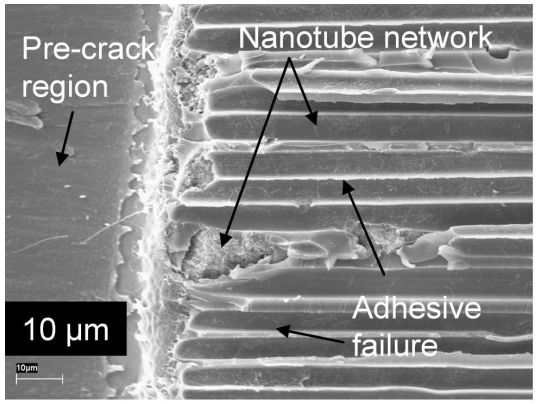

(b) 0 mm (Delamination initiation)

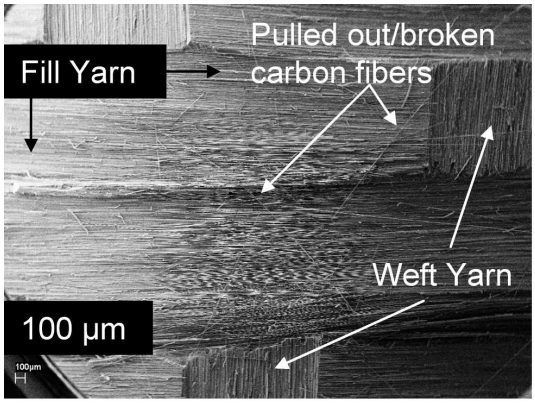

(c) 20 mm from delamination initiation

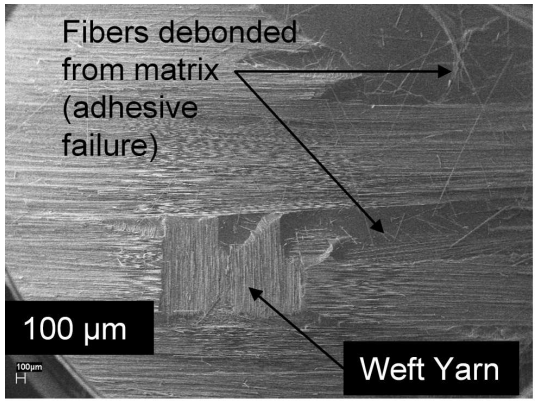

(d) 30 mm from delamination initiation

Fig. 46. Low magnification SEM images of the delamination surface from the panel with pristine SWCNTs.

in Fig. 30, distanced from the starter crack (end of PTFE insert). SEM images are included for samples 1P2 and 2P3, as a representation of samples with pristine nanotubes and functionalized nanotubes, respectively. The results will be presented first for the sample with pristine nanotubes at low then high magnification, followed by results for the sample with functionalized nanotubes also at low then high magnification. Fig. 46(a) and 46(b) includes the SEM images at low magnification of the crack initiation for the 1P2 sample. Fig. 46(a) shows mostly carbon fibers in fill yarn while Fig. 46(b) shows carbon nanotube network at the delamination initiation site

and also on fiber-matrix debonded surfaces. A few fibers can be seen pulled out or broken and fill/weft yarns are also seen without matrix coating. Fig. 46(c) and 46(d) shows the SEM images at 20 and 30 mm from the delamination initiation. The pattern is very similar to that of the delamination edge marking consistent behavior over the delamination process. These images point to adhesive failure (i.e. and failure of adhesion at fiber-matrix interface), in which there is a relatively clean separation between the fiber and the matrix. Fig. 47 shows the surfaces of specimen 1P2 at high magnification. These images show the presence of nanotube bundles on the fabric surface in the form of a network distributed over the fabric surface. The nanotubes form a network which is visible at both the carbon fiber surfaces and on the carbon fiber impressions as shown in Fig. 47(a) and Fig. 47(b) respectively. The presence of nanotubes on the carbon fibers (Fig. 47(a)) and the carbon fiber impressions on matrix (Fig. 47(b)), and the absence of a continuous matrix layer covering these carbon fibers indicate fiber-matrix debonding, further supporting that adhesive failure is the key contributor to the delamination mechanism. However, the presence of long nanotubes of about a micron to few microns also indicated potential for fiber bridging and crack bridging mechanisms that could contribute to an increase in fracture toughness [129]. This mechanism was corroborated by Fig. 47(c) which showed nanotubes dangling from epoxy separated from carbon fiber (as indicated by white ellipse). In Fig. 47(c), the dangling nanotubes were either broken or pulled out of the matrix. The images of fracture surfaces of the pristine nanotubes sample indicated fracture mechanisms which might have lead to the small increase in fracture toughness. As indicated by SEM images in Fig. 46 and 47, the crack propagated through the nanotube network leaving some nanotubes on the carbon fibers (Fig. 47(a)) as well as on the matrix (Fig. 47(b)). Disentanglement of nanotube bundles and broken or pulled out nanotubes as seen in Fig. 47(c), indicated mechanisms for energy dissipation, that

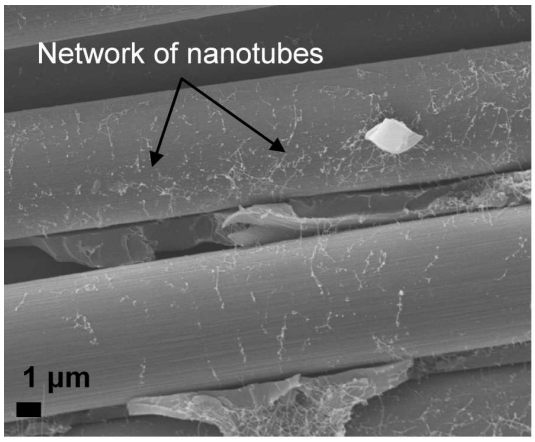

(a) Pristine SWCNTs on carbon fibers forming entangled network

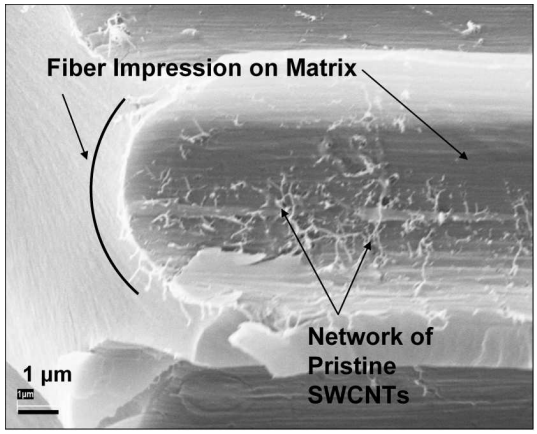

(b) Pristine SWCNTs on matrix impression after fiber debonded from the surface showing poor fiber-matrix bonding

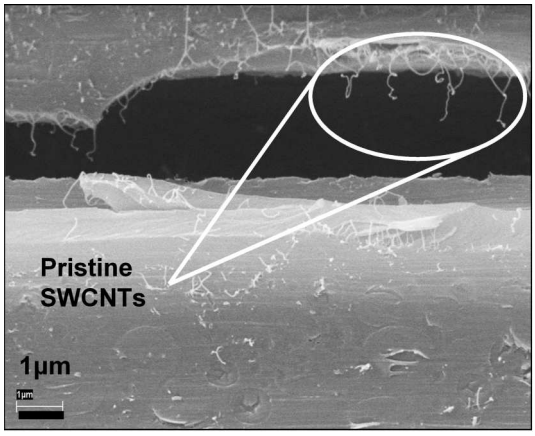

(c) Pulled out/ broken SWCNTs after crack bridging

Fig. 47. SEM images of observed mechanisms in the panel with pristine SWCNTs.

could lead to increased fracture toughness. Secondly, the pristine nanotubes were mostly found on the surfaces of either the fiber or the matrix indicating poor bonding. This poor affinity could be a result of the absence of a chemical functional group on the pristine nanotubes. Therefore the effect of pristine nanotubes on the matrix properties might be insignificant. This observation supports the DCB results, from which it has been observed that the load displacement curves follow approximately same shape as base laminate without nanotubes. Only one curve shows unstable crack extension of about 20 mm and may be an outlier due to uneven distribution of nanotubes resulting in enough interaction of a cluster of nanotubes with epoxy matrix to delay the crack propagation. Fig. 48 includes low magnification images for sample 2P3, which contains the functionalized nanotubes. The images in Fig. 48(a) and 48(b) show the delamination initiation edge. Fig. 48(c) includes an image taken 10 mm from the delamination initation, and Fig. 48(d) is taken at 30 mm from the delamination initiation. These images, like those for the samples with pristine nanotubes, show some broken or pulled out carbon fibers at the surface. However, these images also show bands of epoxy which span large portions of the images which have smooth surfaces. The presence of the functionalized nanotubes therefore facilitates a combination of adhesive failure at the fiber-matrix interface, and cohesive failure through the epoxy as shown in the images. Fig. 48(d) indicating smooth matrix surface at approximately 30 mm from the delamination initiation edge for specimen 2P3 confirms brittle crack propagation as observed from Figure 10 representing sudden decrease in G_{Ic} and large delamination extension. Fig. 49 includes SEM images at high magnification of a specimen with functionalized nanotubes. Areas in which the matrix material remains on the fiber after the crack passed through the matrix are visible in Fig. 49(a). This intact fiber-matrix interface is further evidence of cohesive failure. It has been observed in Fig. 49(b) and 49(c), that the functionalized

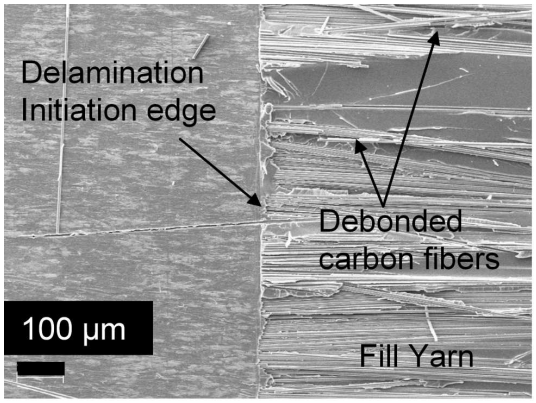

(a) 0 mm (Delamination initiation)

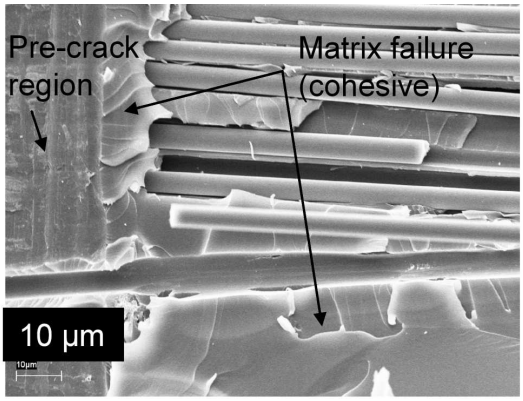

(b) 0 mm (Delamination initiation)

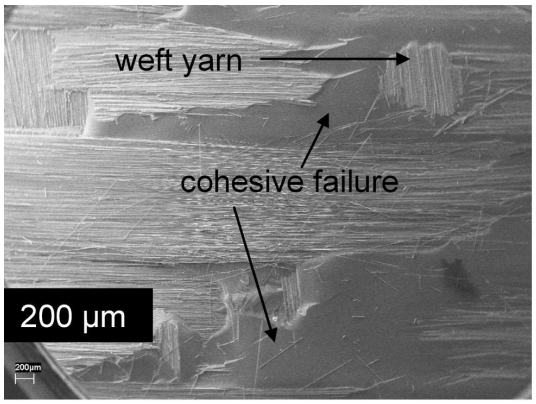

(c) 10 mm from delamination initiation

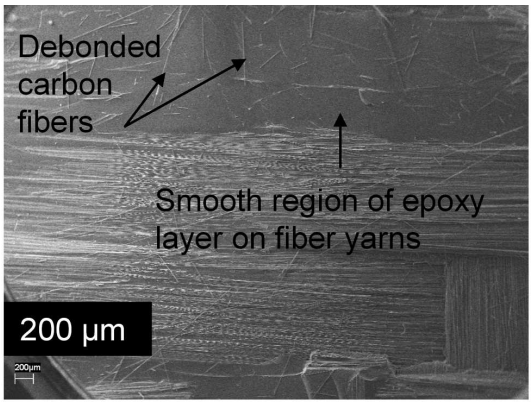

(d) 30 mm from delamination initiation

Fig. 48. Low magnification SEM images of the delamination surface from the panel with silane functionalized SWCNTs.

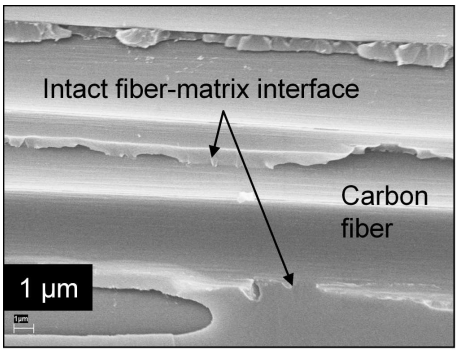

(a) Remnant matrix on the ply surface

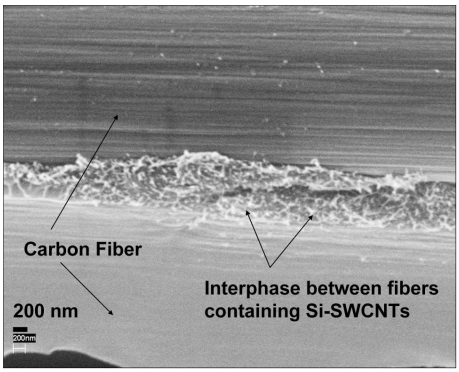

(b) Functionalized SWCNTs forming an interphase region between two carbon fibers

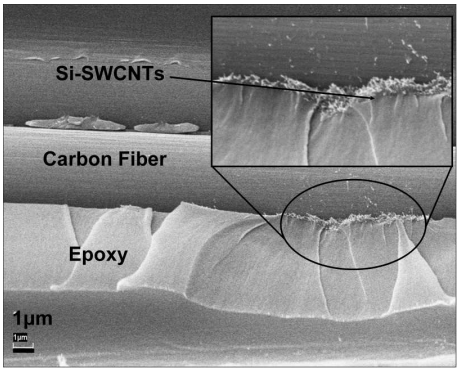

(c) Enhanced fiber-matrix bonding where nanotubes are present

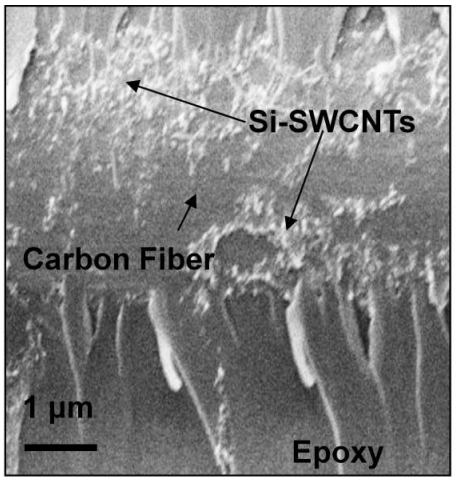

(d) Microcracks pattern due to better bonding between matrix and carbon fiber as a result of silane functionalized SWCNTs

Fig. 49. SEM images of observed mechanisms in the panel with silane functionalized SWCNTs.

nanotubes are sparsely scattered on the fibers as well as matrix, indicating inhomogeneous distribution. In fact, very few nanotubes were visible on the fracture surface, and not in the form of an extensive network as in the case of samples with pristine nanotubes. Due to the chemical functionalization process, the nanotubes were typically cut short in length due to acid reaction, as well as debundled into smaller ropes of nanotubes. In Fig. 49(b), a nanotube rich region has been observed between two carbon fibers. Here the nanotubes were spread throughout the epoxy matrix between the fibers indicating better dispersion of nanotubes and compatibility with the epoxy matrix. It also indicated that the carbon fiber-epoxy matrix bonding has been improved by the presence of nanotube rich interphase region. Another location that the nanotubes are visible is between the carbon fiber and the matrix (Fig. 49(c)) where their ends are visible protruding out from the edge of the epoxy.

In Fig. 49(c) and 49(d), microcracks are initiated near nanotube rich areas which are very different from the rest of the fracture surface where nanotubes were not present. Fig. 49(b) and Fig. 49(d) indicating nanotube rich regions and better fiber-matrix bonding are taken from a region which is approximately 10 mm away from the delamination initiation edge for specimen 2P3. These images are taken from the vicinity of the peak G_{Ic} value just before large delamination extension. So these images can be correlated to the particular G_{Ic} (632 J/m^2) value corresponding to 9 mm of delamination extension for the same specimen 2P3 from Figure 10. This is the peak G_{Ic} value before the start of large delamination extension. These SEM results indicate that the presence of functionalized nanotubes resulted in better fiber-matrix bonding, which would require higher energy to break the bonds. Secondly, the silane functional group has better affinity towards epoxy matrix which might result in higher resistance to fiber pullout, absorbing more energy in the process. However, the functionalized nanotubes were sparsely distributed on the fabric surface which

may be because of the absence of nanotube networks and hence easier transfer of these nanotubes to another plane through the separation between carbon fiber tows during resin transfer process under vacuum. Thus the energy required to propagate the delamination through nanotube rich areas of epoxy would be much higher than required for delamination propagation through areas without any nanotubes (along the surface of the carbon fibers or in matrix regions where there are no nanotubes) [109, 129]. This combination of failure mechanisms indicates possible explanation for the unstable delamination extension through 25 to 30 mm. Absence of these large unstable crack growths in the panels with pristine nanotubes indicates a more homogeneous distribution of long SWCNTs that could have helped in stabilizing the crack growth along with higher G_{Ic}. Similar indications were made by Tong et al.[129], who developed a mechanistic model to show an increase in G_{Ic} by increasing nanotube length and density. The pristine and functionalized nanotubes therefore have shown different failure mechanisms, resulting in large part from the level of compatibility with epoxy matrix and the level of dispersion. In short, it has been observed from the above fractographic analysis of delamination surfaces that pristine nanotubes could help in bridging cracks while functionalized nanotubes could provide better fiber-matrix bonding and therefore a more substantial amount of cohesive failure in addition to the adhesive failure observed for the pristine nanotubes.

C. Summary

1. Interlaminar Shear Strength

A study was performed to determine the effect of selective use of single walled carbon nanotubes on the interlaminar shear strength of a conventional carbon fiber- epoxy composite. The VARTM processing was used to fabricate three different types of

composite laminates and a novel spraying technique was used for selective placement of the nanotubes. One laminate had no nanotubes making it base material, while the other two laminate types consisted of pristine and silane functionalized SWCNTs in the mid-plane. Short beam shear testing of these laminates showed about a 4.4% increase in short beam strength of the functionalized nanotubes composite as compared to the base material and about 2.6% increase with respect to the composite with pristine nanotubes. The composite with pristine nanotubes showed about 1.8% increase with respect to the base material. It cannot be said that there is any significant improvement in ILSS by addition of nanotubes, but the results are better compared to some of recently reported results mentioned in discussion section that showed decrease in ILSS for multiscale composites modified by nanoparticles. The silane functionalized nanotubes also resulted in a decrease in the number of cracks formed as observed from the edge of the specimens indicating reduction in damage accumulation. The SEM microscopy images showed differences in fracture surfaces between pristine and silane treated interfaces with the fiber-matrix interface intact in the later case. This result indicates possibility of interlaminar toughening due to the presence of functionalized nanotubes without decreasing the shear strength.

2. Interlaminar Fracture Toughness

The multi-scale laminates consisting of macro-scale woven plies of micron sized carbon fibers were produced using VARTM method with selective placement of nano-scale carbon nanotubes at the mid-plane of the laminate using the spraying technique. The initiation G_{Ic} did not show any significant change for the panels with pristine and functionalized nanotubes as compared to the panel without nanotubes. However, the specimens with functionalized nanotubes showed a large unstable crack growth mechanism(20 to 30 mm). The reasons for the large unstable crack growth were in-

vestigated using SEM fractography of the delamination surfaces. It was found to be due to modified fiber-matrix bonding at the location of functionalized nanotubes rich interphase regions which enhanced the bonding of silane functionalized nanotubes with the epoxy matrix and reducing the fiber-matrix debonding which is one of the energy dissipation mechanisms, as evident from the SEM images. The functionalization process also resulted in better dispersion of nanotubes, however, the distribution of functionalized nanotubes on the ply surface was inhomogeneous due to the out of plane transfer of disentangled nanotubes through the gaps in weave structure. The fiber bridging mechanisms were also suppressed as a result of smaller nanotube lengths due to this particular chemical functionalization process.

SEM images showed comparatively better coverage of the fabric ply by the pristine nanotubes, compared to the functionalized nanotubes. The entanglement of long pristine nanotubes can help in bridging cracks as observed from SEM fractography. The crack propagation was observed to be much more stable in these specimens as seen from the R-curves. A different functionalization with similar dispersion characteristics but which will have longer nanotubes forming entangled networks could help in getting homogeneous coverage of functionalized nanotubes on the ply.

It is also suggested that a synergistic combination of functionalized and non-functionalized nanotubes could provide a better approach in enhancing the interlaminar properties. The functionalized nanotubes could provide better resistance to delamination initiation due to enhanced adhesion properties of fiber-matrix interface while long pristine nanotubes could stabilize the crack propagation through crack bridging mechanism as observed in the present work.

CHAPTER V

MULTISCALE UNIDIRECTIONAL PRE-PREG COMPOSITE LAMINATES

Carbon nanotube reinforced polymer matrix nanocomposites are finding a lot of attention due to enhanced electrical, thermal and in some cases mechanical properties [4, 5, 8, 11, 18, 78]. The laminated composites are widely used for structural applications in aerospace and automotive industry. The matrix dominated properties such as transverse modulus and in-plane shear of these laminated composites are weaker due to limiting modulus and strength of polymer matrix. Thus the use of traditional composites has been limited to some extent. The reinforcement of traditional laminated composites with nanoscale particulates has been recently reported in an effort to improve the mechanical properties [64, 66, 67, 121, 130, 131]. The addition of nanoparticles, such as carbon nanotubes or carbon nanofibers, also introduces a possibility of making multifunctional laminated composites. Thus, there is a need to improve all matrix dominated properties to enhance the potential of traditional laminated composites in structural applications.

Yokozeki et al. [107] reinforced carbon fiber/epoxy laminates with cup-stacked carbon nanotubes (CSCNT) i.e. carbon nanofibers and reported about 6% increase in transverse stiffness and no improvement in longitudinal stiffness for 5 wt% of CSCNT. Cho et al. [132] reported about 7% improvement in in-plane shear modulus of carbon fiber/epoxy laminates by introducing 3 wt% of graphite nanoplatelet. Recently Zhou et al. [133] reported 22% improvement in flexural strength with addition of 2 wt% carbon nanofibers in carbon fabric/epoxy composites.

In the current work, multifunctional multi-scale composites suitable for structural aerospace applications are processed, characterized and modeled. Stacked layers of unidirectional pre-preg laminae forms the macro-scale (cm), while carbon-fibers (mi-

crons) surrounded by polymer and carbon nanotubes forms the micro-scale. Carbon nanotubes (nm) surrounded by polymer matrix forms the nano-scale interactions of the proposed system. The material system consists of unidirectional IM7 carbon fibers pre-impregnated with toughened epoxy matrix (RS-47). Single wall carbon nanotubes with and without covalent functionalization (amide group) are introduced between laminae layers and form an interphase layer. Extremely small weight fraction of carbon nanotubes (0.5 wt% and 1 wt%) is used in this study. Addition of carbon nanotubes is expected to provide anisotropic multifunctionality to these composite laminates with negligible added weight to the original carbon fiber laminate. Such laminated composite system consisting of micro/nanostructured reinforcements requires appropriate characterization and modeling at different length scales to understand the physics behind the measured material property and establish structure-property co-relation.

A. Experimental Procedure

1. Materials

The pre-preg material is procured from YLA Inc. through NASA Langley Research Center, VA. The uni-directional carbon fibers (IM7) are pre-impregnated with a toughened epoxy matrix (RS-47 system). The polymer chemistry is proprietary information of YLA Inc. and thus, the combination of epoxy monomers and toughening agent is unknown. However, RS-47 is a high curing temperature epoxy and is expected to have an aromatic curing agent bonding basic epoxide groups. The epoxy system can be a di-functional epoxy (e.g. DGEBA, di-glycidyl ether of bi-sphenol A) or a tetra-functional epoxy (e.g. TGDDM, tetra-glycidyl ether of diamino-diphenylmethane) or a combination of both. The toughening agent is most likely polyethersulphone (PES)

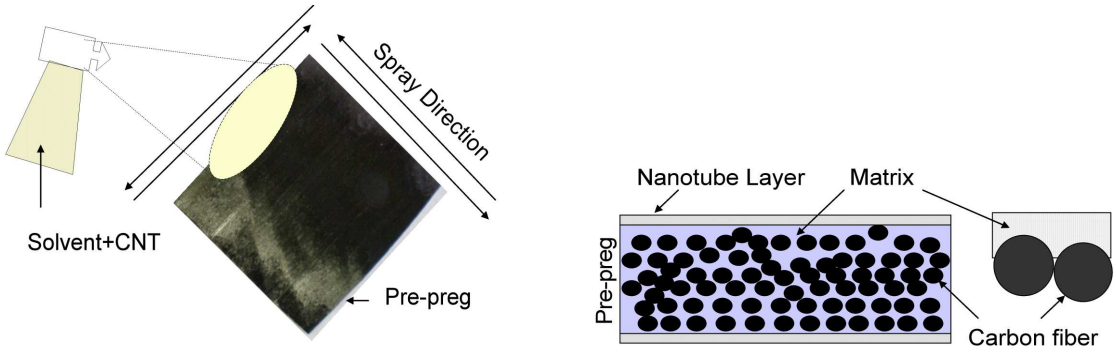

(a) (b)

Fig. 50. Nanotube spraying set-up. 50(a) Spraying Technique for UDPP 50(b) UDPP cross-section after spray process.

which is a very common toughener used in epoxy resin systems. Purified single wall carbon nanotubes are obtained from Rice University. The nanotubes are functionalized at NanoRidge Inc. and Houston. A functional group (amide) is chosen based on compatibility with the toughened epoxy system. The functionalization process is not disclosed due to intellectual property rights of NanoRidge Inc.

2. Processing Methods

a. Three Point Bending Test Panels

The unidirectional pre-preg (UDPP) layers are sprayed with a solution of single walled carbon nanotubes dispersed in ethanol solvent as shown in Fig. 50(a). Each pre-preg layer is sprayed on both sides with nanotube-solvent solution and the solvent is allowed to evaporate under room temperature and atmospheric pressure conditions. Fig. 50(b) shows the cross-section of a pre-preg with deposited layer of nanotubes after solvent evaporation. Ten layers of such modified pre-preg layers are stacked with all fibers facing the same direction, i.e. and stacking sequence of [0]10. The zero degree direction represents the longitudinal direction of the fibers. The stacked

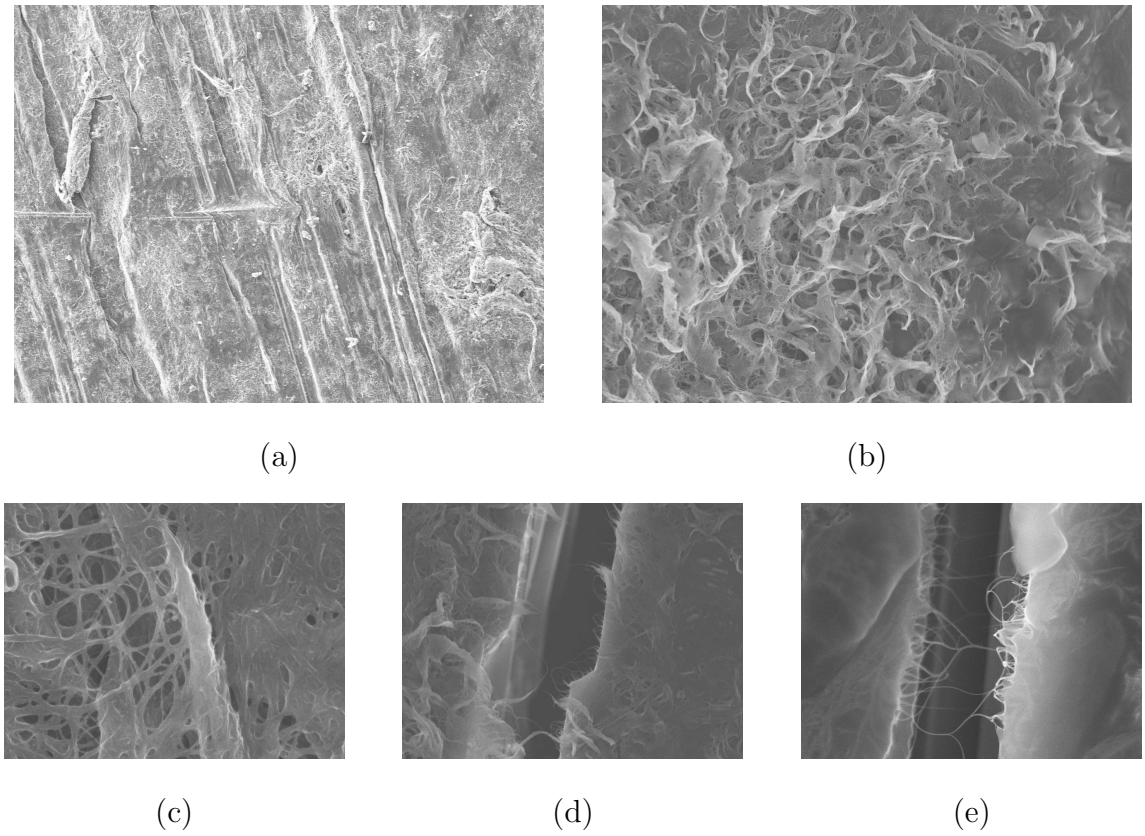

Fig. 51. SEM micrographs showing sprayed pre-preg layers before processing. 51(a) Low magnification image of sprayed pre-preg, 51(b) Thermoplastic toughener phase seems to be broken, 51(c) Big entangled bundles of nanotube ropes, 51(d) Curled nanotube ropes after bridging cracks, 51(e) Embedded nanotubes are observed in the matrix.

pre-preg layers are placed between two metal plates coated with release agent on the inner side. These metal plates are then transferred on a hot press between rectangular platens of hot press and a pressure of about 2000 lb is applied. The curing process for the pre-preg system involved gradual heating of the platens to the temperature of 350 F. The platens are held together at 350 F and 2000 lb pressure for two hours. Later the platens are cooled using water cooling system to gradually decrease the temperature to room temperature. Fig. 51 shows high magnification images of the pre-pregs before stacking them to get the laminated composite. The thermoplastic

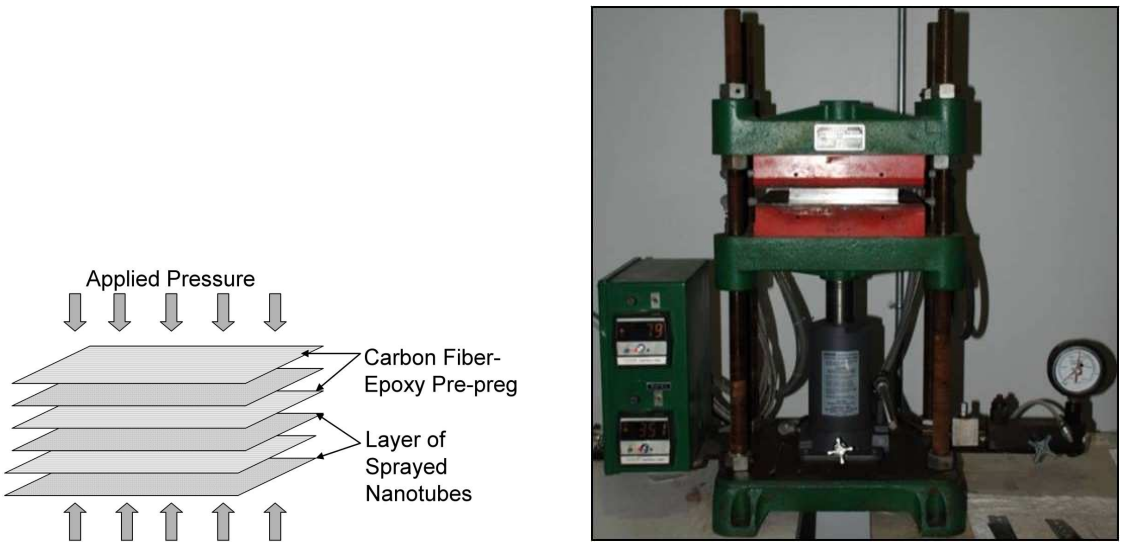

(a) (b)

Fig. 52. Schematic of processing set-up containing stacked UDPP and hot-press. 50(a) Stacked pre-pregs being pressed under hot press platens, 50(b) Hot-press set-up.

phase (Fig. 51(b)) seems to be broken into fibrils forming spherulite like structures as observed at few spots on the lamina, may be due to some chemical reaction with solvent. The nanotubes are present in the form of entangled network throughout the lamina surface (Fig. 51(c)) which indicates good distribution of nanotubes. Presence of nanotubes embedded well in the matrix and a possible crack bridging mechanism are observed in Figures 51(d) and 51(e). The local volume fraction of nanotubes just between the interphase between two laminae would be much more higher than as calculated based on weight fraction of each lamina. This concept of local volume fraction has been discussed in detail in the modeling section. Five laminates are processed using the above procedure and set-up as shown in Fig. 52. The weight percent of nanotubes is with respect to the total weight of the pre-preg layers. One laminate is a base laminate with no nanotubes, second is a laminate with 0.5 wt% of purified SWCNTs, third laminate contains 0.5 wt% of amide functionalized nanotubes

Table VIII. Fiber volume fraction of all pre-preg laminates

Laminate number	Constituents	Fiber volume fraction
1	No SWCNTs	60%
2	Pristine SWCNTs (0.5 wt%)	57 %
3	Amide functionalized SWCNTs (0.5 wt%)	61%
4	Amide functionalized SWCNTs (1.0 wt%)	55%

and fourth laminate contains 1.0 wt% of amide functionalized nanotubes. The carbon-fiber volume fraction of the laminates is given in Table VIII. The fiber volume fractions are calculated by density measurement test. The density of the composite is measured by weighing the composite specimen in water and in air and then the known densities of fiber and matrix is utilized to finally calculate the fiber volume fraction.

b. In-plane Shear Test Panels

The in-plane shear tests require panels with $\pm 45^{\circ}$ fiber orientation. Two more panels are processed for in-plane shear tests, one with amide functionalized nanotubes and one control panel without nanotubes. For the nanotubes modified panel, all pre-preg layers are sprayed with nanotubes on both sides. The number of pre-preg layers were eight in each panel. Apart from orientation of the pre-pregs in $\pm 45^{\circ}$ direction and number of layers in each panel, the rest of the processing method remains the same as explained previous section.

c. Double Cantilever Beam Test Panels

The single wall carbon nanotubes were functionalized with amide reactive group using a proprietary process by NanoRidge. The dispersion study is presented earlier showing good dispersion and better matrix-CNT bonding by use of amide functionalization. Nanotubes were dispersed in ethanol and sonicated for one hour using bath sonicator. These nanotubes were then sprayed on only one side of three pre-preg laminae. Pre-preg laminae were allowed to dry for about 6 hours at room temperature and placed in vacuum oven at 30^oC and full vacuum for overnight. This process allowed the evaporation of ethanol. The three sprayed pre-preg laminae were placed in the center plane of a 40 layer stacked laminae all facing 0° i.e. unidirectional stacking sequence. Three middle layers were chosen to increase the possibility of keeping the delamination growth in the center plane and preventing any crack jump from mid-plane to adjacent planes. Each lamina was carefully placed on top of another lamina and then pressed using a roller to remove any air between the laminae. Then the paper backing on the other side of the pre-preg was removed and above stacking process was repeated till 40 layers were stacked together. Hot press was used to compress these stacked laminae between two metal platens at 2000 lb pressure (8890 N). The curing cycle involved slowly heating the platens to 350 F (178^oC) and holding at this temperature for two hours followed by slow cooling to room temperature. The complete process took about 4 hours to prepare one panel. This process was repeated to get four panels, i.e. and base panel without nanotubes, control panel with solvent spraying process but no nanotubes, panel with pristine nanotubes and panel with amide functionalized nanotubes.

Specimen Preparation

The specimens were cut according to ASTM-5528 standards with length of 7 inches

(15.24 cm) and width of 1 inch (2.54 cm) with an accuracy of ±0.1 mm. The upper and lower specimen surfaces were roughened using grinding paper where the piano hinges were to be bonded. The surfaces of the piano hinges were also sanded to prepare rough surfaces for better bonding, and then the surface was cleaned with isopropanol to remove any contamination. The specimens were dried for four days at 60^oC in a oven to remove moisture absorbed during the cutting process. Two-part epoxy adhesive was used to bond the piano hinges, and the specimens were placed in an oven for 6 hours at 60^oC to cure the epoxy adhesive. The specimen edges were sprayed with white paint, and a scale with 1 mm resolution was placed on one of the edges of each specimen for monitoring crack propagation.

3. Characterization Methods

a. Three Point Bending Test

Specimens are cut from the laminates in two directions. The specimens cut along the length of the specimen are called longitudinal specimens and the specimens cut in a direction perpendicular to the fiber direction are called transverse specimens. All specimens for bending tests are 45 mm long, 10 mm wide and 1 mm thick. Three point bending tests are performed as per ASTM standards D-790. The specimens are tested till failure. MTS Insight table top machine is used to test the specimens using 35 kN load cell for force measurement. The test set-up is shown in Fig. 53. Euler-Bernoulli beam theory is used to find the modulus and strength of the laminate as given below by Eqs. 5.1 and 5.2 respectively:

$$E = \frac{mL^3}{4bd^3} \tag{5.1}$$

$$T = \frac{3F_{max}L}{2bd^2} \tag{5.2}$$

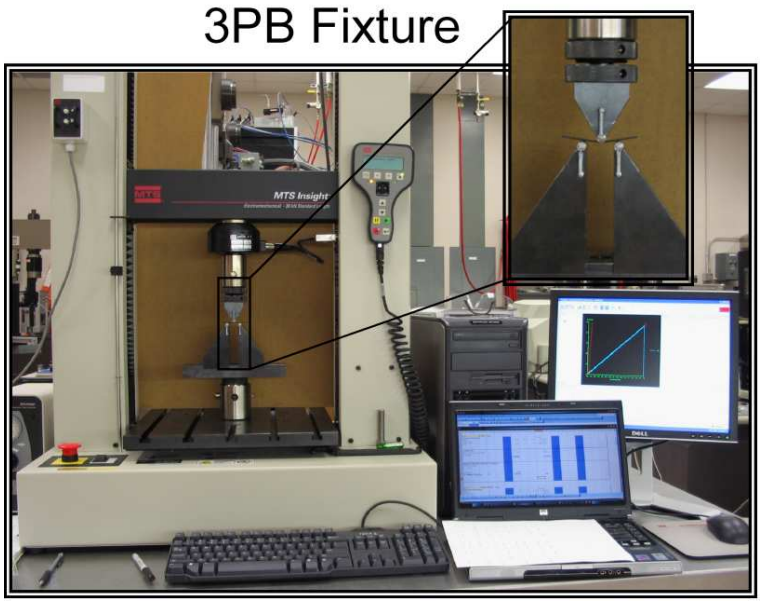

Fig. 53. Three point bending test set-up.

Where E is the modulus, m is the slope of load-displacement curve, L is the span length, b is the width of the specimen, d is the depth or thickness of the specimen, T is the strength of the laminate, F_{max} is the failure load or maximum applicable load.

b. In-plane Shear Test

In-plane shear tests are guided by the ASTM standards D-3518. Rectangular specimens are cut from the $[\pm 45^o]_{2s}$ panels with dimensions of 140 mm by 15 mm by 1.2 mm (length, width and thickness respectively). The specimen edges are polished to a smooth finish. Center surface of each specimen is roughened and cleaned using isopropanol for mounting strain gages. The strain gages were of type CEA-06-125UT-350 and purchased from Vishay Micro-measurement division. Strain gage bonding is performed using standard technique suggested by strain gage manufacturer. Strain gages are mounted on the center of each specimen to measure strains in longitudinal as well as transverse direction. Quarter bridge circuits are used for each strain gage

and out-put voltage is measured using NI signal processing board. Labview software is used to display and measure the strains. MTS 100 Kips (445 kN) test frame is used with 8.9 kN (2000 lb) load cell for tension testing. The specimens are tested till 3% strain. The test set-up is shown in Fig. 54. All tests are displacement controlled with head displacement rate of 2 mm/min. The data acquisition rate for strain gages and load-displacement measurement is 10 data points per second. The specimens are gripped using emery cloth. Extensometers are used to measure longitudinal strain and compare with strain gage measurement. The maximum in-plane shear stress is

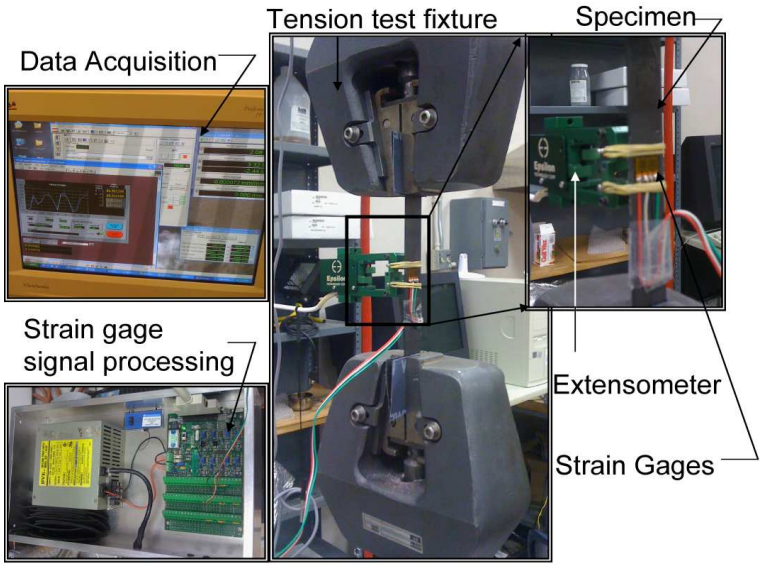

Fig. 54. In-plane shear test set-up.

calculated using Eq. 5.3 and the shear strain is calculated using Eq. 5.4.

$$\tau_{12}{}^{m} = \frac{P_m}{2A} \tag{5.3}$$

$$\gamma_{12i} = \varepsilon_{xi} - \varepsilon_{yi} \tag{5.4}$$

Where τ_{12} is the maximum in-plane shear stress, P_m is the maximum load at maximum shear strain during the test, A is the cross-sectional area, γ_{12i} is the shear strain at

the i-th data point, ε_{xi} is the longitudinal strain at the i-th data point and ε_{yi} is the lateral (transverse) shear strain at the i-th data point. The shear modulus is calculated from the slope of the linear region of the shear stress-shear strain plot. The shear stress at each data point is calculated by Eq. 5.3 by replacing maximum load by incremental load at each data point.

c. Double Cantilever Beam Test

The ASTM D-5528 standard was followed for performing the DCB tests at room temperature using a electrical power supplied test frame (MTS table top system). A 35 KN load cell with 0.05 N resolution was used for force measurement. Parameters P, δ , and a represent force, applied displacement, and delamination length, respectively. Crack propagation was monitored on a video screen connected to a video camera set at magnification of about 15X and focused on the crack tip at all times as the crack progressed. The test was conducted under displacement control at a displacement rate of 1.27 mm/min. Crack extension was recorded every millimeter of crack growth for stable crack growths. The crack was allowed to propagate through a distance of at least 70 mm, after which the specimen was unloaded at a rate of 2.54 mm/min. The same procedure was repeated for the five specimens from each panel.

d. Microscopy

Transmission electron microscopy of functionalized and as-received pristine single wall carbon nanotubes is performed using JEOL-2010 microscope for characterizing the nanotube dispersion. The fracture surfaces generated as a result of three point bending tests and in-plane shear tests are investigated using scanning electron microscopy and optical microscopy. SEM is performed using the JSM-7500F cold emission microscope to characterize the microstructure of the composites and study the fracture

mechanisms. Optical microscopy is performed using Leica inverted section microscope for investigating the morphology of the fracture surfaces and crack formation on the edges of the composite laminates.

B. Model Description

The macroscale properties (longitudinal, transverse and in-plane shear modulus) of symmetric balanced laminates are modeled using classical laminate theory. Each unidirectional pre-preg lamina is considered as quasihomogeneous and transversely isotropic. The interphase layer between two laminae consists of polymer, unidirectional carbon fibers and randomly oriented nanotubes and thus, considered as transversely isotropic. A schematic of the realistic system is shown in Fig. 55. A simple system with the interphase layer consisting of only polymer and randomly oriented nanotubes is shown in Appendix B along with results for that case. In Appendix B, the interphase layer is considered as an interleaf because additional epoxy layer is introduced into the composite. The following case consisting of unidirectional carbon fibers in the interphase region forms a more realistic case study based on the experiments. There is no additional epoxy introduced in the experiments as only CNTs are sprayed on the top of the pre-preg layers. These CNTs penetrate the pre-preg consisting of matrix and carbon fibers during the lamination process and forms a thin layer of nanotube rich interphase layer. Such concept has been represented in Fig. 55. The top and bottom interphase layer of each lamina is represented by a 2.5 μm layer. The remaining 95 μm layer consists of only epoxy and unidirectional carbon fibers. Thus, there is a 5 μm layer between two pre-preg layers. Another case study is performed by changing the interphase thickness between two lamina as 50 μm. Individual lamina properties are computed using the rule of mixtures and the interphase layer, i.e. and

nanocomposite layer properties are obtained by using Mori-Tanaka micromechanics method utilizing orientation distribution function for random orientation of fibers. The laminate analysis is performed using CompositePro design and analysis software by Peak Composites, Inc. The exact volume fraction of sprayed nanotubes in the interphase layer is complicated to compute. The nanotubes are weighed as 0.5% of the weight of one carbon fiber lamina and converted to fiber areal weight or fiber areal density. Thus the amount of nanotubes is quantified as the weight of nanotubes per unit area of the pre-preg lamina. The fiber areal density is also known for the carbon fibers in each lamina and if it is divided by the density of the carbon fiber lamina then the thickness of lamina can be calculated. This calculated lamina thickness is experimentally validated by measuring the actual thickness of a lamina. Similar concept is utilized to find the thickness of the interphase layer. The thickness of the

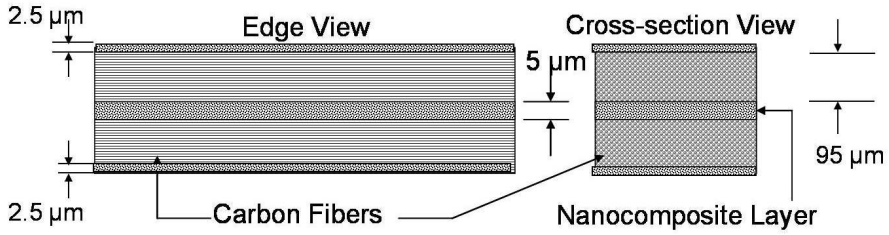

Fig. 55. Edge view and cross-section view of a nanocomposites layer between two unidirectional pre-pregs.

interphase layer can thus be represented as a ratio of the CNT areal weight density and the density of the carbon nanotubes.The volume fraction of carbon fibers in the pre-preg lamina is the ratio of the volume of carbon fiber and the total volume of the carbon fibers and matrix. The volume fraction of the CNTs in the interphase layer is the ratio of the volume of CNTs to the total volume consisting of CNTs, epoxy and carbon fibers. The concept of areal weight density reduces the volume fraction equation to the ratio of thicknesses. Thus the localized volume fraction of carbon

nanotubes in the interphase layer is given as the ratio of the thickness of CNT layer thickness to the thickness of the pre-preg. The 0.5 weight% of sprayed CNTs are thus converted to local volume fraction of 10.9% using the current approach. Thus there should be a significant effect of the interphase layer on the matrix dominated properties. This hypothesis is tested using classical laminate theory. A flow chart explaining the analytical steps in classical laminate theory are presented in Appendix B.

Longitudinal, transverse and shear moduli are calculated for different stacking sequences of laminates as described below:

- Laminate without nanotubes - stacking sequence $[0^\circ]_1 0$, resulting in 10 layer laminate.

- Laminate with alternate layers of pre-preg and nanocomposite layers (NC) as shown in Fig. 55. The nanocomposite layer consists of carbon fibers reinforced in modified epoxy with carbon nanotubes. Each lamina consists of three layers, i.e. 2.5 μm layer of nanocomposite, 95 μm layer of unidirectional carbon fiber pre-preg followed by 2.5 μm layer of nanocomposite. The laminate theory is applied to find single pre-preg lamina property which is the combination of above mentioned three layers with stacking sequence $[NC/0^\circ/NC]$.

- Final laminate consists of 10 layers of above mentioned lamina which individually consists of 3 layers each.

The nanotubes are incorporated into the laminate in three major ways as follows

1. First case consists of nanotubes randomly oriented in the matrix phase throughout the lamina and thus throughout the laminate. So there is no interphase layer between two pre-pregs.

2. Second case consists of nanotubes forming 5 μm interphase layers between two pre-pregs. The unidirectional lamina thickness is adjusted accordingly so that the total laminate thickness remains same as the first case and also there is no additional epoxy introduced.

3. Third case is similar to second case with the exception of the thickness of the interphase layer, which is 50 μm in this case and the unidirectional lamina thickness is again adjusted to keep the laminate thickness same as above two cases.

Each individual case as mentioned above consists of three sub-cases to account for neat epoxy and varying weight fractions of nanotubes as described below:

1. First sub-case consists of neat epoxy only.

2. Second sub-case consists of the nanocomposite layer with 0.5 wt% pristine single wall carbon nanotubes (CFRP+0.5%PSW).

3. Third sub-case consists of the nanocomposite layer with 1.0 wt% pristine single wall carbon nanotubes (CFRP+1%PSW).

The process of determining laminate longitudinal, transverse and shear moduli consists of following steps:

Step 1: Enter fiber and epoxy properties and get pre-preg layer properties. In this case, IM7 carbon fibers properties are used along with RS-47 toughened epoxy matrix properties. The neat epoxy properties were taken from experiments.

Step 2: The nanocomposite properties are calculated from Mori-Tanaka method of micromechanics using orientation averaging to get properties for randomly oriented nanotubes.

Step 3: Find layer stiffness referred to principal material axes, which is equivalent

to transformed stiffness as the local layer axes and global laminate axes coincide. Perform the process for three layer composite then replace single layer properties in the final ten layer composites such that each single layer represents combination of three layers.

Step 4: Calculate A, B, D matrix considering individual pre-preg layer thickness.

Step 5: Calculate laminate engineering constants i.e. transverse, shear and longitudinal modulus in terms of A-B-D matrix components.

The details of the overall process of classical laminate analysis are presented in Appendix B.

C. Results and Discussion

The functionalization of nanotubes results in better dispersion of nanotubes consisting of smaller diameter bundles as shown by the TEM images in Fig. 56. In addition

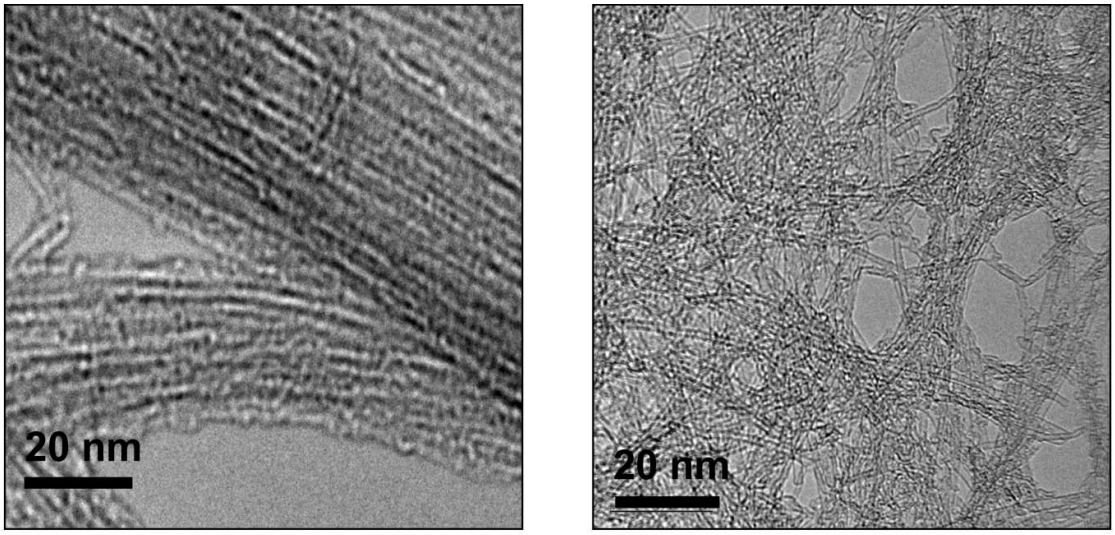

(a) (b)

Fig. 56. TEM micrographs of nanotubes in solvent before spraying on pre-pregs.56(a) Spraying Technique for UDPP 56(b) UDPP cross-section after spray process.

to forming better nanotube dispersion, the functional group (amide) is expected to participate in cross-link formation with epoxide groups, thus becoming integral part of the network of epoxy. The nanotubes network after spraying on pre-preg layers and after solvent evaporation is represented in Fig. 57. It is important to note that even 0.5 wt% of nanotubes forms quite dense network on the pre-preg layers as shown by Fig. 51(c). The interphase layers with 0.5 wt% and 1 wt% of nanotubes is expected to result in different thickness of the nanotube rich region between the pre-pregs.

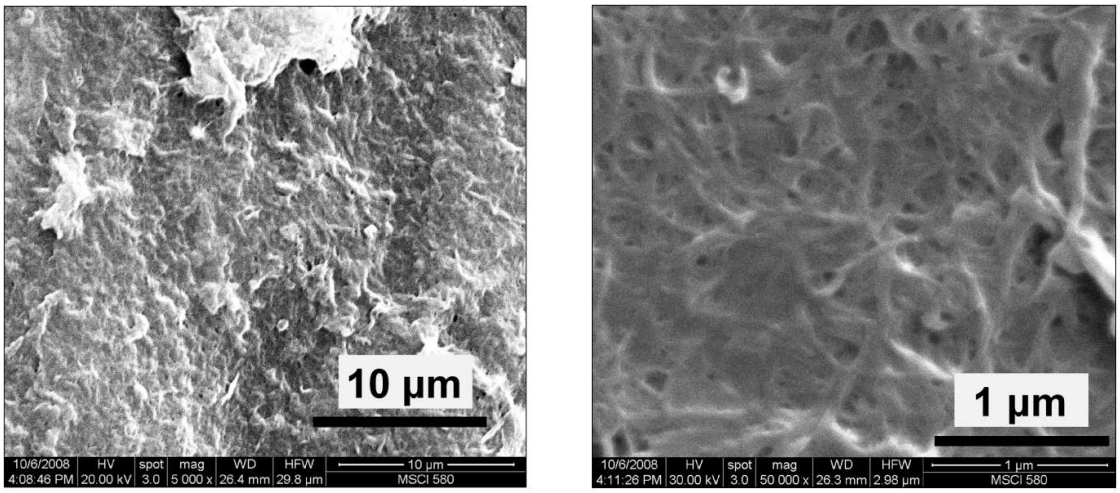

(a) (b)

Fig. 57. SEM micrograph of network of nanotubes after spraying on pre-preg layers.

1. Transverse and Longitudinal Properties

The longitudinal and transverse properties of pre-preg laminates, as a result of three point bending tests, are presented in Table IX and Table X respectively. The longitudinal properties, i.e. and modulus and strength do not show any significant effect of nanotubes and all values lie within the coefficient of variation. The fiber properties dominate the longitudinal properties of the laminated composites and accordingly, extremely small weight percent of nanotubes is not expected to affect properties in

Table IX. Longitudinal modulus and strength of pre-preg laminates

Panels	Modulus (GPa)	Strength (MPa)
No SWCNTs	149 ± 3%	2.5 ± 2%
Pristine SWCNTs (0.5 wt%)	154 ± 2%	2.5 ± 3%
Amide functionalized SWCNTs (0.5 wt%)	158 ± 4%	2.3 ± 2%
Amide functionalized SWCNTs (1.0 wt%)	145 ± 6%	2.3 ± 2%

Table X. Transverse modulus and strength of pre-preg laminates

Panels	Modulus (GPa)	Strength (MPa)
No SWCNTs	8.4 ± 4%	155 ± 8%
Pristine SWCNTs (0.5 wt%)	9.7 ± 2%	136 ± 13%
Amide functionalized SWCNTs (0.5 wt%)	9.4 ± 5%	128 ± 4%
Amide functionalized SWCNTs (1.0 wt%)	10.1 ± 7%	144 ± 11%

longitudinal direction.

The transverse properties show some significant effect of the addition of nanotubes as seen from Table X. The specimens with 0.5 wt% pristine nanotubes show about 15% increase in the transverse modulus, while the specimens with 0.5 wt% and 1 wt% amide functionalized nanotubes show about 12% and 20% increase in the transverse modulus respectively. The transverse strength shows a decrease by addition of nanotubes. The decrease in strength indicates the possibility of a weaker interphase surrounding the functionalized nanotubes, resulting in poor load transfer ability.

2. Mechanisms of Fracture

Three point bending tests were performed until the specimens fractured. Scanning electron microscopy was used to study the cross-sections of the fractured surfaces of the above specimens. Differences in failure mechanisms are shown in following figures. The toughening agent in the epoxy results in flake like fracture surfaces indicating non-brittle fracture. One important observation from the SEM images, as shown in Fig. 58, indicates the formation of shear hackles as the energy dissipation mechanisms. In most of the cases with 0.5 wt% pristine or amide functionalized nanotubes, the size of the shearing region between fibers or laminae seems to be around 5 to 7 microns. This observation is utilized in choosing one of the interphase region thickness for the modeling part. Fig. 59 shows the fracture surfaces of specimens without nanotubes and with pristine nanotubes. Fig. 59(a) shows presence of shear hackles between smooth regions running along the length of carbon fibers. The smooth regions indicate either fiber-matrix debonding or brittle crack growth along the top and bottom fiber surface. Fig. 59(b) shows the side view of the hackle formation between fibers. The size of the shear hackles is found to be in the range of 2.5 μm

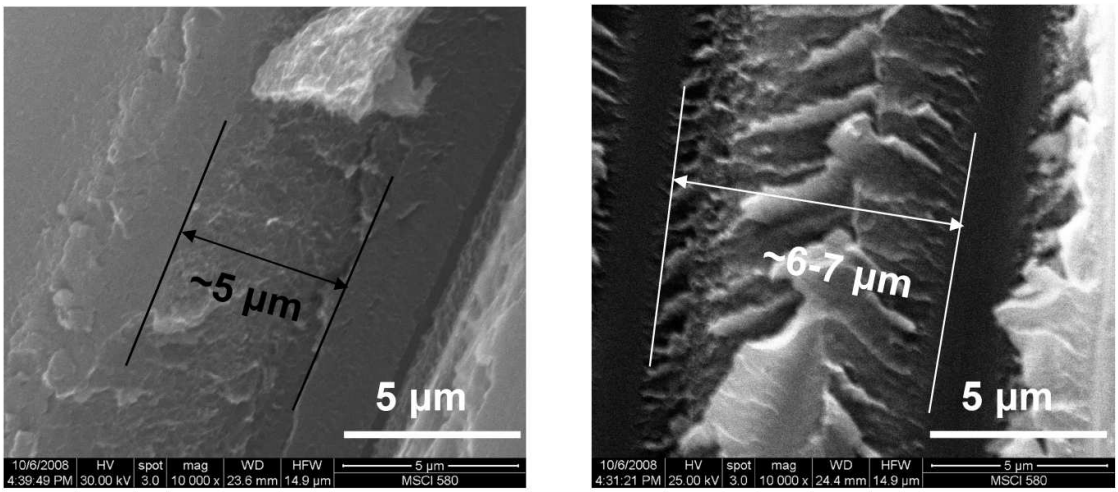

(a) (b)

Fig. 58. Fracture surfaces generated after flexure testing for pre-preg laminates containing amide functionalized nanotubes.

to 4.5 μm in length i.e. distance between two fiber surfaces perpendicular to crack propagation direction and 0.5 μm to 1.7 μm in width along the crack propagation direction. Presence of voids (black circles in top left corner of image) can be seen on the shear hackles area in Fig. 59(c). Figures 59(d) and 59(e) shows suppression of the shear hackles formation, especially for the regions where pristine CNTs are prominently visible. Higher magnification image in Fig. 59(f) shows the presence of network of pristine CNTs on the shear hackles/flakes. Few nanotubes or ropes of nanotubes are running across the shear hackles. The lower right corner of the Fig. 59(f) shows suppressed shear hackle (no large flakes) and presence of entangled pristine nanotubes running across the surface. The lower left corner of the Fig. 59(f) shows fully developed shear hackle and there are no nanotubes visible on this hackle or bridging this hackle with another hackle. These observations indicate that the presence of nanotube network might be suppressing or preventing the formation of the shear hackle surfaces. Fig. 60 shows the shear hackle formation in specimens with

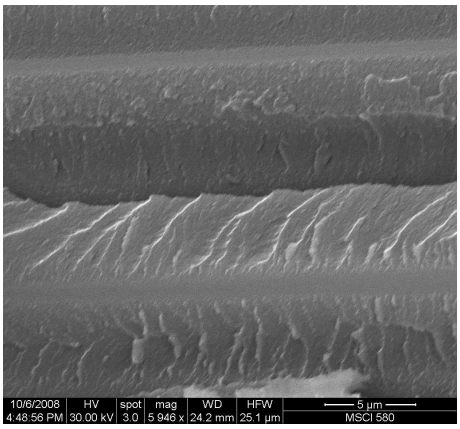

(a) Presence of shear hackles on specimen without CNTs

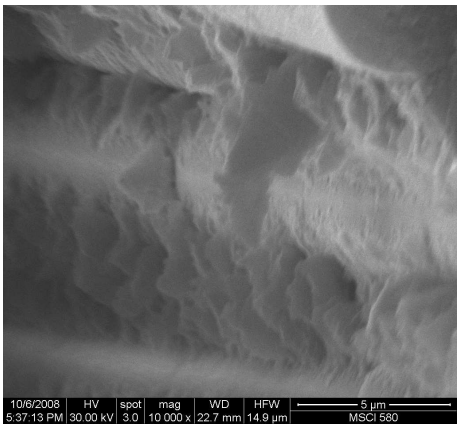

(b) Presence of large shear hackles between debonded fibers on specimen without CNTs

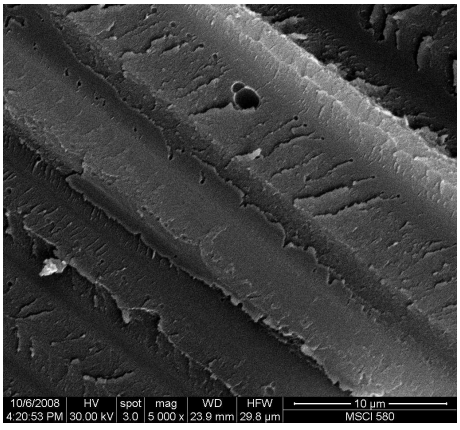

(c) Holes are observed at some places on shear hackles

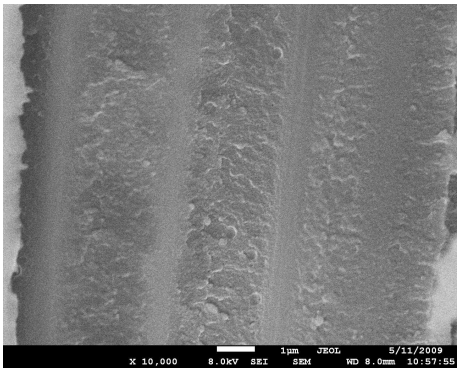

(d) Suppressed shear hackles

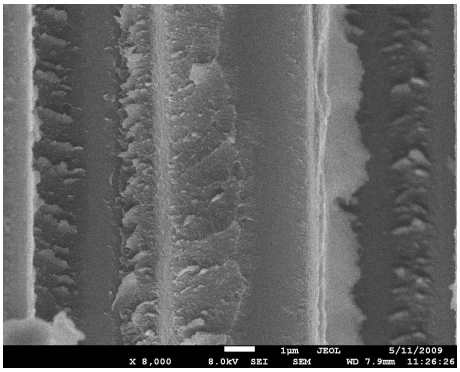

(e) Less hackles are observed in the CNT rich region

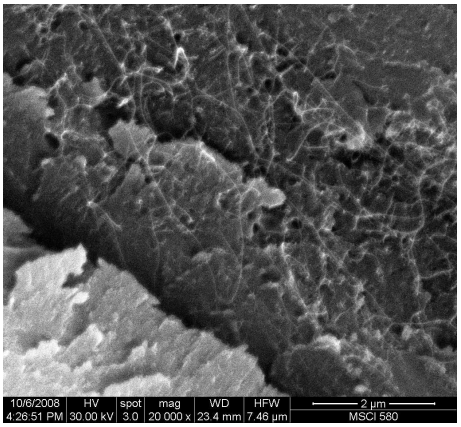

(f) Network of pristine nanotubes on near the flakes fracture surface

Fig. 59. SEM micrographs of fracture surfaces obtained by flexure test.

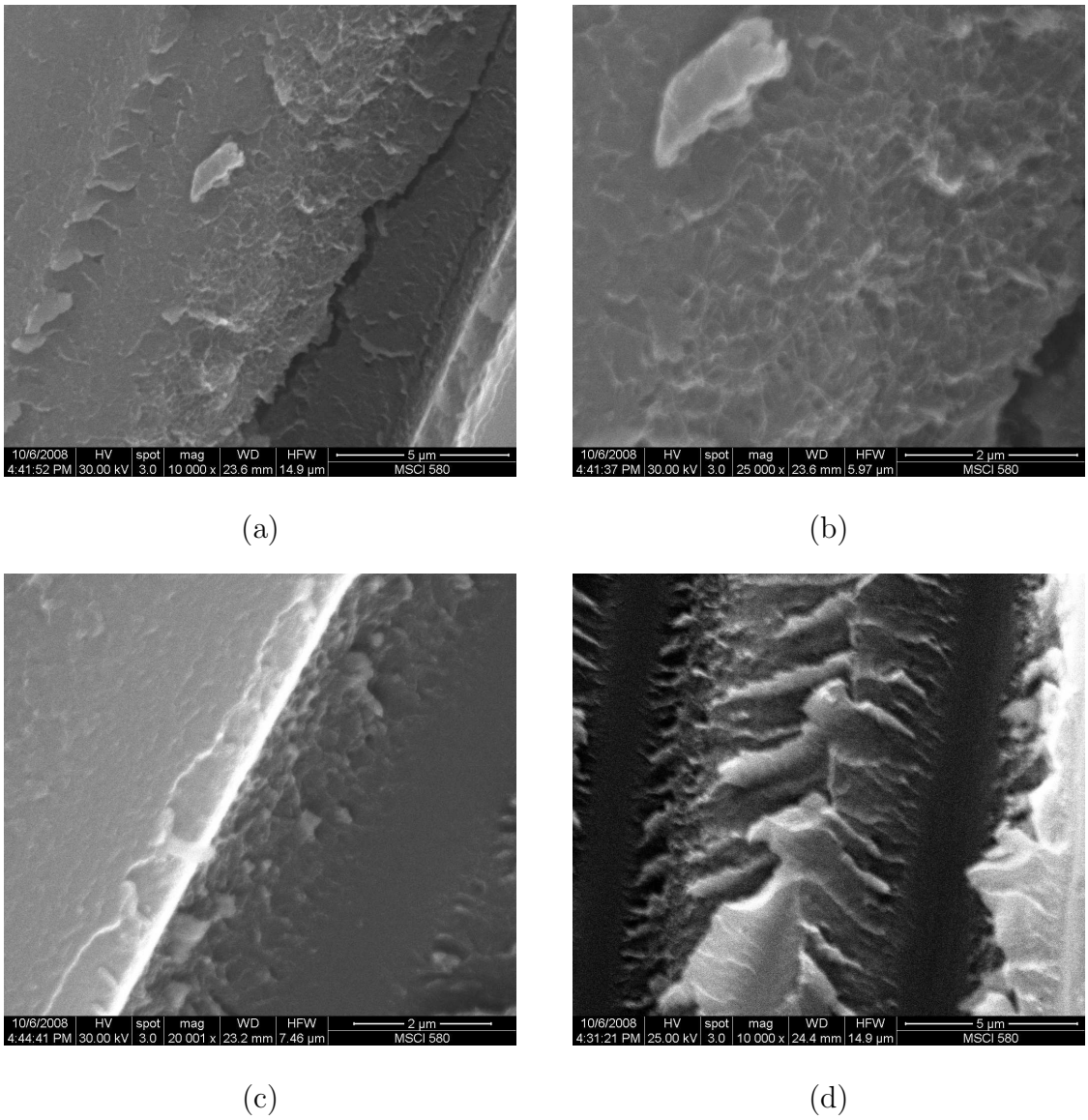

Fig. 60. SEM micrographs showing morphology of shear hackles in amide CNT modified specimens. 60(a) Smaller shear hackles and matrix cracking, 60(b) High magnification image showing network of amide CNTs in the shear hackles, 60(c) Start of scaling in shear hackles, 60(d) Fully developed shear hackle surfaces showing different length scales of shear hackles.

amide functionalized CNTs. Fig. 60(a) shows smaller hackle sizes (suppressed behavior) and also a crack developed through the matrix along the direction of the crack growth. Fig. 60(b) shows higher magnification of the region and presence of network of amide functionalized CNTs. Fig. 60(c) shows shear hackles but of comparatively smaller sizes, most likely due to the presence of nanotubes. Fig. 60(d) shows a very different type of shear hackle formation with different length scales of hackle formation. Smaller shear hackles can be seen closer to the clean fiber-matrix debonding surfaces and then scales into larger size shear hackles closer to the center of the area between two debonded fibers. This scale transition might be an indication of moving away from the CNT rich region i.e. region of suppressed hackles to fully developed hackles. Fig. 61 showing hackle surfaces on amide CNT modified specimens further corroborates the earlier observation of suppression of shear hackles from the specimens with pristine nanotubes. Fig. 61(b) shows reduced sizes of the shear hackles as compared to the specimens with no nanotubes as shown in Fig. 59(b). Presence of matrix on the carbon fiber surface (Fig. 61(a)) shows good fiber-matrix bonding. Fig. 61(c) and Fig. 61(d) shows smaller (suppressed) shear hackle formation at the locations of dispersed amide functionalized CNTs. Fig. 62 shows formation of scale like mechanism on some surfaces without shear hackles. Fig. 62(a) shows matrix cracking leading to scale like mechanism and Fig. 62(c) showing presence of amide CNT network well embedded in the epoxy matrix. The above images shows that there is a reduction in the amount of shear hackle formation by addition of both pristine and functionalized nanotubes. At certain places, suppressed or smaller sized shear hackles or scaled shear hackles are found. Some images show presence of voids in specimen with pristine CNTs and presence of matrix cracking instead of shear hackles in the specimen with amide CNTs. A decrease in the transverse strength which is a matrix dominated property might be due to the above mentioned observations.

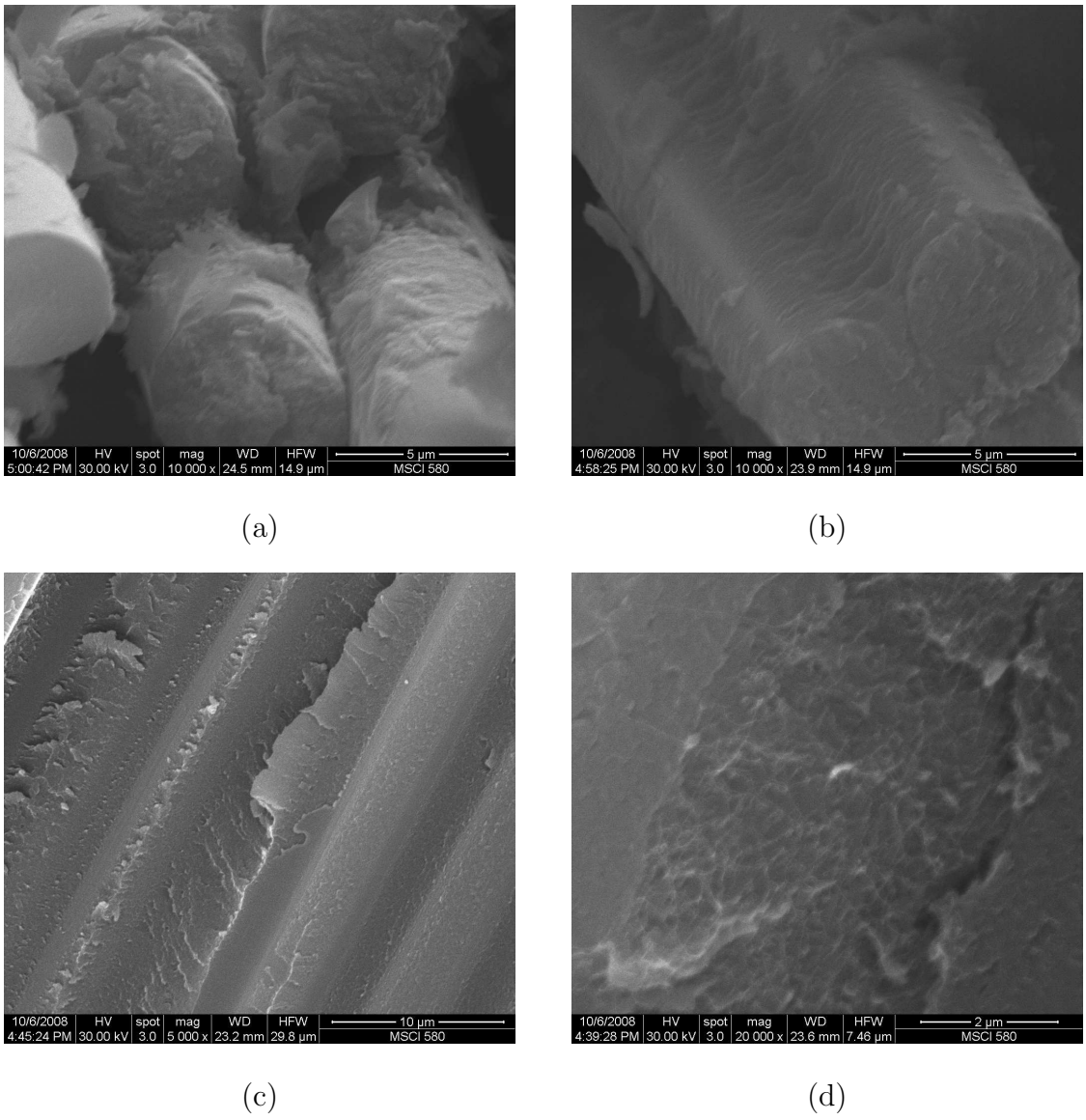

Fig. 61. SEM micrographs of fracture surfaces for amide CNT modified specimens post flexure test. 61(a) Presence of matrix on the carbon fiber (side view), 61(b) Reduced shear hackles size from side view, 61(c) Suppressed shear hackle mechanism, 61(d) Dispersion of amide CNTs in shear hackles.

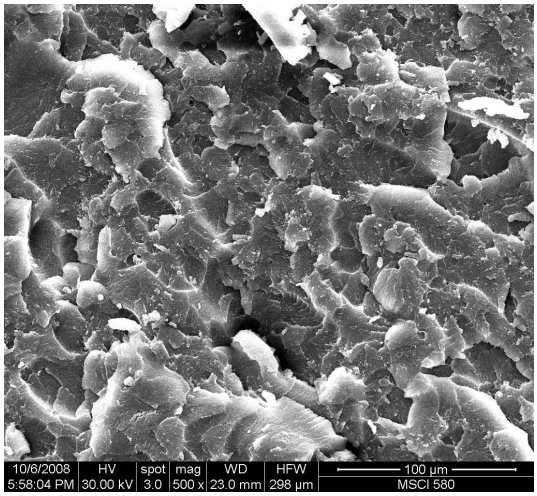

(a)

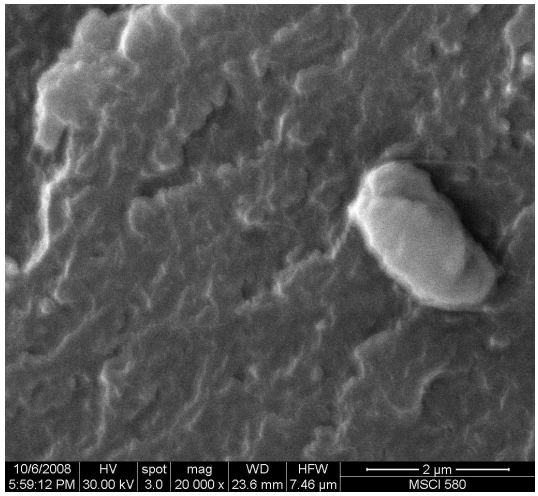

(b)

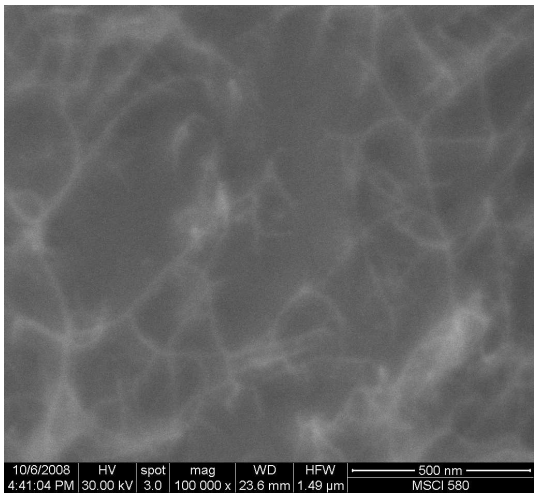

(c)

Fig. 62. SEM micrographs at no shear hackle surfaces for amide CNT modified specimens post flexure test. 62(a) Presence of matrix cracking forming scales like mechanism, 62(b) Higher magnification view of the scales mechanism, 62(c) Presence of embedded network of amide CNTs.

Table XI. In-plane shear properties of pre-preg laminates

Panels	Modulus (GPa)	Strength (MPa)
No SWCNTs	4.2	58.3
Amide functionalized SWCNTs (0.5 wt%)	1.4	33.4

The suppression of shear hackle mechanism might further lead to a reduction in shear properties as well as fracture toughness of the laminated composite.

3. In-plane Shear Strength and Modulus

The in-plane shear modulus is a matrix dominated property. The addition of nanotubes to the matrix region is expected to improve the shear properties by introducing nano-scale mechanisms. The in-plane shear properties are presented in Table XI. It shows that the in-plane shear modulus and in-plane shear strength decreases by addition of 0.5 wt% amide functionalized nanotubes. The images from previous section indicating suppression of shear hackle mechanisms seem to be a strong reason for reduction in shear properties. Another reason for the decrease might be due to insufficient evaporation of solvent from the pre-preg surfaces resulting in plasticizing effect of solvent on the matrix. Scanning electron microscopy images of the sheared planes of specimens after in-plane shear testing are shown Fig. 63. Lot of fiber debonding (Fig. 63(a)) and shear hackles (Fig. 63(b)) are observed on the surface of lamina without nanotubes. The mechanism of formation of shear hackles seems to be suppressed on the lamina with amide functionalized nanotubes (Fig. 63(c)). However, CNT bridging mechanisms were observed at some places as indicated by curled CNTs,most likely after being pulled out of the matrix (Fig. 63(d)). Certain places on the lamina showed phase separation of the thermoplastic toughener phase in the form of fibrils

originating from a single point (Fig. 63(e)). There might be a combination of reasons including suppressed shear hackle formation, toughener phase separation and presence of solvent, for the suppression of shear properties.

4. Classical Laminate Analysis

Fig. 64, 65 and 66 shows the modeling results from classical laminate theory for longitudinal, transverse and shear modulus respectively. The IM7/RS-47 system is chosen for comparative analysis. There are nine horizontal bars in each figure. The first three results at the bottom are for 10 layer composites without any interphase layer. First bottom bar is for control laminate without nanotubes and next two cases are for 0.5 and 1.0 wt% nanotubes distributed randomly throughout the matrix of the laminate. The next three cases in the middle region of each figure represents composite laminates with 5 μm interphase layers. The bottom bar in the middle three bars represent the neat epoxy interphase layer and the upper two bars represent 0.5 and 1.0 wt% pristine nanotubes as labeled on each figure. Top most three bars are exactly similar to middle three bars with the exception that in this case, each interphase layers is 50 μm thick.

Fig. 64 shows that there is no effect on the longitudinal modulus as a result of addition of nanotubes, whether throughout the matrix or in the interphase layer. The longitudinal modulus of the composite laminate in the direction of the unidirectional carbon fibers is a fiber dominated property. There is a large difference between the matrix properties and fiber properties and thus slight improvement in matrix property has no effect on the overall laminate longitudinal modulus. The results as shown in Fig. 65 indicate an increase in the transverse modulus by addition of nanotubes. The higher weight fraction of nanotubes show a greater impact as compared to the lower weight fraction of pristine nanotubes. The best results are obtained when 1 wt%

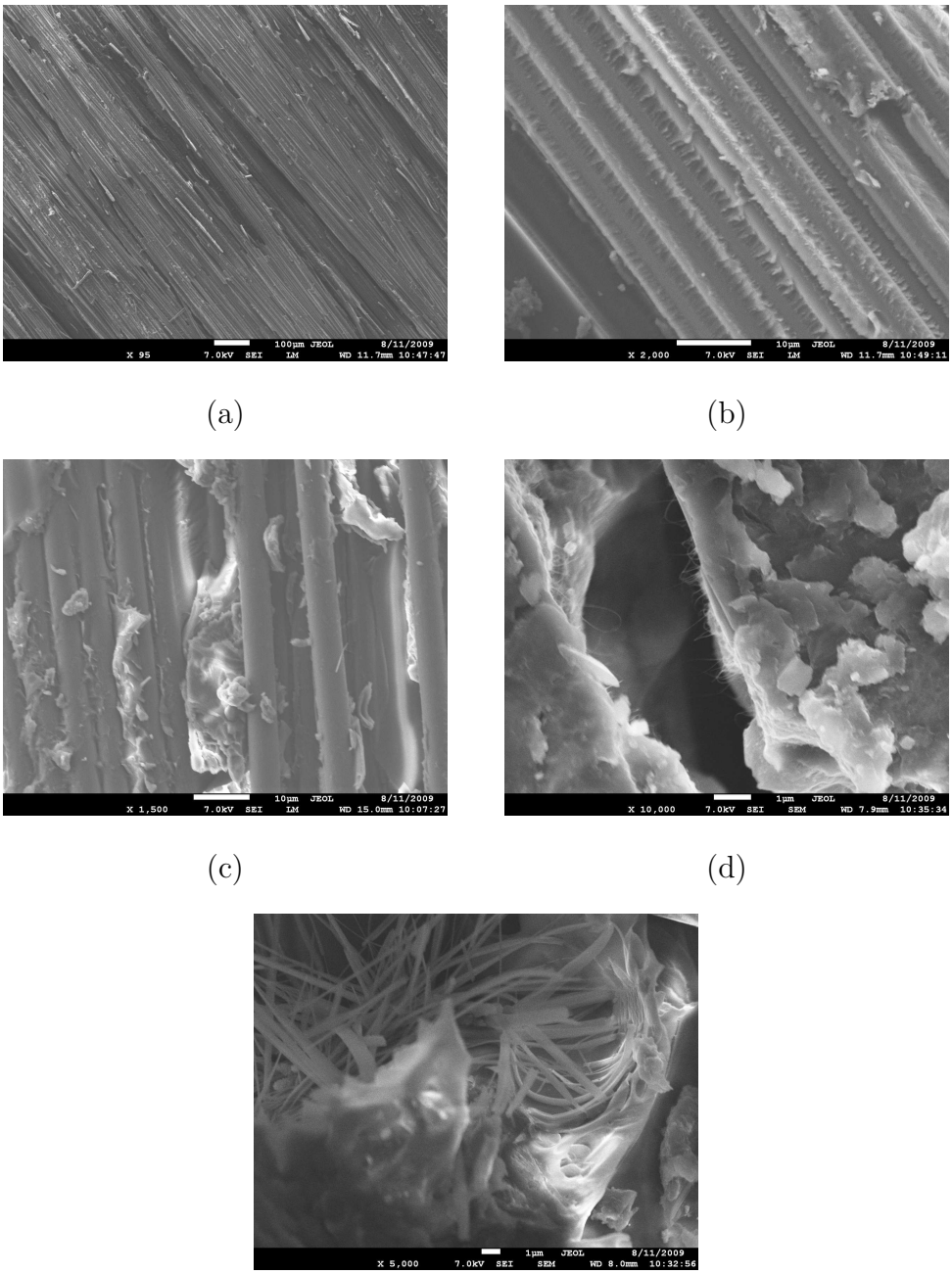

(a) (b) (c) (d) (e)

Fig. 63. SEM micrographs of sheared lamina after in-plane shear test. 63(a) Sheared lamina without CNTs showing fiber matrix debonding, 63(b) Presence of shear hackles between debonded fibers on lamina without CNTs, 63(c) No shear hackles on lamina with amide CNTs, 63(d) Curled nanotube ropes pulled out after bridging cracks, 63(e) Fibrils of thermoplastic phase are observed in the matrix.

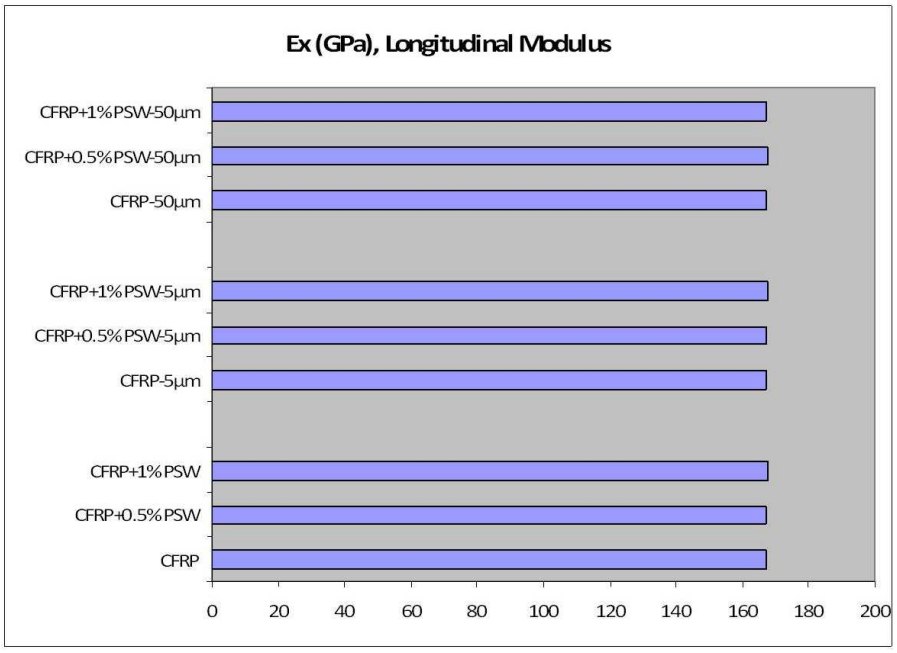

Fig. 64. Longitudinal modulus of different laminates from classical laminate theory.

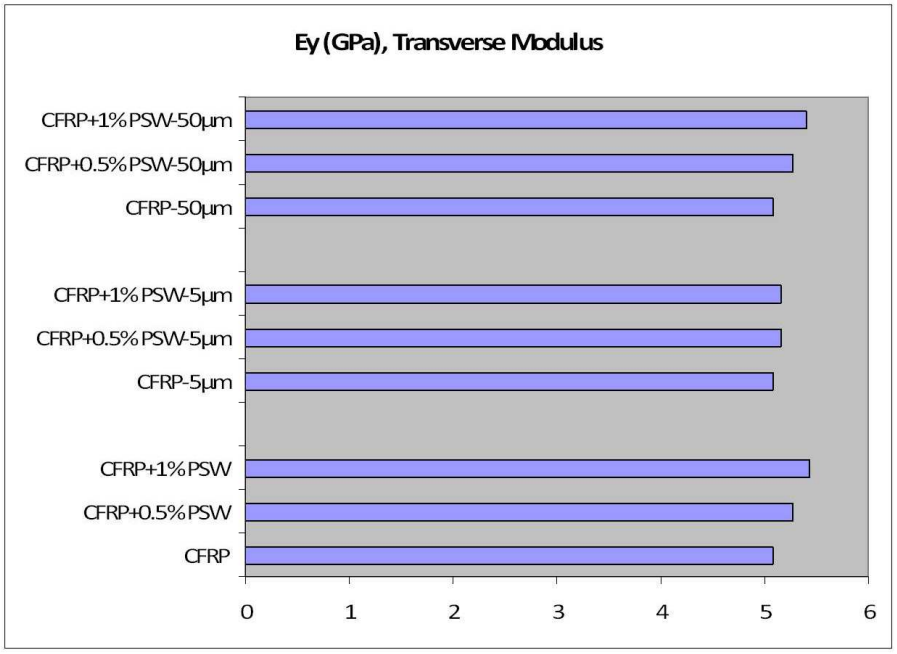

Fig. 65. Transverse modulus of different laminates from classical laminate theory.

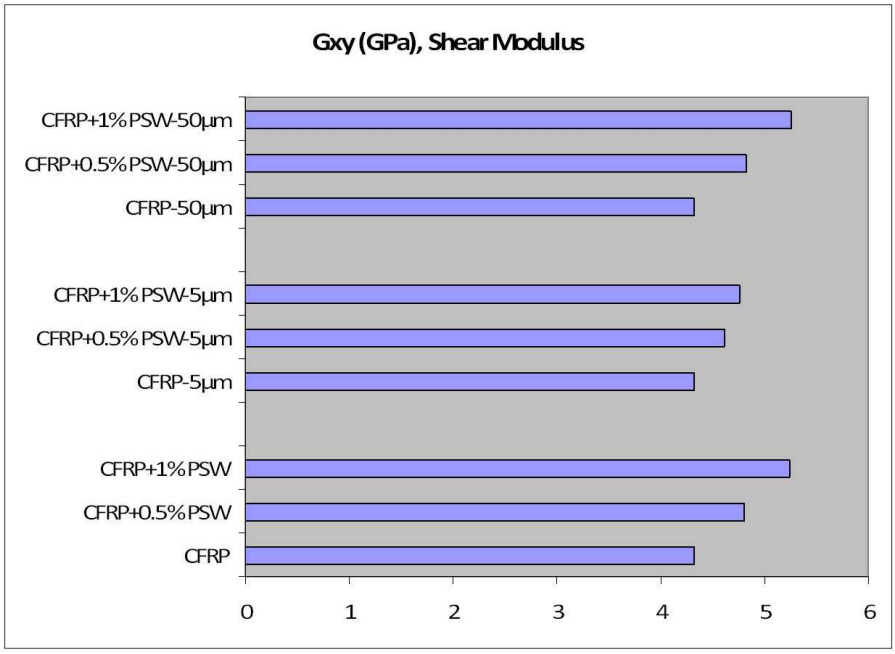

Fig. 66. In-plane shear modulus of different laminates from classical laminate theory.

nanotubes are present throughout the matrix, followed by, when 0.5 wt% nanotubes are present throughout the matrix. The improvement in transverse modulus is about 6% and 12% for specimens with two weight fractions respectively, and is in close agreement with the experimentally observed increase of 6% for specimens with 0.5 wt% of pristine nanotubes.

The introduction of thin layers of 5 μm thickness does not show significant effect as compared to the composite containing 5 μm layers of neat epoxy. However, the presence of 50 μm layers of nanotubes shows significant improvement of about 12% in the transverse modulus (of 1 wt% specimens) over the composite containing 50 μm layers of neat epoxy. The in-plane shear modulus, which is also a matrix dominated property, shows almost similar behavior as transverse properties(Fig. 66). The maximum improvement is for the case of 1 wt% nanotubes present throughout the matrix system instead of just in the interphase layers. In all the modeling cases

presented here, when the nanotube reinforced epoxy nanocomposite interphase layer is introduced between pre-preg layers, it does not result in any increase in the matrix volume fraction and no corresponding decrease in the carbon fiber volume fraction. The actual experiment also does not involve introduction of additional epoxy, so there is no change in the total carbon fiber volume fraction. There is a slight decrease in matrix volume fraction to account for the very small amount of nanotubes added.

5. Interlaminar Fracture Toughness

The delamination extensions were noted from a marked scale on the edge, with 1 mm markings during various increments of stable delamination growth. The delamination extension data was taken from the videos of the crack propogation. As observed from videos, the delamination initiation was followed by a small drop in force. The delamination growth was visually observed at this point from the edge of the specimen thus releasing the stored energy to create new fracture surfaces. For all specimens, the initial small force drop or variation from linearity (i.e. change in slope) was followed by an increase in force till a peak. The increase in force corresponds to the presence of fiber bridging, yarn bridging, ply bridging or a combination of these mechanisms. Similar characteristics were observed in CFRP composites by Paris et al. [88]. R- Curves for all tested specimens are shown in Fig. 68. These curves show the change in the strain energy release rate of the specimen as the initial delamination starts growing from the end of a PTFE insert and propagates through the specimen. A non-linearity criterion is used to calculate the initiation values for the critical strain energy release rates which are considered as the interlaminar fracture toughness values for different laminates. According to the non-linearity criterion [88], force and displacement values corresponding to first deviation from linearity on the force-displacement curve is considered as the critical values for initiation of delamination

growth.

The average values of G_{Ic} initiation for three specimens from each panel are presented in Table XII. The average values of G_{Ic} propagation for three specimens

Table XII. Average G_{Ic} at delamination initiation for UDPP composites

Panel	G_{Ic} Initiation (J/m^2)	Drop w.r. to Base (%)	Drop w.r. to Control (%)
Base: No SWCNT	456	-	-
Control: No SWCNT	359	21%	-
Pristine SWCNT	214	53%	40%
Amide Functionalized SWCNT	209	54%	41%

from each panel are presented in Table XIII. The R-curves for base composite are

Table XIII. Average G_{Ic} at delamination propagation for UDPP composites

Panel	G_{Ic} Initiation (J/m^2)	Drop w.r. to Base (%)	Drop w.r. to Control (%)
Base: No SWCNT	1312	-	-
Control: No SWCNT	894	32%	-
Pristine SWCNT	525	60%	41%
Amide Functionalized SWCNT	314	76%	65%

shown in Fig. 68(a). The initiation values are taken for 0 mm value of delamination extension and the propagation values are averaged from 10 mm to 70 mm. Increase in G_{Ic} after initiation of delamination indicates fiber bridging mechanisms. Actually the G_{Ic} should drop as the crack propagates, however, as the fiber bridging develops i.e. fibers from lower plane bridging with the upper plane, the energy required

to propagate the delamination increases as additional energy is required to debond the bridging fibers from one of the planes or ultimate failure of fibers. Ideally after some initial fiber bridging, the R-curve should show a plateau indicating equilibrium response for delamination propagation. However, as observed in the specimens from base laminate, only specimen B4 showed some plateau region, otherwise a continuous increase in G_{Ic} until 70 mm of extension was observed indicating an extensive fiber bridging. As indicated in Tables XII and XIII, the base laminate has very high G_{Ic} initiation and propagation values indicating highly toughened systems due to the presence of thermoplastic toughener phase.

Fig. 67 shows load-displacement curves for one representative specimen from each

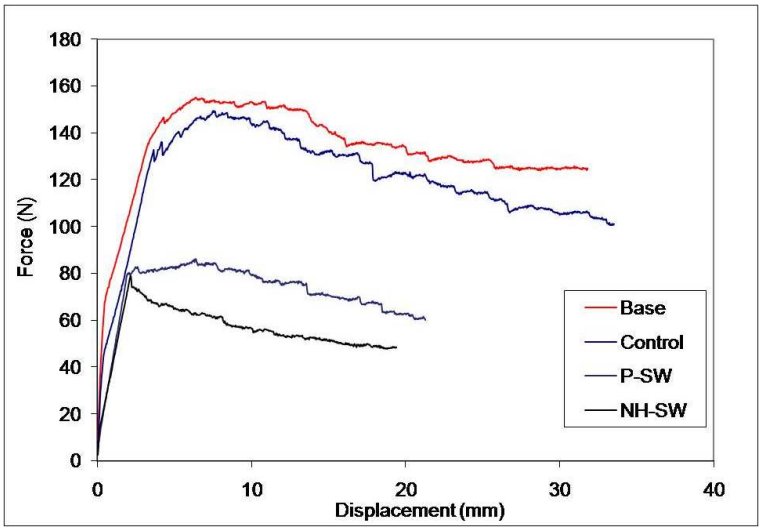

Fig. 67. Load-displacement response of the representative specimens from the unidirectional pre-preg composites.

pre-preg composite panel. It shows that the fiber-bridging mechanism has been greatly suppressed in specimens with amide functionalized nanotubes. Also the area under the curves has been reduced for the pristine and the amide functionalized nanotubes indicating reduced energy dissipation.

Fig. 68(b) shows R-curve for control specimens. Control specimens were prepared

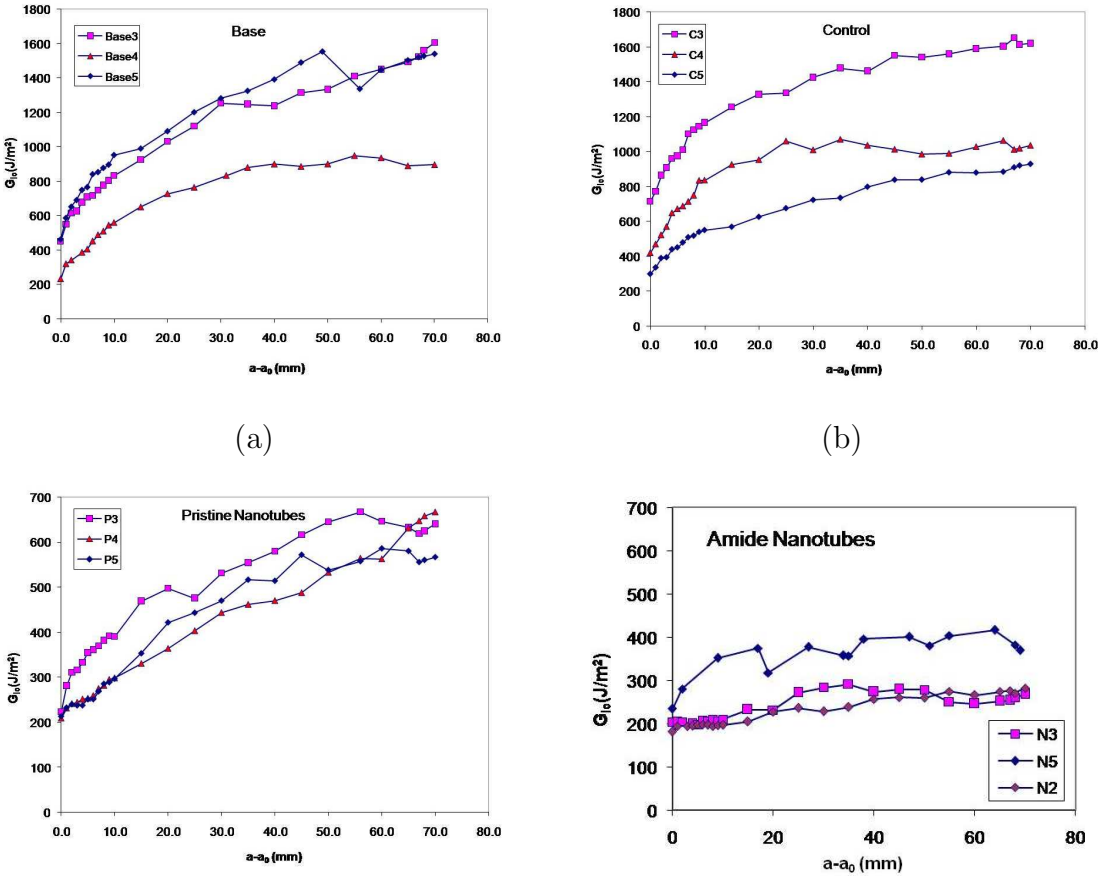

Fig. 68. R-Curves from DCB test of unidirectional pre-preg composites. 68(a) Base composite without CNTs, 68(b) Control composite without nanotubes (solvent evaporated), 68(c) Composite modified with pristine CNTs, 68(d) Composite modified with amide functionalized CNTs.

to separate the effect of solvent spraying and evaporation from the effect of purely nanotube modification. This will also help in finding if the solvent reacts with the toughener phase or has some kind of plasticizing effect on the composite toughness. As seen from Fig. 68(b), all curves showed plateau behaviour after about 20 mm of delamination extension. This indicates reduced fiber bridging as compared with the base composites. Also the G_{Ic} initiation decreased by 21% and G_{Ic} propagation decreased by 32% as seen from Tables XII and XIII.

Fig. 68(c) shows R-curve response for composite with pristine nanotubes in the middle three planes. The plateau regions are not observed as compared to control specimens indicating continuous fiber bridging until 70 mm of delamination extension. However, the G_{Ic} initiation decreased by 40% and 53% compared to control and base specimens and G_{Ic} propagation decreased by 41% and 60% compared to control and base specimens respectively as seen from Tables XII and XIII. This is a large drop in fracture toughness even after considering large variation in results. Microstructural investigation is needed to find the reasons for this large decrease.

Fig. 68(d) shows R-curve response for composite with amide functionalized nanotubes modifying the middle three planes. These are very different curves from the previous R-curves. Two of the specimens, N3 and N5 showed total suppression of fiber bridging mechanisms. There is almost no increase in G_{Ic} after the delamination is initiated and the crack propagated through the specimen showing plateau regions in these R-curves. Only specimen N4 showed some fiber bridging until 50 mm of delamination extension. The G_{Ic} initiation decreased by 41% and 65% compared to control and base specimens and G_{Ic} propagation decreased by 54% and 76% compared to control and base specimens respectively as seen from Tables XII and XIII. The drop in G_{Ic} initiation is comparable to composite with pristine nanotubes, however, the drop in G_{Ic} propagation is very high even after considering large variation

in results. It is extremely important to study the delamination fracture surfaces to get an insight into such reduction in fracture toughness results.

6. Mechanisms of Delamination

Fig. 69 shows SEM micrographs of delamination surfaces of base composite specimens. The presence of debonded fibers, most likely, after fiber bridging can be seen from low magnification images. Also the main mechanism of toughness seems to be the formation of shear hackles in these specimens. The shear deformation of matrix in the form of shear hackles is the contributor for the high interlaminar fracture toughness of the base composites. The dimensions of the shear hackles are noted from the high magnification images. The fiber-matrix bonding also seems to be good as presented in Fig. 69(e), due to the presence of sizing on the carbon fibers. As seen from Fig. 70 for control specimens, the delamination fracture surfaces are almost similar to base composites. Presence of debonded fibers can be seen on the delamination plane, however, the size of the flakes in the shear hackles seems to be reduced along with reduced amount of shear hackle zones. This can possibly explain the reduction in G_{Ic} for control specimens. Fig.71 shows delamination fracture surfaces for pristine CNT modified mid-planes. The low magnification images show suppression of shear hackle formation as well as reduced flake sizes in the shear hackles. The higher magnification images in Fig.72 show presence of entangled network of pristine nanotubes. Again suppression of shear hackle mechanism can be seen, however, a new mechanism of CNT stretching is noticed in these images. The entangled network of pristine nanotubes seems to be stretched in shearing direction i.e. 45° to the direction of the crack propagation. The formation of shear hackles seems to be a major contributor in toughness improvement compared to the CNT stretching mechanism. The observed decrease in G_{Ic} is somewhat explained from the mechanisms observed from

(a) Delamination surface showing debonded (or post bridging) fibers

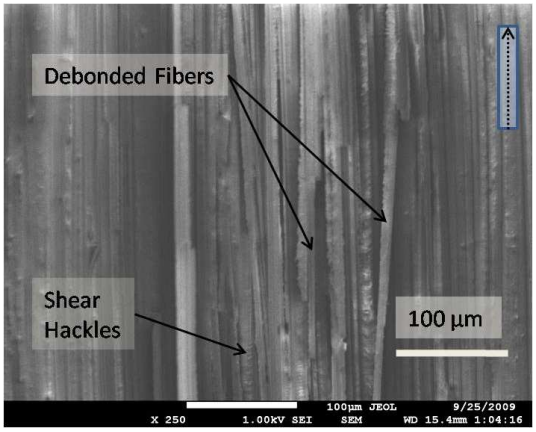

(b) Debonding and hackles

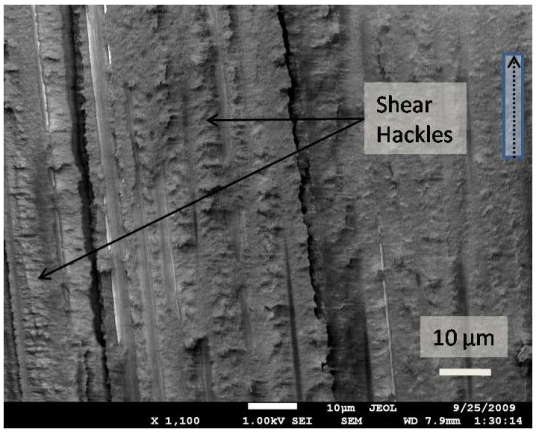

(c) Substantial shear hackle formation

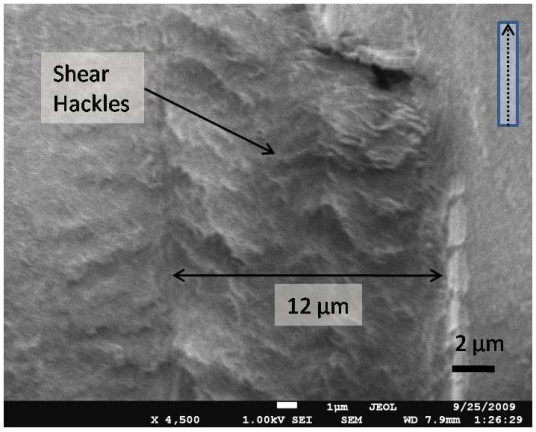

(d) Large shear hackles

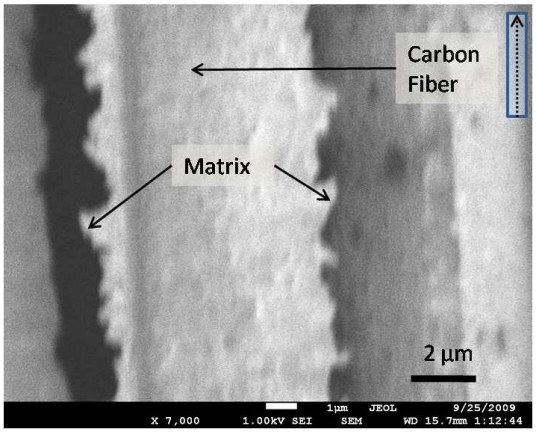

(e) Matrix bonding to fiber

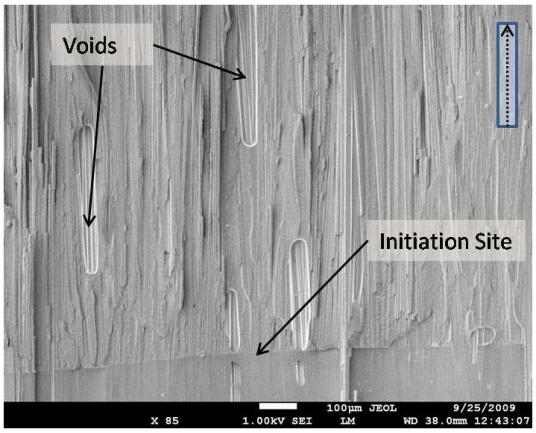

(f) Presence of voids on the delamination plane

Fig. 69. Delamination fracture surfaces of base UDPP composites.

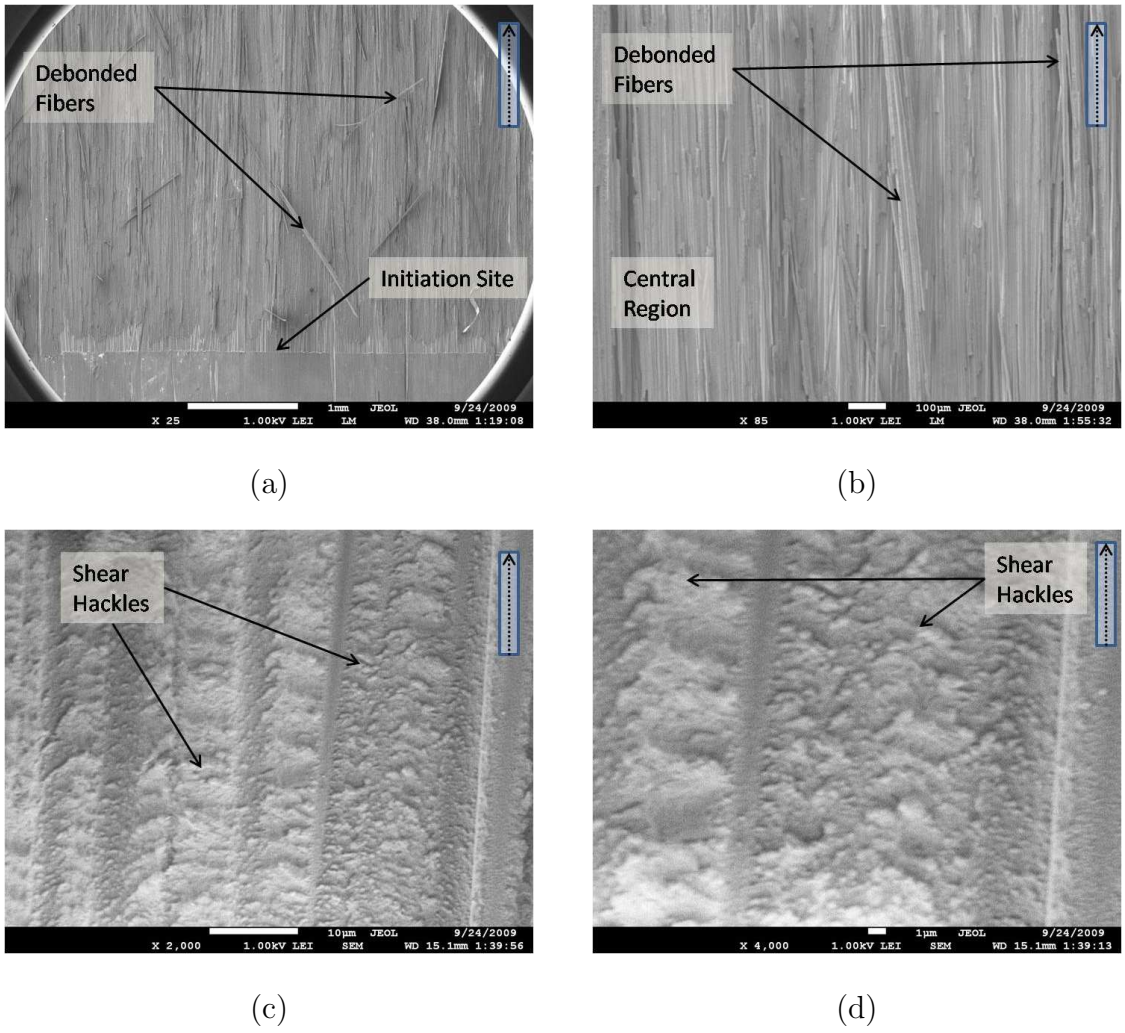

(a) (b)

(c) (d)

Fig. 70. Delamination fracture surfaces of control UDPP composites. 70(a) Delamination surface at initiation site showing debonded (or post bridging) fibers, 70(b) Delamination surface along crack propagation path, 70(c) Lower magnification showing shear hackle formation, 70(d) Higher magnification of the shear hackles.

these images. Although more investigation is necessary to pin point the details of the toughness decrease. Fig. 73 indicates spherulite formation in the specimen with amide functionalized nanotubes. Higher magnification images shows the fibrils in the spherulites and some of such surfaces seems to be flat compared to the surrounding matrix deformation. These images are peculiar to only specimens with functionalized CNTs, indicating some reaction of toughener phase with the amide reactive group resulting in phase separation in the composites. Such spherulite formation can hinder the formation of shear hackles. Fig. 74 shows presence of white spots/regions on the delamination surfaces. These white regions are observed in only the specimens with amide functionalized CNTs. Such white regions are also an indication of chemical reaction of the amide reactive group with the toughened RS-47 matrix. The matrix consists of two epoxies (DGEBA and TGDDM), curing agent (DDS) and a thermoplastic toughener phase (most likely PES). However, it is not clear at this point about which phase reacts with the functional group on the nanotubes.

The higher magnification images show suppression of matrix deformation in these white regions. This will contribute to a reduction in fracture toughness, as matrix deformation is extremely important mechanism for providing toughness to the composite material.

Fig. 75 shows higher magnification images to further investigate the fracture mechanisms. First observation is that the network of nanotubes is quite extensive and the local volume fraction of CNTs seems to be much higher than global volume fraction. The main reason for this is due to the localization of the CNT rich area in the interphase region between two pre-pregs. Second observation is the formation of voids and break down of matrix in the form of fibrils indicating crazing/croiding like mechanism. Third observation is the stretching of nanotube bundles at 45° direction indicating shearing forces on this surface. The most important observation is

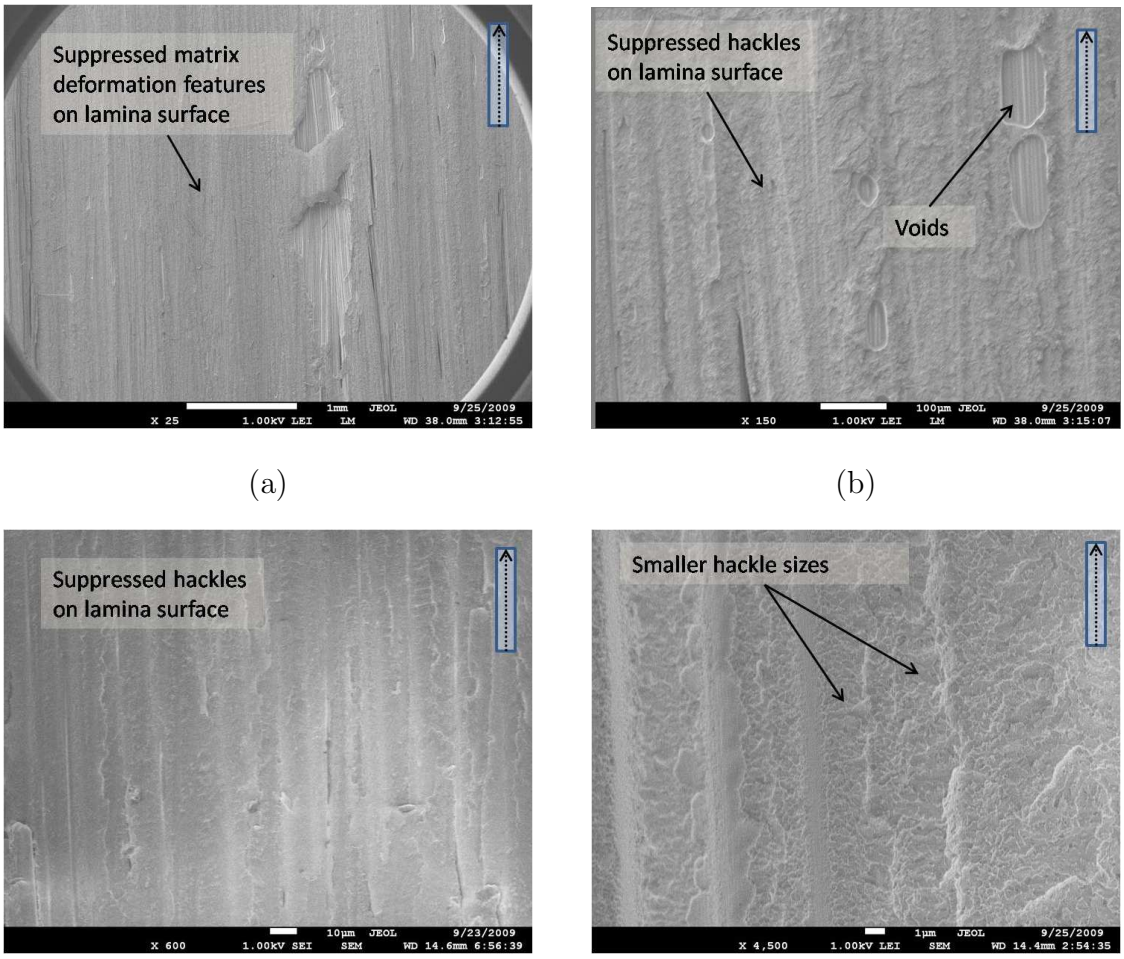

(a) (b)

(c) (d)

Fig. 71. Delamination fracture surfaces of pristine CNT modified UDPP composites. 71(a) Delamination surface showing suppressed matrix deformation, 71(b) Presence of voids at few spots, 71(c) Comparatively clean delamination surface (suppressed shear), 71(d) Reduced sizes of the shear hackles.

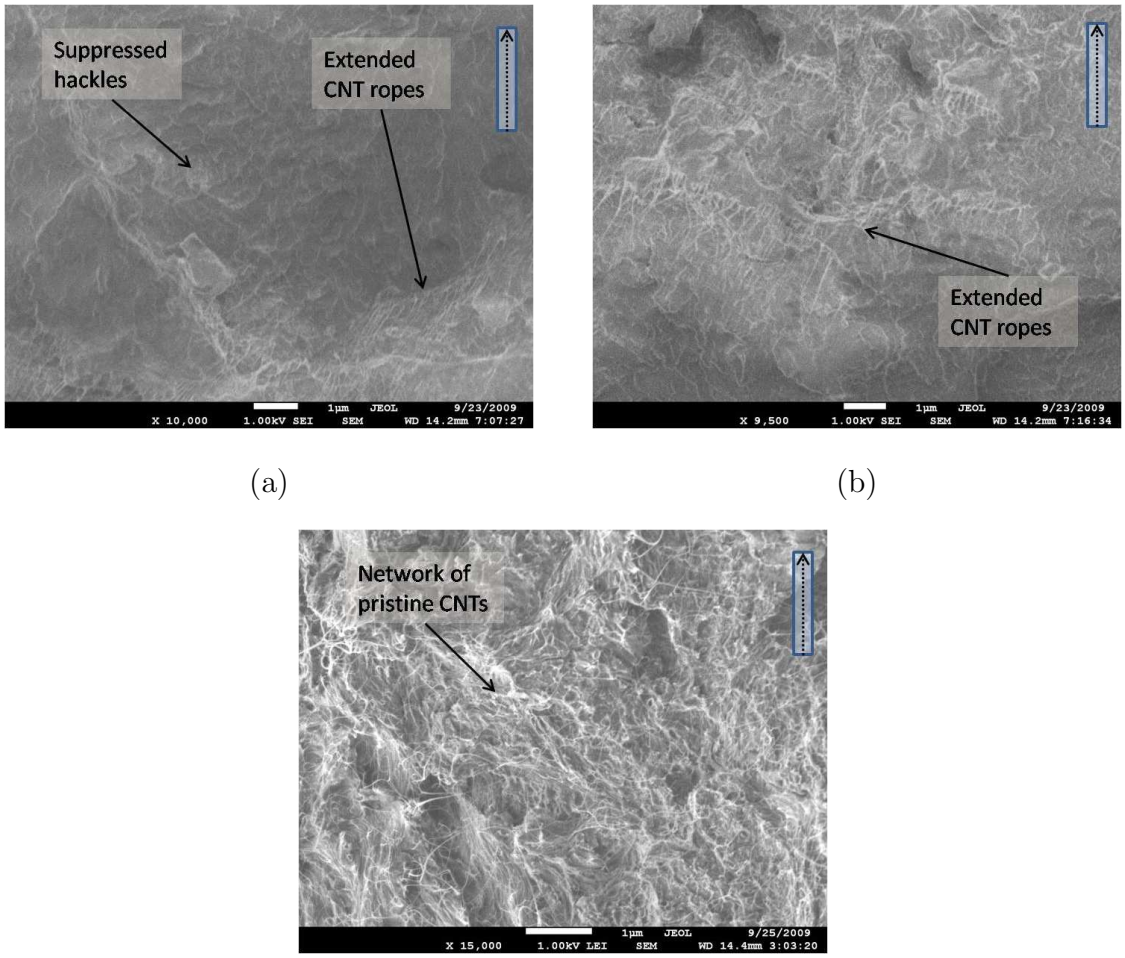

Fig. 72. Higher magnification of delamination fracture surfaces of pristine CNT modified UDPP composites. 72(a) Suppressed shear hackles and stretched pristine CNT ropes, 72(b) Higher magnification of extended (stretched) ropes in the shearing direction (45° to crack propagation direction), 72(c) Presence of entangled network of pristine CNTs.

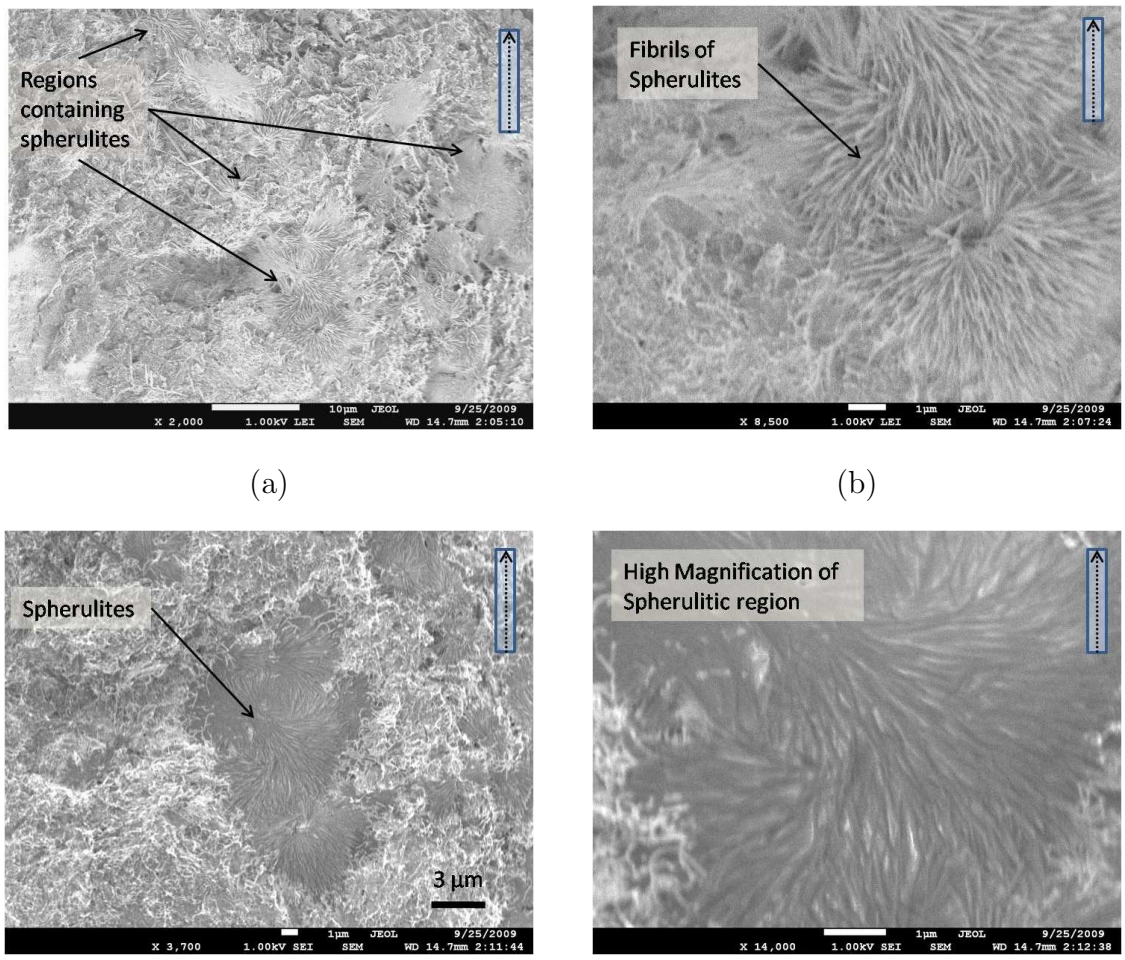

(a) (b)

(c) (d)

Fig. 73. Spherulites on amide functionalized CNT modified UDPP composites. 73(a) Presence of spherulites on the delamination fracture surface, 73(b) Higher magnification image showing fibrils of spherulites, 73(c) Flat surfaces in the spherulites region, 73(d) Higher magnification of the flat surfaces in spherulitic region.

the large suppression of shear hackle mechanism and presence of undeformed matrix regions on the delamination plane. These observations strongly support the observation of reduced shear properties and reduced fracture toughness of composites with amide functionalized nanotubes. This research provided some initial assessments for the reduction in fracture toughness by addition of pristine or amide functionalized nanotubes. It is extremely important to continue this study for better explanation of toughening mechanisms and to prevent fracture toughness reduction in composites.

7. Electrical Conductivity

The electrical conductivity of unidirectional pre-preg composites is very high because of the high volume fraction of carbon fibers which are very conductive 10^3 S/cm. These carbon fibers form conducting percolation network due to contact and thus are already percolated systems as shown in Fig. 76. No improvement has been observed by introducing carbon nanotubes in all layers of the pre-preg composites. Thus the electrical conductivity improvement of the matrix has not be transferred to such systems at laminate scale. The electrical conductivity of laminates containing low conductivity fibers (glass, silicon carbide, etc.) might be an area of impact for transferring matrix conductivity at the laminate scale.

D. Summary

The main contributions presented in this chapter are summarized as follows:

1. A new material system is produced by introduction of pristine and amide functionalized single wall carbon nanotubes in unidirectional carbon fiber reinforced toughened epoxy matrix composite laminates.
2. About 20% improvement is found in the transverse modulus by adding just 1.0 wt%

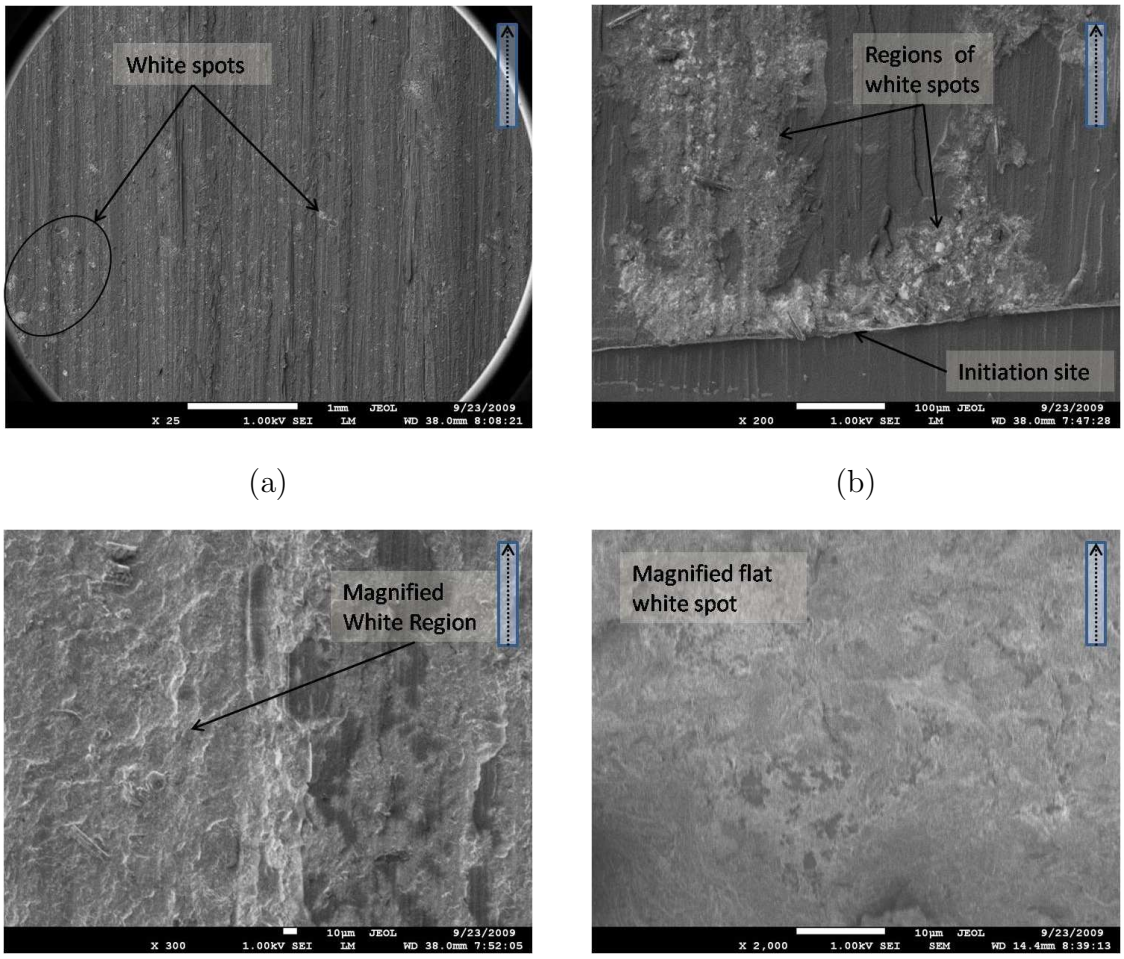

Fig. 74. Delamination fracture surfaces of amide functionalized CNT modified UDPP composites. 74(a) Presence of white spots on the delamination fracture surface, 74(b) Large white regions near initiation site, 74(c) Higher magnification of the white region, 74(d) Higher magnification shows flat surfaces in white region.

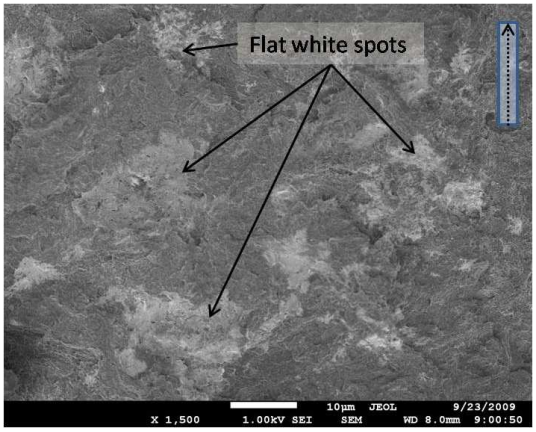

(a) White spots on the delamination fracture surface

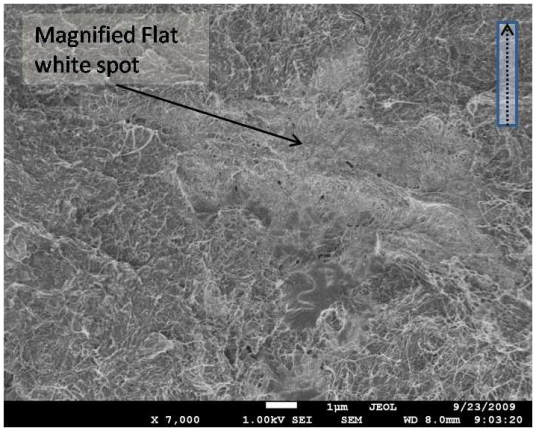

(b) Magnified white spots

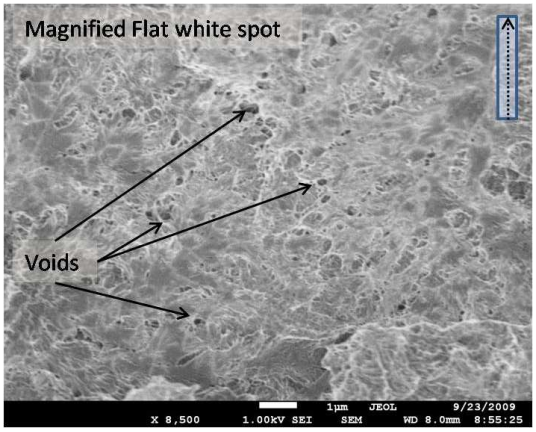

(c) Presence of voids in the white region

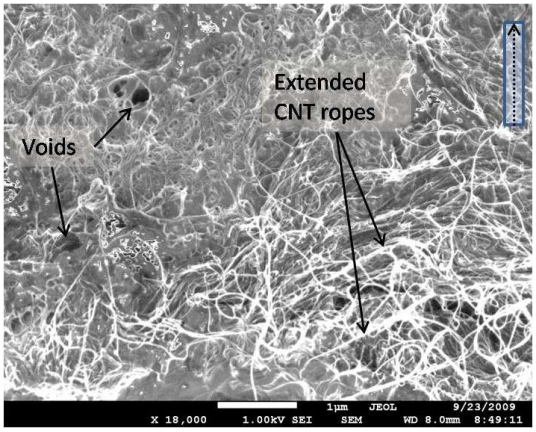

(d) Voids and extended CNT ropes

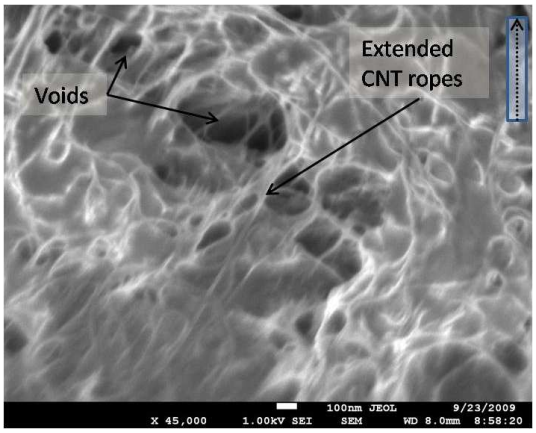

(e) Voids and extended (stretched ropes) in shearing direction

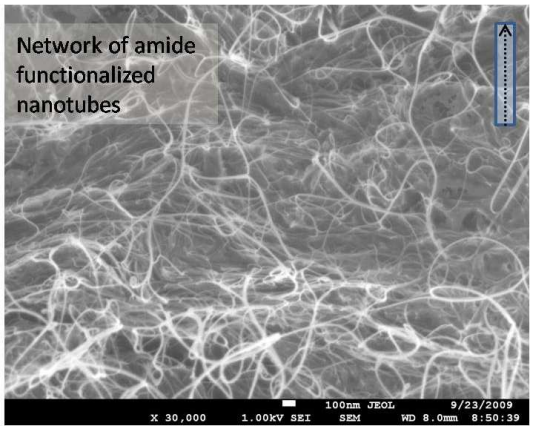

(f) Presence of entangled and embedded network of amide functionalized CNTs

Fig. 75. Higher magnification of delamination fracture surfaces of amide functionalized CNT modified UDPP composites.

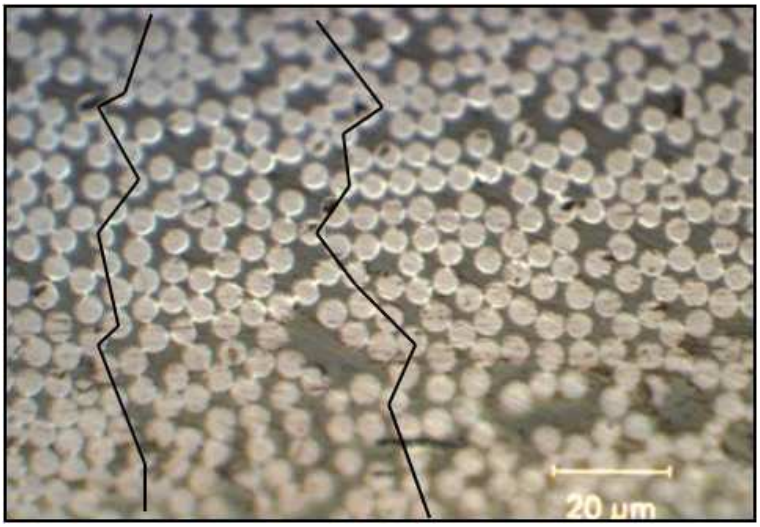

Fig. 76. Formation of percolation network in unidirectional fiber composite laminate.

of amide functionalized nanotubes. However, the in-plane shear modulus is found to be decreased due to functionalized nanotubes.

3. The transverse strength and the shear strength are found to be reduced by addition of functionalized nanotubes.

4. Possible reason for reduction in strength is due to insufficient evaporation of solvent after spraying process or due to modified stoichiometric proportion of amine group in the epoxy system resulting in additional amine group from functionalization that can act as plasticizing agent.

5. Classical laminate analysis is used to model a representative laminate system consisting of interphase layers of nanocomposites.

6. The predictions from the model are somewhat comparable with experimental measurements, except for the case of in-plane shear modulus. However, much more work needs to be done in modeling part to be able predict the response of these complex systems.

7. There is a large reduction in interlaminar fracture toughness of composites with

pristine and amide functionalized nanotubes. Some of the mechanisms that might be responsible for this behavior have been identified in this research.

8. Formation of shear hackles is seen to be the main contributor of toughness in RS-47 matrix based composites and suppression of this mechanism along with suppressed fiber bridging resulted in reduction of initiation and propagation fracture toughness in these composites.

The research topic of toughening laminated composites using carbon nanotubes is still very new and the concepts of toughening process are still unclear in such composites. The understanding of the exact role played by the nanotube reinforcement in the toughening process requires much more work and only some initial understanding has been provided based on the observations from the current work.

CHAPTER VI

SUMMARY AND FUTURE CHALLENGES

A. Summary and Significance of Present Work

The key outcomes from the present research are the development of processing methods and characterization methodology for multi-scale multi-functional composites based on the epoxy resin. The research objectives lead to setting up of processing methods for nanocomposites using cast molding method, vacuum assisted resin tranfer molding method for woven carbon fiber composites with spraying technique for selective placement of nanotubes and hot press method for unidirectional carbon fiber pre-preg based composites. Good quality nanocomposites, woven fabric composite laminates and unidirectional fiber composite laminates are obtained by way of this research.

After establishing processing technique, a characterization methodology is established for investigating multi-functional properties of such composites. Nanocomposites are tested to investigate the interaction of various types of carbon nanotubes (pristine SW, functionalized SW, XD) with the epoxy resin. Fracture mechanisms are identified based on high resolution fractography of such nanocomposites. The observed mechanisms are important to identify plausible contribution by introduction of carbon nanotubes in the brittle epoxy matrix.

The effect of carbon nanotubes on the interlaminar fracture of traditional advanced composites for aerospace applications containing woven as well as unidirectional fibers are evaluated through multi-scale characterization and testing. In this process, some of the structure-property relationships are identified in such material systems, providing a physical understanding of the mechanisms introduced due to

localized dispersion of carbon nanotubes by selective placement into the composites. Microscopic investigation played an important role in explaining the mechanical testing results for the interlaminar fracture toughness and the interlaminar shear strength. The fundamental understanding of the exact role of the dispersed nanophase and contribution to the macro-scale properties is still mostly unclear and more work is needed for providing such an understanding. The present research work shows a small attempt in that direction.

In addition to establishing a methodology for processing and characterization of multi-scale multi-functional composites, the generated data can be used across a range of length scales to validate micromechanics, fracture or damage mechanics based models along with computational chemistry based molecular dynamics simulations for multi-scale modeling of the proposed system.

B. Future Challenges

The understanding of the exact role of the nano/micro dispersed phases in the toughening process of advanced composites is an open question. More experimental work is needed to establish better structure-property relationships and improve the understanding of fracture processes at the nanoscale. In addition, significant modeling efforts are needed to understand the behavior of fracture processes at the nanoscale and its impact on the macroscale properties.

REFERENCES

[1] M. Strock, "Types of carbon nanotubes. available [online]: http://www.nanoscienceworks.org," 2006.

[2] S. Iijima, "Helical microtubules of graphitic carbon," *Nature*, vol. 354, pp. 56, 1991.

[3] M. F. Yu, B. Files, S. Arepalli, and R.S. Ruoff, "Tensile loading of ropes of single wall carbon nanotubes and their mechanical properties," *Physical Review Letters*, vol. 84, no. 24, pp. 5552, 2000.

[4] J. Zhu, J. D. Kim, H. Q. Peng, J. L. Margrave, V. N. Khabashesku, and E. V. Barrera, "Improving the dispersion and integration of single-walled carbon nanotubes in epoxy composites through functionalization," *Nano Letters*, vol. 3, no. 8, pp. 1107–1113, 2003.

[5] J. Zhu, Peng H.Q., M. Rodriguez, J.L. Margrave, V.N. Khabasheskhu, A.M. Imam, K. Lozano, and E.V. Barrera, "Reinforcing epoxy polymer composites through covalent integration of functionalized nanotubes," *Advanced Functional Materials*, vol. 14, no. 7, pp. 643–648, 2004.

[6] A. K. Dutta, D. Penumadu, and B. Files, "Nanoindentation testing for evaluating modulus and hardness of swcnt reinforced epoxy composites," *Journal of Materials Research*, vol. 19, no. 1, pp. 158, 2004.

[7] X. Li, H. Gao, W. A. Scrivens, D. Fei, X. Xu, M. A. Sutton, A. P. Reynolds, and M. L. Myrick, "Nanomechanical characterization of swcnt reinforced epoxy composites," *Nanotechnology*, vol. 15, pp. 1416, 2004.

[8] P.R. Thakre, D.C. Lagoudas, J. Zhu, E.V. Barrera, and T.S. Gates, "Effect of functionalization and weight fraction of single wall carbon nanotubes on mechanical properties of epoxy nanocomposites," in *Proc. International Conference on Computational and Experimental Engineering Sciences (ICCES)*, Chennai, India, 2005.

[9] A. S. dos Santos, T. D. N. Leite, C. A. Furtado, C. Welter, L. C. Pardini, and G. G. Silva, "Morphology, thermal expansion, and electrical conductivity of multiwalled carbon nanotube/epoxy composites," *Journal of Applied Polymer Science*, vol. 108, no. 2, pp. 979–986, 2008.

[10] D. Zilli, S. Goyanes, M. M. Escobar, C. Chiliotte, V. Bekeris, A. L. Cukierman, and G. H. Rubiolo, "Comparative analysis of electric, magnetic, and mechanical properties of epoxy matrix composites with different contents of multiple walled carbon nanotubes," *Polymer Composites*, vol. 28, no. 5, pp. 612–617, 2007.

[11] E. T. Thostenson and T. W. Chou, "Processing-structure-multi-functional property relationship in carbon nanotube/epoxy composites," *Carbon*, vol. 44, no. 14, pp. 3022–3029, 2006.

[12] M. Moniruzzaman and K. I. Winey, "Polymer nanocomposites containing carbon nanotubes," *Macromolecules*, vol. 39, no. 16, pp. 5194–5205, 2006.

[13] H. Miyagawa, M. Misra, and A. K. Mohanty, "Mechanical properties of carbon nanotubes and their polymer nanocomposites," *Journal of Nanoscience and Nanotechnology*, vol. 5, no. 10, pp. 1593–1615, 2005.

[14] C. A. Martin, J. K. W. Sandler, A. H. Windle, M. K. Schwarz, W. Bauhofer, K. Schulte, and M. S. P. Shaffer, "Electric field-induced aligned multi-wall

carbon nanotube networks in epoxy composites," *Polymer*, vol. 46, no. 3, pp. 877–886, 2005.

[15] M. J. Biercuk, M. C. Llaguno, M. Radosavljevic, J. K. Hyun, A. T. Johnson, and J. E. Fischer, "Carbon nanotube composites for thermal management," *Applied Physics Letters*, vol. 80, no. 15, pp. 2767–2769, 2002.

[16] T. Prasse, L. Flandin, K. Schulte, and W. Bauhofer, "In situ observation of electric field induced agglomeration of carbon black in epoxy resin," *Applied Physics Letters*, vol. 72, no. 22, pp. 2903–2905, 1998.

[17] T. Prasse and W. Bauhofer, "Electrically structured inhomogeneous conductivity in carbon black-filled epoxy resins," *Kunststoffe-Plast Europe*, vol. 92, no. 2, pp. 74–75, 2002.

[18] F. H. Gojny, M. H. G. Wichmann, B. Fiedler, I. A. Kinloch, W. Bauhofer, A. H. Windle, and K. Schulte, "Evaluation and identification of electrical and thermal conduction mechanisms in carbon nanotube/epoxy composites," *Polymer*, vol. 47, no. 6, pp. 2036–2045, 2006.

[19] A. Moisala, Q. Li, I. A. Kinloch, and A. H. Windle, "Thermal and electrical conductivity of single- and multi-walled carbon nanotube-epoxy composites," *Composites Science and Technology*, vol. 66, no. 10, pp. 1285–1288, 2006.

[20] H. Chen, H. Muthuraman, P. Stokes, J. H. Zou, X. Liu, J. H. Wang, Q. Huo, S. I. Khondaker, and L. Zhai, "Dispersion of carbon nanotubes and polymer nanocomposite fabrication using trifluoroacetic acid as a co-solvent," *Nanotechnology*, vol. 18, no. 41, pp. –, 2007.

[21] N. Grossiord, J. Loos, O. Regev, and C. E. Koning, "Toolbox for dispersing

carbon nanotubes into polymers to get conductive nanocomposites," *Chemistry of Materials*, vol. 18, no. 5, pp. 1089–1099, 2006.

[22] J. Li, P. C. Ma, W. S. Chow, C. K. To, B. Z. Tang, and J. K. Kim, "Correlations between percolation threshold, dispersion state, and aspect ratio of carbon nanotubes," *Advanced Functional Materials*, vol. 17, no. 16, pp. 3207–3215, 2007.

[23] C. A. Martin, J. K. W. Sandler, M. S. P. Shaffer, M. K. Schwarz, W. Bauhofer, K. Schulte, and A. H. Windle, "Formation of percolating networks in multi-wall carbon-nanotube-epoxy composites," *Composites Science and Technology*, vol. 64, no. 15, pp. 2309–2316, 2004.

[24] M. H. G. Wichmann, J. Sumfleth, B. Fiedler, F. H. Gojny, and K. Schulte, "Multiwall carbon nanotube/epoxy composites produced by a masterbatch process," *Mechanics of Composite Materials*, vol. 42, no. 5, pp. 395–406, 2006.

[25] K. T. Lau, M. Lu, and K. Liao, "Improved mechanical properties of coiled carbon nanotubes reinforced epoxy nanocomposites," *Composites Part A-Applied Science and Manufacturing*, vol. 37, no. 10, pp. 1837–1840, 2006.

[26] L. J. Lanticse, Y. Tanabe, K. Matsui, Y. Kaburagi, K. Suda, M. Hoteida, M. Endo, and E. Yasuda, "Shear-induced preferential alignment of carbon nanotubes resulted in anisotropic electrical conductivity of polymer composites," *Carbon*, vol. 44, no. 14, pp. 3078–3086, 2006.

[27] G. Pecastaings, P. Delhaes, A. Derre, H. Saadaoui, F. Carmona, and S. Cui, "Role of interfacial effects in carbon nanotube/epoxy nanocomposite behavior," *Journal of Nanoscience and Nanotechnology*, vol. 4, no. 7, pp. 838–843, 2004.

[28] R. Krishnamoorti, "Strategies for dispersing nanoparticles in polymers," *MRS Bulletin*, vol. 32, no. 4, pp. 341–347, 2007.

[29] C. A. Mitchell, J. L. Bahr, S. Arepalli, J. M. Tour, and R. Krishnamoorti, "Dispersion of functionalized carbon nanotubes in polystyrene," *Macromolecules*, vol. 35, no. 23, pp. 8825–8830, 2002.

[30] S. Bal, "Influence of dispersion states of carbon nanotubes on mechanical and electrical properties of epoxy nanocomposites," *Journal of Scientific & Industrial Research*, vol. 66, no. 9, pp. 752–756, 2007.

[31] L. Liu and J. C. Grunlan, "Clay assisted dispersion of carbon nanotubes in conductive epoxy nanocomposites," *Advanced Functional Materials*, vol. 17, no. 14, pp. 2343–2348, 2007.

[32] H. Miyagawa and L. T. Drzal, "Thermo-physical and impact properties of epoxy nanocomposites reinforced by single-wall carbon nanotubes," *Polymer*, vol. 45, no. 15, pp. 5163–5170, 2004.

[33] J. Sandler, M. S. P. Shaffer, T. Prasse, W. Bauhofer, K. Schulte, and A. H. Windle, "Development of a dispersion process for carbon nanotubes in an epoxy matrix and the resulting electrical properties," *Polymer*, vol. 40, no. 21, pp. 5967–5971, 1999.

[34] L. Valentini, D. Puglia, E. Frulloni, I. Armentano, J.M. Kenny, and S. Santucci, "Dielectric behavior of epoxy matrix/single-walled carbon nanotube composites," *Composites Science and Technology*, vol. 64, pp. 23–33, 2004.

[35] J.B. Bai and A. Allaoui, "Effect of the length and the aggregate size of mwnts on the improvement efficiency of the mechanical and electrical properties of

nanocomposites - experimental investigation," *Composites: Part A*, vol. 34, pp. 689–694, 2003.

[36] G.D. Seidel and D.C. Lagoudas, "A micromechanics model for the electrical conductivity of nanotube-polymer nanocomposites," *Journal of Composite Materials*, vol. 43, no. 9, pp. 917–941, 2009.

[37] R. H. Schmidt, I. A. Kinloch, A. N. Burgess, and A. H. Windle, "The effect of aggregation on the electrical conductivity of spin-coated polymer/carbon nanotube composite films," *Langmuir*, vol. 23, no. 10, pp. 5707–5712, 2007.

[38] J. K. W. Sandler, J. E. Kirk, I. A. Kinloch, M. S. P. Shaffer, and A. H. Windle, "Ultra-low electrical percolation threshold in carbon-nanotube-epoxy composites," *Polymer*, vol. 44, no. 19, pp. 5893–5899, 2003.

[39] S. M. Yuen, C. C. M. Ma, H. H. Wu, H. C. Kuan, W. J. Chen, S. H. Liao, C. W. Hsu, and H. L. Wu, "Preparation and thermal, electrical, and morphological properties of multiwalled carbon nanotube and epoxy composites," *Journal of Applied Polymer Science*, vol. 103, no. 2, pp. 1272–1278, 2007.

[40] K. I. Winey, T. Kashiwagi, and M. F. Mu, "Improving electrical conductivity and thermal properties of polymers by the addition of carbon nanotubes as fillers," *Mrs Bulletin*, vol. 32, no. 4, pp. 348–353, 2007.

[41] P. C. Ma, J. K. Kim, and B. Z. Tang, "Effects of silane functionalization on the properties of carbon nanotube/epoxy nanocomposites," *Composites Science and Technology*, vol. 67, no. 14, pp. 2965–2972, 2007.

[42] C. Y. Li, E. T. Thostenson, and T. W. Chou, "Dominant role of tunneling

resistance in the electrical conductivity of carbon nanotube-based composites," *Applied Physics Letters*, vol. 91, no. 22, pp. –, 2007.

[43] L. Gao, X. F. Zhou, and Y. L. Ding, "Effective thermal and electrical conductivity of carbon nanotube composites," *Chemical Physics Letters*, vol. 434, no. 4-6, pp. 297–300, 2007.

[44] S. Bal and S. S. Samal, "Carbon nanotube reinforced polymer composites - a state of the art," *Bulletin of Materials Science*, vol. 30, no. 4, pp. 379–386, 2007.

[45] K. Schulte, F. H. Gojny, M. H. G. Wichmann, J. Sumfleth, and B. Fiedler, "Polymer nanocomposites: Chances, risks and potential to improve the mechanical and physical properties," *Materialwissenschaft Und Werkstofftechnik*, vol. 37, no. 9, pp. 698–703, 2006.

[46] Y. S. Song and J. R. Youn, "Influence of dispersion states of carbon nanotubes on physical properties of epoxy nanocomposites," *Carbon*, vol. 43, no. 7, pp. 1378–1385, 2005.

[47] Y. J. Kim, T. S. Shin, H. D. Choi, J. H. Kwon, Y. C. Chung, and H. G. Yoon, "Electrical conductivity of chemically modified multiwalled carbon nanotube/epoxy composites," *Carbon*, vol. 43, no. 1, pp. 23–30, 2005.

[48] S. Barrau, P. Demont, C. Maraval, A. Bernes, and C. Lacabanne, "Glass transition temperature depression at the percolation threshold in carbon nanotube-epoxy resin and polypyrrole-epoxy resin composites," *Macromolecular Rapid Communications*, vol. 26, no. 5, pp. 390–394, 2005.

[49] B. Kim, J. Lee, and I. S. Yu, "Electrical properties of single-wall carbon nanotube and epoxy composites," *Journal of Applied Physics*, vol. 94, no. 10, pp. 6724–6728, 2003.

[50] A. Allaoui, S. Bai, H. M. Cheng, and J. B. Bai, "Mechanical and electrical properties of a mwnt/epoxy composite," *Composites Science and Technology*, vol. 62, no. 15, pp. 1993–1998, 2002.

[51] A.J. Brunner and P. Flueler, "Prospects in fracture mechanics of engineering laminates," *Engineering Fracture Mechanics*, vol. 72, pp. 899–908, 2005.

[52] T.W. Chou, *Microstructural Design of Fiber Composites*, Cambridge University Press, Cambridge, 1992.

[53] I.M. Daniel and O. Ishai, *Engineering Mechanics of Composite Materials*, Oxford University Press, Oxford, 1994.

[54] N. Sela and O. Ishai, "Interlaminar fracture toughness and toughening of laminated composite materials: A review," *Composites*, vol. 20, no. 5, pp. 423–435, 1989.

[55] S.W. Tsai and H.T. Hahn, *Introduction to Composite Materials*, Technomic Publishing Company, Lancaster, 1980.

[56] J. Njuguna and K. Pielichowski, "Polymer nanocomposites for aerospace applications: Properties," *Advanced Engineering Materials*, vol. 5, no. 11, pp. 769–778, 2003.

[57] J. Njuguna, K. Pielichowski, and J.R. Alcock, "Epoxy-based fibre reinforced nanocomposites," *Advanced Engineering Materials*, vol. 9, no. 10, pp. 835–847, 2007.

[58] R.A. Jurf and R.B. Pipes, "Interlaminar fracture of composite materials," *Journal of Composite Materials*, vol. 16, pp. 386–394, 1982.

[59] J. Whitney, C.E. Browning, and W. Hoogsteden, "A double cantilever beam test for characterizing mode i delamination of composite materials," *Journal of Reinforced Plastics and Composites*, vol. 1, no. 297-313, 1982.

[60] T.K. O'Brien, "Interlaminar fracture of composites," *NASA TM 85768*, 1984.

[61] N.S. Choi, A.J. Kinloch, and J.G. Williams, "Delamination fracture of multidirectional carbon-fiber/epoxy composites under mode i, mode ii and mixed-mode i/ii loading," *Journal of Composite Materials*, vol. 33, no. 1, pp. 73–100, 1999.

[62] E. Bekyarova, E.T. Thostenson, A. Yu, H. Kim, J. Gao, J. Tang, H.T. Hahn, T.-W. Chou, M.E. Itkis, and R.C. Haddon, "Multiscale carbon nanotube - carbon fiber reinforcement for advanced epoxy composites," *American Chemical Society*, vol. 23, pp. 3970–3974, 2007.

[63] E. Bekyarova, E.T. Thostenson, A. Yu, M.E. Itkis, Fakhrutdinov D., T.-W. Chou, and R.C. Haddon, "Functionalized single-walled carbon nanotubes for carbon fiber-epoxy composites," *Journal of Physical Chemistry C*, vol. 111, pp. 17865–17871, 2007.

[64] P.R. Thakre, D.C. Lagoudas, J. Zhu, E.V. Barrera, and T.S. Gates, "Processing and characterization of epoxy/swcnt/ woven carbon fabric composites," in *Proc. 47th AIAA/ASME/ASCE/AHS/ASC Structures, Structural Dynamics and Materials Conference*, Newport, RI, 2006, vol. AIAA 2006-1857.

[65] E.T. Thostenson, W.Z. Li, D.Z. Wang, Z.F. Ren, and T.W. Chou, "Carbon nan-

otube/carbon fiber hybrid multiscale composites," *Journal of Applied Physics*, vol. 91, no. 9, pp. 6034–6037, 2002.

[66] V. P. Veedu, A. Cao, X. Li, K. Ma, C. Soldano, S. Kar, P. M. Ajayan, and M. N. Ghasemi-Nejhad, "Multifunctional composites using reinforced laminae with carbon-nanotube forests," *Nature Materials*, vol. 5, no. 6, pp. 457–462, 2006.

[67] M.H.G. Wichmann, J. Sumfleth, F.H. Gojny, M. Quaresimin, B. Fiedler, and K. Schulte, "Glass-fiber-reinforced composites with enhanced mechanical and electrical properties- benefits and limitations of a nanoparticle modified matrix," *Engineering Fracture Mechanics*, vol. 73, pp. 2346–2359, 2006.

[68] E. Garcia, B. Wardle, deVilloria R., R. Guzman de Villoria, S. Wicks, K. Ishiguro, N. Yamamoto, and A. Hart, "Aligned carbon nanotube reinforcement of advanced composite ply interfaces," in *Proc. 49th AIAA/ASME/ASCE/AHS/ASC Structures, Structural Dynamics, and Materials Conference, April 7-10*, Schaumberg, IL, 2008, vol. AIAA-2008-1768.

[69] E.J. Garcia, A.J. Hart, and B.L. Wardle, "Long carbon nanotubes grown on the surface of fibers for hybrid composites," *AIAA Journal*, vol. 46, no. 6, pp. 1405–1412, 2008.

[70] N. Yamamoto and B. Wardle, "Electrical and thermal properties of hybrid woven composites reinforced with aligned carbon nanotubes," in *Proc. 49th AIAA/ASME/ASCE/AHS/ASC Structures, Structural Dynamics, and Materials Conference, April 7-10*, Schaumberg, IL, 2008.

[71] A.J. Kinloch, D.L. Maxwell, and R.J. Young, "The fracture of hybrid-

particulate composites," *Journal of Materials Science*, vol. 20, pp. 4169–4184, 1985.

[72] M-S. Sohn and X-Z. Hu, "Delamination behavior of carbon fibre/epoxy composite laminates with short fibre reinforcement," *Scripta Metallurgica et Materialia*, vol. 30, no. 11, pp. 1467–1472, 1994.

[73] S. Shin and J. Jang, "The effect of thermoplastic coating on the mechanical properties of woven fabric carbon/epoxy composites," *Journal of Materials Science*, vol. 35, pp. 2047–2054, 2000.

[74] D. Stevanovic, S. Kalyanasundaram, A. Lowe, and P.-Y.B. Jar, "Mode i and mode ii delamination properties of glass/vinyl-ester composite toughened by particulate modified interlayers," *Composite Science and Technology*, vol. 63, pp. 1949–1964, 2003.

[75] V. Kostopoulos, "Enhancement of the mechanical performance of carbon fiber reinforced epoxy resin composites by the introduction of carbon nanofibers(cnf)," in *Proc. 47 th AIAA/ASME/ASCE/AHS/ASC Structures, Structural Dynamics, and Materials Conference*, Newport, RI, 2006, pp. 1–10.

[76] S. J. V. Frankland, V. M. Harik, G. M. Odegard, D. W. Brenner, and T. S. Gates, "The stress-strain behavior of polymer-nanotube composites from molecular dynamics simulation," *Composites Science and Technology*, vol. 63, no. 11, pp. 1655–1661, 2003.

[77] T. S. Gates, G. M. Odegard, S. J. V. Frankland, and T. C. Clancy, "Computational materials: Multi-scale modeling and simulation of nanostructured materials," *Composites Science and Technology*, vol. 65, no. 15-16, pp. 2416–2434, 2005.

[78] V. G. Hadjiev, D. C. Lagoudas, E. S. Oh, P. Thakre, D. Davis, B. S. Files, L. Yowell, S. Arepalli, J. L. Bahr, and J. M. Tour, "Buckling instabilities of octadecylamine functionalized carbon nanotubes embedded in epoxy," *Composites Science and Technology*, vol. 66, no. 1, pp. 128–136, 2006.

[79] D. C. Lagoudas, P.R. Thakre, and A.A. Benzerga, "Nanoindentation of cnt reinforced epoxy nanocomposites," in *Proc. Sixteenth European Conference on Fracture (ECF16)*, Greece, 2006.

[80] G. M. Odegard, T. S. Gates, K. E. Wise, C. Park, and E. J. Siochi, "Constitutive modeling of nanotube-reinforced polymer composites," *Composites Science and Technology*, vol. 63, no. 11, pp. 1671–1687, 2003.

[81] J. C. Riddick, S. J. V. Frankland, and T. S. Gates, "Multiscale analysis of delamination of carbon fiber-epoxy laminates with carbon nanotubes," in *Proc. 47 th AIAA/ASME/ASCE/AHS/ASC Structures, Structural Dynamics, and Materials Conference*, Newport, RI, 2006, pp. 1–12.

[82] G. D. Seidel and D. C. Lagoudas, "Micromechanical analysis of the effective elastic properties of carbon nanotube reinforced composites," *Mechanics of Materials*, vol. 38, no. 8-10, pp. 884–907, 2006.

[83] E. T. Thostenson, Z. F. Ren, and T. W. Chou, "Advances in the science and technology of carbon nanotubes and their composites: A review," *Composites Science and Technology*, vol. 61, no. 13, pp. 1899–1912, 2001.

[84] D. C. Hammerand, G. D. Seidel, and D. C. Lagoudas, "Computational micromechanics of clustering and interphase effects in carbon nanotube composites," *Mechanics of Advanced Materials and Structures*, vol. 14, no. 4, pp. 277–294, 2007.

[85] J. Zhu, V.N. Khabasheskhu, A.M. Imam, R. Crane, K. Lozano, and E.V. Barrera, "Processing and properties of polymer composites reinforced by functionalized swcnts," *Materials Science Forum*, vol. 475-479, pp. 1059–1062, 2005.

[86] "Astm d 5528 - standard test method for mode i interlaminar fracture toughness of unidirectional fiber-reinforced polymer matrix composites," Tech. Rep., 01.

[87] A. B. de Morais, M. F. de Moura, J.P.M. Goncalves, and P.P. Camanho, "Analysis of crack propagation in double cantilever beam tests of multidirectional laminates," *Mechanics of Materials*, vol. 35, pp. 641–652, 2003.

[88] I. Paris, P.J. Minguet, and T.K. O' Brien, "Comparison of delamination characterization for im7/8552 composite woven and tape laminates," in *Composite Materials: Testing and Design, ASTM STP 1436*, C. E. Bakis, Ed., West Conshohocken, PA, 2003.

[89] P. Hansen and R. Martin, "Dcb, 4enf and mmb delamination characterisation of s2/8552 and im7/8552," *Technical Report N68171-98-M-5177, United States Army, European Research Office Of the US Army, London, England*, 1999.

[90] L. Flandin, T. Prasse, R. Schueler, K. Schulte, W. Bauhofer, and J. Y. Cavaille, "Anomalous percolation transition in carbon-black-epoxy composite materials," *Physical Review B*, vol. 59, no. 22, pp. 14349–14355, 1999.

[91] W. C. Oliver and G. M. Pharr, "An improved technique for determining hardness and elastic modulus using load and displacement sensing indentation experiments," *Journal of Materials Research*, vol. 7, no. 6, pp. 1564, 1992.

[92] W. C. Oliver and G. M. Pharr, "Measurement of hardness and elastic modulus

by instrumented indentation: Advances in understanding and refinements to methodology," *Journal of Materials Research*, vol. 19, no. 1, pp. 3, 2004.

[93] C. Arends, *Polymer Toughening*, CRC Press, New York, 1996.

[94] R.S. Prasher, J-Y. Chang, I. Sauciuc, S. Narasimhan, D. Chau, G. Chrysler, A. Myers, S. Prstic, and C. Hu, "Nano and micro technology based next generation package level cooling solutions," *Intel Technology Journal*, vol. 9, no. 4, pp. 285, 2005.

[95] T. Prasse, A. Ivankov, J. Sandler, K. Schulte, and W. Bauhofer, "Imaging of conductive filler networks in heterogeneous materials by scanning kelvin microscopy," *Journal of Applied Polymer Science*, vol. 82, no. 13, pp. 3381–3386, 2001.

[96] "Carbon nanotube properties. available [online]: http://www.cnanotech.com/products/materials.html," .

[97] K. Tao, S. Y. Yang, J. C. Grunlan, Y. S. Kim, B. L. Dang, Y. J. Deng, R. L. Thomas, B. L. Wilson, and X. Wei, "Effects of carbon nanotube fillers on the curing processes of epoxy resin-based composites," *Journal of Applied Polymer Science*, vol. 102, no. 6, pp. 5248–5254, 2006.

[98] M. Grujicic, G. Cao, and W.N. Roy, "A computational analysis of the percolation threshold and the electrical conductivity of carbon nanotubes filled polymeric materials," *Journal of Materials Science*, vol. 39, pp. 4441–4449, 2004.

[99] Z. Ounaies, C. Park, K.E. Wise, E.J. Siochi, and J.S. Harrison, "Electrical

properties of single wall carbon nanotube reinforced polyimide composites," *Composites Science and Technology*, vol. 63, pp. 1637–1646, 2003.

[100] K. E. Atkinson and C. Kiely, "The influence of fibre surface properties on the mode of failure in carbon-fibre/epoxy composites," *Composites Science and Technology*, vol. 58, pp. 1917–1922, 1998.

[101] T. Duvis and C.D. Papaspyrides, "Carbon-epoxy composites based on fibers coated with nylon 6,6: Hygrothermal ageing versus interlaminar shear strength," *Polymers for Advanced Technologies*, vol. 5, pp. 444–450, 1994.

[102] B. Fernandez, F. Mujika, A. De Benito, and I. Mondragon, "Mechanical characterization of woven carbon fabric composites with poly(methyl methacrylate)-modified epoxy matrices," *Polymer Composites*, vol. 24, no. 5, pp. 640–654, 2003.

[103] B. Fernandez, A. Arbelaiz, A. Valea, F. Mujika, and I. Mondragon, "A comparative study on the influence of epoxy sizings on the mechancal performance of woven carbon fiber-epoxy composites," *Polymer Composites*, vol. 25, no. 3, pp. 319–330, 2004.

[104] R. Kamiya and T.-W. Chou, "Strength and failure behavior of stitched carbon/epoxy composites," *Metallurgical and Materials Transactions A*, vol. 31(A), pp. 899–909, 2000.

[105] E. Garcia, A. Hart, B. Wardle, and A. Slocum, "Fabrication and testing of long carbon nanotubes grown on the surface of fibers for hybrid composites," in *Proc. 47th AIAA/ASME/ASCE/AHS/ASC Structures, Structural Dynamics, and Materials Conference, May 1-4*, Newport, RI, 2006.

[106] J. Zhu, A. Imam, R. Crane, K. Lozano, V. N. Khabashesku, and E. V. Barrera, "Processing a glass fiber reinforced vinyl ester composite with nanotube enhancement of interlaminar shear strength," *Composites Science and Technology*, vol. 67, no. 7-8, pp. 1509–1517, 2007.

[107] T. Yokozeki, Y. Iwahori, and S. Ishiwata, "Matrix cracking behaviors in carbon fiber/epoxy laminates filled with cup-stacked carbon nanotubes (cscnts)," *Composites Part A*, vol. 38, pp. 917–924, 2007.

[108] K. Adhikari, P. Hubert, B. Simard, and A. Johnston, "Effect of localized application of swnt modified epoxy on the interlaminar shear strength of carbon fibre laminates," in *Proc. 47th AIAA/ASME/ASCE/AHS/ASC Structures, Structural Dynamics and Materials Conference*, Newport, RI, 2006.

[109] F. H. Gojny, M. H. G. Wichmann, U. Kopke, B. Fiedler, and K. Schulte, "Carbon nanotube-reinforced epoxy-composites: Enhanced stiffness and fracture toughness at low nanotube content," *Composites Science and Technology*, vol. 64, no. 15, pp. 2363–2371, 2004.

[110] C.A. Berg, J. Tirosh, and M. Israeli, "Analysis of short beam bending of fiber reinforced composites," in *Proc. Composite Materials: Testing and Desing (Second Conference), ASTM STP 497, ASTM*, 1972, pp. 206–218.

[111] B.K. Daniels, N.K. Harakas, and R.C. Jackson, "Short beam shear tests on graphite fiber composites," *Fibre Science and Technology*, vol. 3, pp. 187–208, 1971.

[112] F. Rosselli and M.H. Santare, "Comparison of the short beam shear (sbs) and interlaminar shear device (isd) tests," *Composites Part A*, vol. 28A, pp. 587–594, 1997.

[113] E. Sideridis and G.A. Papadopoulos, "Short-beam and three-point-bending tests for the study of shear and flexural properties in unidirectional-fiber-reinforced epoxy composites," *Journal of Applied Polymer Science*, vol. 93, pp. 63–74, 2004.

[114] J. L. Sullivan and H. Van Oene, "An elasticity analysis for the generally and specially orthotropic beams subjected to concentrated loads," *Composites Science and Technology*, vol. 27, pp. 182–191, 1986.

[115] J.M. Whitney and C.E. Browning, "On short beam shear tests for composite materials," *Materials Mechanics*, vol. 25, pp. 294–300, 1985.

[116] J.M. Whitney, *Structural Analysis Of Laminated Anisotropic Plates*, Technomic Publishing Company, Inc., Lancaster, 1987.

[117] M.R. Wisnom, "Modelling of stable and unstable fracture of short beam shear specimens," *Composites*, vol. 25, no. 6, pp. 394–400, 1994.

[118] "Astm d 2344-00: Standard test method for short-beam strength of polymer matrix composite materials and their laminates," vol. 15. D2344 edition, 2000.

[119] S. Hashemi, A. J. Kinloch, and J. G. Williams, "Corrections needed in double-cantilever beam tests for assessing the interlaminar failure of fibre-composites," *Journal of Materials Science Letters*, vol. 8, pp. 125–129, 1989.

[120] S.-J. Park and J.-S. Jin, "Effect of silane coupling agent on mechanical interfacial properties of glass fiber-reinforced unsaturated polyester composites," *Journal of Polymer Science: Part B: Polymer Physics*, vol. 41, pp. 55–62, 2002.

[121] J. Zhu, A. Imam, R. Crane, K. Lozano, V. Khabasheshku, and E.V. Barrera, "Processing a glass fiber reinforced vinyl ester composite with nanotube en-

hancement of interlaminar shear strength," *Composites Science and Technology*, vol. 67, pp. 1509–1517, 2007.

[122] J. Qiu, C. Zhang, B. Wang, and R. Liang, "Carbon nanotube integrated multifunctional multiscale composites," *Nanotechnology*, vol. 18, pp. 1–11, 2007.

[123] D. Dean, A.M. Obore, S. Richmond, and E. Nyairo, "Multiscale fiber-reinforced nanocomposites: Synthesis, processing and properties," *Composites Science and Technology*, vol. 66, pp. 2135–2142, 2006.

[124] L. Liu, Z.-M. Huang, C.L. He, and X.J. Han, "Mechanical performance of laminated composites incorporated with nanofibrous membranes," *Materials Science and Engineering A*, vol. 435-436, pp. 309–317, 2006.

[125] N. Alif, L.A. Carlsson, and L. Boogh, "The effect of weave pattern and crack propagation direction on mode-i delamination resistance of woven glass and carbon composites," *Composites Part B*, vol. 29B, pp. 603–611, 1998.

[126] A. B. de Morais, M. F. de Moura, A. T. Marques, and P. T. de Castro, "Mode i interlaminar fracture of carbon/epoxy cross-ply composites," *Composites Science and Technology*, vol. 62, pp. 679–686, 2002.

[127] W. Richards Thissell, A. K. Zurek, and F. Addessio, "Mechanical properties and failure mechanisms of carbon fiber reinforced epoxy laminated composites," *Proc. AIP Conference*, vol. 370, no. 1, pp. 551–554, 2006.

[128] R.H. Martin, "Delamination characterization of woven glass/polyester composites," *Journal of Composites Technology and Research*, vol. 19, no. 1, pp. 20–28, 1997.

[129] L. Y. Tong, X. N. Sun, and P. Tan, "Effect of long multi-walled carbon nanotubes on delamination toughness of laminated composites," *Journal of Composite Materials*, vol. 42, no. 1, pp. 5–23, 2008.

[130] E. Bekyarova, E. T. Thostenson, A. Yu, M. E. Itkis, D. Fakhrutdinov, T. W. Chou, and R. C. Haddon, "Functionalized single-walled carbon nanotubes for carbon fiber-epoxy composites," *Journal of Physical Chemistry C*, vol. 111, no. 48, pp. 17865–17871, 2007.

[131] F. H. Gojny, M. H. G. Wichmann, B. Fiedler, W. Bauhofer, and K. Schulte, "Influence of nano-modification on the mechanical and electrical properties of conventional fibre-reinforced composites," *Composites Part A-Applied Science and Manufacturing*, vol. 36, no. 11, pp. 1525–1535, 2005.

[132] J. Cho and I. M. Daniel, "Reinforcement of carbon/epoxy composites with multi-wall carbon nanotubes and dispersion enhancing block copolymers," *Scripta Materialia*, vol. 58, pp. 533–536, 2008.

[133] Y. X. Zhou, F. Pervin, S. Jeelani, and P. K. Mallick, "Improvement in mechanical properties of carbon fabric-epoxy composite using carbon nanofibers," *Journal of Materials Processing Technology*, vol. 198, pp. 445–453, 2008.

[134] L. Sun, G.L. Warren, J.Y. O'Reilly, W.N. Everett, S.M. Lee, D. Davis, D. Lagoudas, and H.-J. Sue, "Mechanical properties of surface-functionalized swcnt/epoxy composites," *Carbon*, vol. 46, pp. 320–328, 2008.

APPENDIX A

FRACTURE TOUGHNESS OF NANOCOMPOSITES

Nanocomposite Fracture Toughness

Mechanical properties from Gojny et al. [18]

Table 1
Mechanical properties of nanoparticle reinforced composites

	Filler type/content (wt%)	Young's modulus (MPa)	Ultimate tensile strength (MPa)	Fracture toughness K_{Ic} (MPa $m^{1/2}$)
Epoxy	**0.0**	**2599 (±81)**	**63.80 (±1.09)**	**0.65 (±0.062)**
Epoxy/CB	0.1	2752 (±144)	63.28 (±0.85)	0.76 (±0.030)
	0.3	2796 (±34)	63.13 (±0.59)	0.86 (±0.063)
	0.5	2830 (±60)	65.34 (±0.82)	0.85 (±0.034)
Epoxy/SWCNT	0.05	2681 (±80)	65.84 (±0.64)	0.72 (±0.014)
	0.1	2691 (±31)	66.34 (±1.11)	0.80 (±0.041)
	0.3	2812 (±90)	67.28 (±0.63)	0.73 (±0.028)
Epoxy/DWCNT	0.1	2785 (±23)	62.43 (±1.08)	0.76 (±0.043)
	0.3	2885 (±88)	67.77 (±0.40)	0.85 (±0.031)
	0.5	2790 (±29)	67.66 (±0.50)	0.85 (±0.064)
Epoxy/DWCNT–NH_2	0.1	2610 (±104)	63.62 (±0.68)	0.77 (±0.024)
	0.3	**2944 (±50)**	**67.02 (±0.19)**	**0.92 (±0.017)**
	0.5	**2978 (±24)**	**69.13 (±0.61)**	**0.93 (±0.030)**
Epoxy/MWCNT	0.1	2780 (±40)	62.97 (±0.25)	0.79 (±0.048)
	0.3	2765 (±53)	63.17 (±0.13)	0.80 (±0.028)
	0.5	2609 (±13)[a]	61.52 (0.19)[a]	[a]
Epoxy/MWCNT–NH_2	0.1	2884 (±32)	64.67 (±0.13)	0.81 (±0.029)
	0.3	2819 (±45)	63.64 (0.21)	0.85 (±0.013)
	0.5	2820 (±15)	64.27 (±0.32)	0.84 (±0.028)

[a] High viscosity disabled degassing – composite contained numerous voids.

Mechanical properties from Sue et al. [134]

Mechanical Properties of the Bulk Epoxy/SWCNT Nanocomposites (0.5 wt %)

Property	Neat epoxy	Epoxy/ P-SWCNT	Epoxy/ O-SWCNT	Epoxy/ F-SWCNT
Young's modulus (GPa)	2.77 ± 0.01	2.84 ± 0.05	3.17 ± 0.01	3.21 ± 0.15
Tensile strength (MPa)	60.1 ± 5.6	74.2 ± 0.5	76.5 ± 3.9	82.7 ± 3.2
Elongation (%)	1.98 ± 0.22	2.57 ± 0.18	2.97 ± 0.40	4.88 ± 0.91
K_{IC} (MPa $m^{1/2}$)	0.78 ± 0.01	0.76 ± 0.03	0.83 ± 0.05	0.93 ± 0.04

K_{IC}, Mode-I critical stress intensity factor.

The above tables show improvement in fracture toughness for epoxy based nanocomposites.

APPENDIX B

DETAILS OF CLASSICAL LAMINATE THEORY MODEL

The following flow chart represents the calculation of elastic constants using classical laminate theory model. This flow chart has been taken from Issac Daniel and Ori Ishai Book on Engineering Mechanics of Composite Materials. The nanocomposite properties were calculated by using Mori-Tanaka micromechanics method and the carbon nanotubes were randomly oriented using orientation averaging method proposed by Entchev-Lagoudas Method.

The local volume fraction of the carbon nanotubes in the nanocomposite layer and the thickness of nanocomposite layer was calculated based on fiber areal weight and density of carbon fibers and carbon nanotubes.

The case for incorporating nanocomposite interleaf between the pre-pregs and the resulting laminate properties have been presented as follows. Edge view and cross-section view of a nanocomposites layer between two unidirectional pre-pregs.

Longitudinal modulus of different laminates from classical laminate theory.

Transverse modulus of different laminates from classical laminate theory.

In-plane shear modulus of different laminates from classical laminate theory

Figures shows the modeling results from classical laminate theory for longitudinal and transverse modulus. The HM Graphite/Epoxy system is chosen for comparative analysis. There are nine horizontal bars in each figure. The first three results are for 10 layer composites only. First one is for control laminate without nanotubes and next two cases are for 10 layer pre-preg laminates modified with nanotube reinforced epoxy. Thus nanotubes exist throughout the matrix. The next six cases are for 22 layer composites by introduction of thin layers of epoxy or nanocomposites

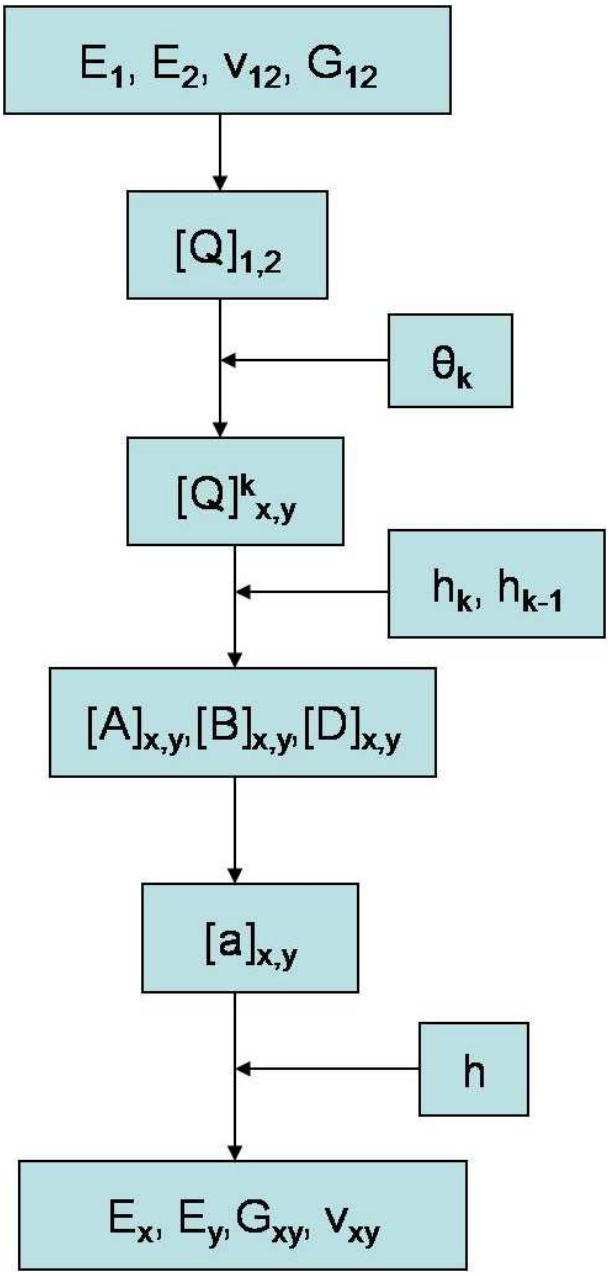
E_1, E_2, v_{12}, G_{12}
$[Q]_{1,2}$
θ_k
$[Q]^k_{x,y}$
h_k, h_{k-1}
$[A]_{x,y}$,$[B]_{x,y}$,$[D]_{x,y}$
$[a]_{x,y}$
h
E_x, E_y,G_{xy}, v_{xy}

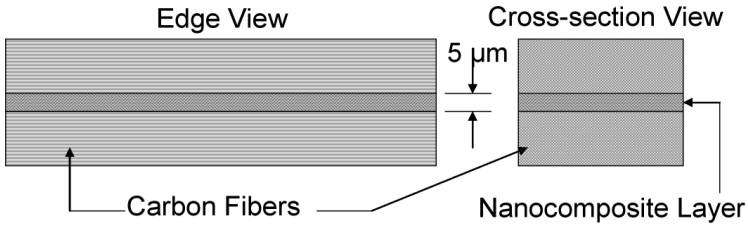

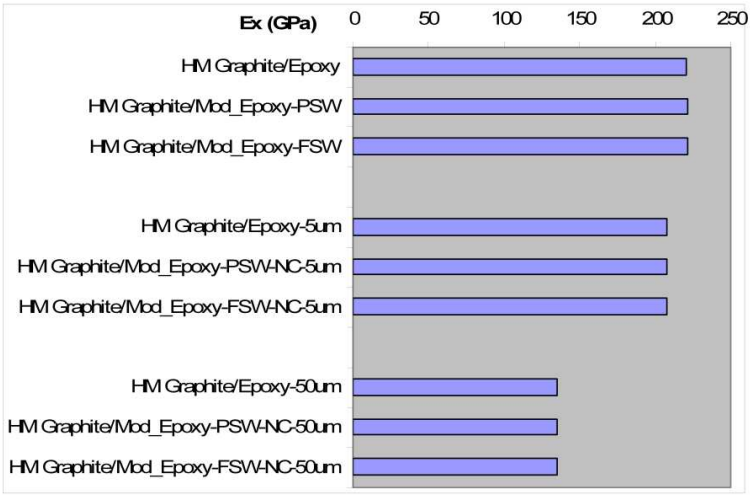

between alternate layers of pre-pregs. When nanocomposite layers are introduced, it is represented by HM Graphite/Mod-Epoxy-NC-PSW for nanocomposite containing pristine nanotubes and HM Graphite/Mod-Epoxy-NC-FSW for nanocomposite containing functionalized nanotubes. The layer thickness is represented by 5 μm or 50 μm. The nanocomposite layer properties are taken from the dynamic mechanical analysis tests on randomly oriented nanotubes reinforced epoxy matrix. There was a 6% and 20% improvement in isotropic elastic modulus of the pristine and the functionalized single wall nanotubes embedded in toughened RS-47 epoxy matrix respectively.

Fig. B shows that there is no effect on the longitudinal modulus as a result of addition of nanotubes. The base laminate longitudinal modulus is higher than the experimental value because high modulus graphite fibers are used for modeling purpose instead of IM7 carbon fibers used for experimental investigation. When the

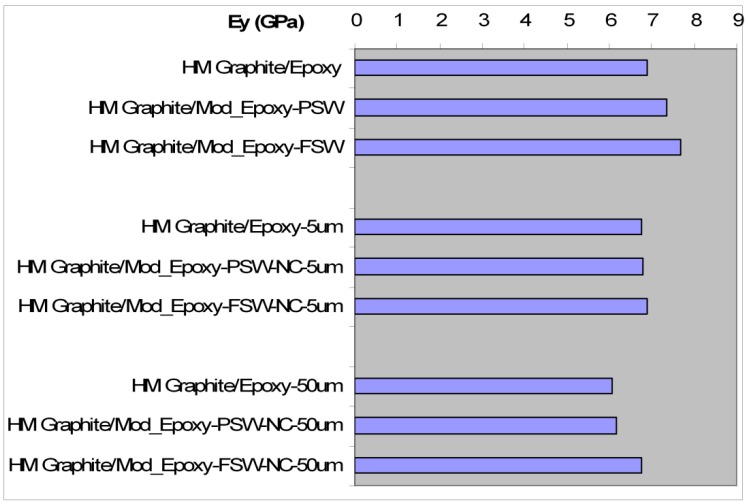

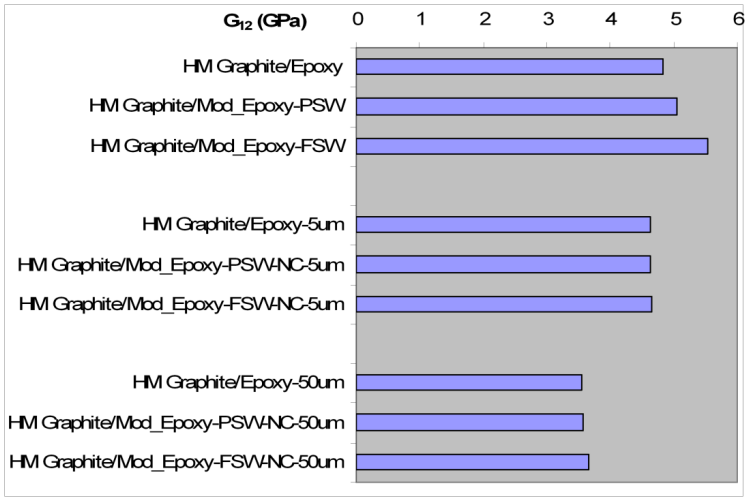

neat epoxy or nanocomposite interphase layer is introduced, it reduces the original volume fraction (60%) of the carbon fibers. Thus we see a decrease in longitudinal modulus, however, the decrease is consistent for laminates with or without nanotubes. Increasing the interphase layer thickness results in further decrease in longitudinal modulus, as there is a further decrease in the carbon fiber volume matrix. So there are two important observations from Fig. B. First, there is no effect on the longitudinal modulus due to the presence of nanotubes, whether throughout the matrix or in the interphase layer. Secondly, addition of the interphase layer and increasing its

thickness results in reducing the longitudinal modulus.

The results as shown in Fig. B indicate an increase in the transverse modulus by addition of nanotubes. The functionalized nanotubes show a greater impact as compared to the pristine nanotubes. The best results are obtained when functionalized nanotubes are present throughout the matrix, followed by, when pristine nanotubes are present throughout the matrix. The improvement in transverse modulus of about 6% and 11% for specimens with pristine and functionalized nanotubes respectively, is in close agreement with the experimentally observed increase of 6% and 12% for specimens with 0.5 wt% of pristine and functionalized nanotubes respectively.

The introduction of thin layers of 5 micron thickness does not show significant effect as compared to the composite containing 5 micron layers of neat epoxy. However, the presence of 50 micron layers of functionalized nanotubes shows significant improvement of about 12% (in the transverse modulus) over the composite containing 50 micron layers of neat epoxy.

The in-plane shear modulus, which is also a matrix dominated property, shows almost similar behavior as transverse properties(Fig. B). The maximum improvement is for the case of functionalized nanotubes present throughout the matrix system instead of just in the interphase layers. In all the modeling cases presented here, when the nanotube reinforced epoxy nanocomposite layer is introduced between pre-preg layers, it results in increased matrix volume fraction and corresponding decrease in the carbon fiber volume fraction. The actual experiment does not involve introduction of additional epoxy, so there is no change in the total carbon fiber volume fraction. This case has been discussed in the modeling section of Chapter V.

VITA

Name: Piyush R. Thakre

Education:

- Texas A&M University, USA
  - Doctor of Philosophy, Materials Science and Engineering (**Ph.D.**)
  - Master of Science, Mechanical Engineering (**M.S.**)
- Nagpur University, India
  - Bachelor of Engineering, Mechanical Engineering (**B.E.**)
    With Distinction (equivalent to Summa Cum Laude)
- Indira Gandhi National Open University, India
  - Diploma In Management (**D.I.M.**)

Address: 223 WERC, 3409 TAMU, College Station, TX 77843-3409

Research Interests:

- Processing of nanoparticles reinforced polymer matrix nanocomposites and fiber reinforced polymer (FRP) composite laminates.

- Damage tolerance and delamination growth in composites, fracture mechanisms in composites and laminate analysis.

- Mechanical, electrical and thermal characterization of multifunctional composites.

- Multi-scale structure-property relationships in nanocomposites and composite laminates using advanced characterization methods.

- Future interests include processing and characterization of advanced structural composites, multifunctional nanocomposites for sensors and actuators, structural health monitoring composite systems, energy harvesting materials and bio-based composite materials.